print
11 2 06
online
www.karger.com/aud

Audiology & Neurotology

Basic Science and Clinical Research in the Auditory and Vestibular Systems and Diseases of the Ear

Micro- and Nanotechnology for Neurotology

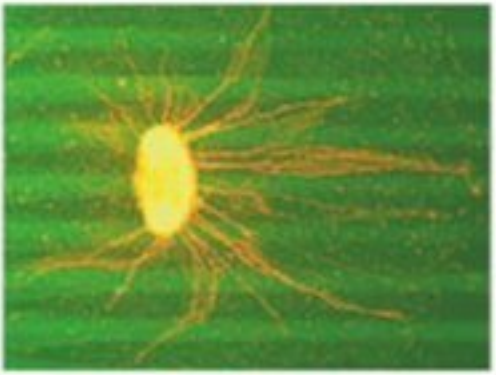

Guest Editor
Fan-Gang Zeng, Irvine, Calif.

KARGER

Audiology & Neurotology

Micro- and Nanotechnology for Neurotology

Guest Editor
Fan-Gang Zeng, Irvine, Calif.

45 figures, 13 in color, and 2 tables, 2006

KARGER

Basel · Freiburg · Paris · London · New York ·
Bangalore · Bangkok · Singapore · Tokyo · Sydney

S. Karger
Medical and Scientific Publishers
Basel • Freiburg • Paris • London
New York • Bangalore • Bangkok
Singapore • Tokyo • Sydney

Printed in Switzerland on acid-free paper by
Reinhardt Druck, Basel
ISBN 3–8055–8100–9

KARGER

Fax +41 61 306 12 34
E-Mail karger@karger.ch
www.karger.com

Audiology & Neurotology

Vol. 11, No. 2, 2006

Contents

KARGER

Fax +41 61 306 12 34
E-Mail karger@karger.ch
www.karger.com

Access to full text and tables of contents, including tentative ones for forthcoming issues: www.karger.com/aud_issues

Audiology & Neurotology

Audiol Neurotol 2006;11:75
DOI: 10.1159/000090678

Published online: January 17, 2006

Editorial

As this special issue of *Audiology & Neurotology* ushers in a new year, the focus on nanotechnology is intended to provoke thoughtful discussion of new areas for research and development in our field. A broad definition of nanotechnology provides the backdrop for this issue:

'The creation of functional materials, devices and systems through control of matter on the nanometer length scale and exploitation of novel phenomena and properties (physical, chemical, biological) at that length scale' (http://www.ipt.arc.nasa.gov/nanotechnology.html).

Given that the scale of a nanometer is less than 1/1000 of the width of a human hair, the field of nanotechnology naturally conjures up a myriad of questions about application and feasibility.

Some background and explanation for why the topic of nanotechnology is both contemporary and momentous may be useful to our readers. The origins of nanotechnology arose from the theoretical work of several scientists. In the 1950s, Richard Feynman proposed a new small scale future that included manipulating and controlling atoms. Feynman's theory has been confirmed by the discovery of new shapes for molecules of carbon including carbon nanotubes, which are far lighter but stronger than steel with superior heat and conductivity characteristics. In 1974, Norio Taniguchi coined the term 'nano-technology' to refer to production technology or micromachining with accuracy and fineness on the scale of the nanometer. Around the same time, Eric Drexler proposed that the biological machinery that already exists in nature could be adapted through molecular manufacturing. He also called this approach 'nanotechnology' and envisioned manufacturing high-performance machines out of a molecular carbon lattice. Even as some scientists have anticipated the revolutionary changes that nanotechnology might bring, controversies associated with nanotechnology have not been small scale – particularly as warnings surfaced of the potential for developing a self-replicating nanorobot with the capacity to destroy the environment.

Even as scientific debate continues regarding the usefulness and safety of nanotechnology, some principles of nanotechnology are already shaping biomedical research. For example, innovative research is already funded and underway on creating synthetic ciliated surfaces through the creation and actuation of sheets of nanorods and investigating the impact of light-driven molecular motors for use in artificial muscle systems. In this issue, we are publishing seven articles that describe how various principles and practices of nanotechnology are being applied to the human ear and hearing. Our goal is to both enlighten our readers about this new research and to stimulate questions and dialogue about the possibilities for nanotechnology in our field.

Jeffrey P. Harris, La Jolla, Calif.

KARGER

Fax +41 61 306 12 34
E-Mail karger@karger.ch
www.karger.com

1420–3030/06/0112–0075$23.50/0

Accessible online at:
www.karger.com/aud

Audiology & Neurotology

Audiol Neurotol 2006;11:76
DOI: 10.1159/000090679

Published online: January 17, 2006

Editorial

Like integrated circuits and personal computers, the emerging micro- and nanotechnologies will fundamentally change the way we live and work in the future. There are two reasons why we should pay attention to the development and impact of these technologies. Firstly, we should prepare for the changes the technologies will likely bring about to our profession and service. Secondly, as audiologists and neurotologists, we deal with perhaps the most sophisticated microelectromechanical system that nature ever built, namely the ear, which can sense vibrations as small as 0.5 nm. Engineers are not only learning the operational principles of the ear to enhance their technological development, but also how to apply the technologies to addressing a host of clinical issues in otology.

The present special issue, consisting of seven invited papers, showcases potential applications of micro- and nanotechnologies to audiology and neurotology. Spelman reviews the development of cochlear implants and discusses future cochlear electrode arrays. Inspired by the working of a fly's ear, Miles and Hoy have microfabricated a directional microphone for hearing aids. Bachman and colleagues use polymers to produce micromechanical resonator arrays that may serve as the microphone and frequency analyzer for an analog cochlear implant. Wittbrodt and colleagues have developed a physical model of the human cochlea using microfabrication. Shkel and Zeng describe a microelectromechanical system vestibular implant prototype. The usage of magnetic nanoparticles for inner ear targeted molecule delivery and middle ear implants is described by Kopke and coworkers. Combining microfluidics and transfected cells, Ryan's group have conducted micropatterning studies to control auditory nerve development and growth.

Although the papers were invited, each went through the same rigorous review process as typical papers submitted to *Audiology & Neurotology*. We thank the reviewers and the editorial managers at Karger for their efficient and high-quality professional service.

Fan-Gang Zeng, Irvine, Calif.

KARGER

Fax +41 61 306 12 34
E-Mail karger@karger.ch
www.karger.com

1420–3030/06/0112–0076$23.50/0

Accessible online at:
www.karger.com/aud

KARGER

Table 1. Electrode arrays described in this paper (see the text for details)

Source	Manufacturing method/substrate	Number of contacts	Used in humans?
Epic Biosonics	automatic/silicon	16	no
Sonn (Raytheon)[a]	automatic/silicon	37	no
Stanford[b]	automatic/polymer	8	no
University of Michigan	automatic/silicon[c]	128	no
Advanced Cochlear Systems	automatic/polymer	72	no
University of Utah	automatic/silicon	100	no
AllHear (House)	manual/wire	1	yes
Med-El	manual/silicone	24	yes
Cochlear Ltd.	manual/silicone	22	yes
Advanced Bionics	manual/silicone	16	yes
LAURA	manual/silicone	48	no

[a] Sonn [1972].
[b] White et al. [1982].
[c] The University of Michigan is also working on hybrid arrays that bury silicon substrates in polymeric carriers.

olds occurred between 100 and 400 Hz [Spelman, 1982]. Despite the frequency-threshold characteristics of neural fibers, signal processing and interference issues made clear the necessity to drive the fibers of the auditory nerve with pulses of short duration, indeed, of widths less than 100 μs [Wilson et al., 1991; Rubinstein and Miller, 1999; Rubinstein et al., 1999]. Clear also was the need to develop arrays with large numbers of electrode contacts, to better approximate the design of the auditory system [Merzenich and White, 1977; Spelman, 1982; Patrick et al., 1990].

Modern cochlear implants consist of a microphone or microphones, an external processor, a transcutaneous data link, an internal processor and an electrode array. This paper deals solely with the electrode array. Other aspects of the cochlear prosthesis are covered in other papers within this issue. The manufacturing techniques, producers and basic properties of the major electrode arrays presented here are summarized in table 1.

Organization of the Paper

Early studies in humans were done with six electrodes that were inserted into the modiolus of the cochlea [Simmons et al., 1964; Simmons, 1966]. That approach has the benefit of bringing electrode contacts into direct proximity with the cells of the auditory nerve, lowering the threshold for electrical excitation. It suffers from the tonotopic organization of the nerve fibers in the modiolus: the fibers' characteristic frequencies are organized in a spiral whose axis is either parallel or orthogonal to the direction of placement of contacts in the array [Geisler, 1998]. Modiolar arrays have not been used commercially at the time of this writing, but are proposed as potential designs for high-density devices because the modiolar approach lends itself to the use of silicon substrates [Badi et al., 2003; Hillman et al., 2003]. Modiolar electrode arrays may possibly be the heart of future implants and will be discussed in more detail below.

The number of patients who have received brainstem auditory implants is small. Brainstem implants are still experimental devices. No commercial device has been distributed widely. Brainstem arrays will not be discussed in this paper.

Current commercial electrode arrays are placed in the scala tympani of the cochlea. This paper will present a view of arrays that have been developed and are currently in use, and describe future designs of the scala tympani array.

Properties of a Cochlear Electrode Array

The length of the cochlea of the human is about 35 mm [Geisler, 1998]. Ideally, a cochlear electrode array would span the entire cochlea, stimulating the full population of auditory neurons that span its length. To excite the speech regions of the cochlea, the contacts of the array should stimulate neurons whose center frequencies extend from 500 to 3000 Hz, that is, the array should span the distance from

14 to 25 mm from the stapes [Greenwood, 1990]. With 25–30000 auditory neurons spread across the cochlea [Geisler, 1998], and the necessity to have 20 independent stimuli to reproduce speech signals in noise [Spelman, 2004], there should be a means by which 20 electric fields could be produced within the 11 mm subtended by the speech frequency region. One way to do so is to drive triads of electrodes to produce potential widths that are approximately one electrode separation apart [Spelman et al., 1995; Jolly et al., 1996; Middlebrooks and Bierer, 2001; Bierer and Middlebrooks, 2004]. That requirement suggests that the cochlear electrode array's contacts should have a pitch that is less than 0.5 mm. If musical sound is desired, the array must extend nearer to the stapes than 14 mm in order to stimulate high-frequency neurons. If the array extends from the highest frequencies to 500 Hz as the lowest frequency, it must span 25 mm and should support at least 50 contacts for music appreciation.

Multipolar stimulation has higher thresholds of excitation than monopolar stimulation [Spelman et al., 1995; Middlebrooks and Bierer, 2001]. The higher thresholds are a consequence of the electric fields produced when electrodes are driven simultaneously to produce focused potential fields [Spelman et al., 1995]. Thresholds can be reduced if the electrode contacts are close to the target neurons [Merzenich and White, 1977; Spelman et al., 1995]. The electrode array should be placed near the modiolar (central) wall of the cochlea. A cochlear electrode array should be flexible to allow relatively easy surgical insertion. Of course, the materials of the array must withstand the hostile milieu of a warm, saline environment and be compatible with biological tissue.

A few properties of an ideal cochlear electrode array are these: flexibility for easy insertion and to minimize damage; a means to ensure proximity to the modiolar wall of the cochlea; high-density fabrication of electrodes; materials that are impervious to saline solutions; biocompatibility; ease of manufacture for low cost. These properties will be discussed below in the sections that describe electrode arrays that are produced for human use and that are in the research stage.

Modiolar Electrode Arrays

Wire Bundle Array: Simmons

Simmons' first attempt to stimulate the auditory nerve in humans was done in a surgical setting during which he exposed and visualized the nerve, obtaining responses to frequencies of 1 kHz and getting spoken responses from the subject [Simmons et al., 1964]. Simmons et al. [1979] implanted volunteers with chronic electrode arrays placed inside the auditory nerve.

Monolithic Array: Normann

Richard Normann's group at the University of Utah is developing a three-dimensional electrode array to stimulate the cells of the auditory nerve [Hillman et al., 2003]. The array consists of silicon needles, the tips of which are plated with platinum and the shanks of which are insulated. Each needle has a 1-mm length, and is spaced from its neighboring needles by 400 μm. The needles are placed on a silicon substrate in groups of 6–19, though the arrays have been produced with as many as 100 contacts [Badi et al., 2003]. The Utah array has been used successfully in animal experiments. It was tested in anesthetized cats. Arrays were driven into the auditory nerve with a pneumatic actuator [Hillman et al., 2003]. The auditory brainstem response was recorded, and the technique produced thresholds of 3–60 μA using pulse widths of 75 μs/phase and biphasic square pulses [Badi et al., 2003]. The contact lengths can be varied, although they were not graded in the experiments described here. The arrays have been implanted for times as long as 52 h. The construction of the arrays is novel and promising for automated manufacture. However, insertion into the auditory nerve may require extensive testing after implantation to learn the tonotopic organization of the contacts for each subject. The proximity to cells should provide more confined excitation of neurons than is available currently.

Early Work: Wire Bundle Arrays

House

William F. House was one of the early entrants into the cochlear implant field, using a single scalar electrode and a 16-kHz carrier, amplitude-modulated with auditory signals to drive the auditory nerve [House and Urban, 1973]. House reported that his patients heard environmental sounds, e.g. doorbells and automobile horns, and had improved speech production when they used the cochlear implant [House and Berliner, 1991], a finding supported by Bilger in his early report on the benefits of cochlear prostheses [Bilger et al., 1977]. The House implant was produced commercially by 3M in 1984 [House and Berliner, 1991]. The House implant is still produced by AllHear (http://www.allhear.com/). However, multi-channel implants make up by far the greatest, and most useful, number of cochlear prostheses that are used today.

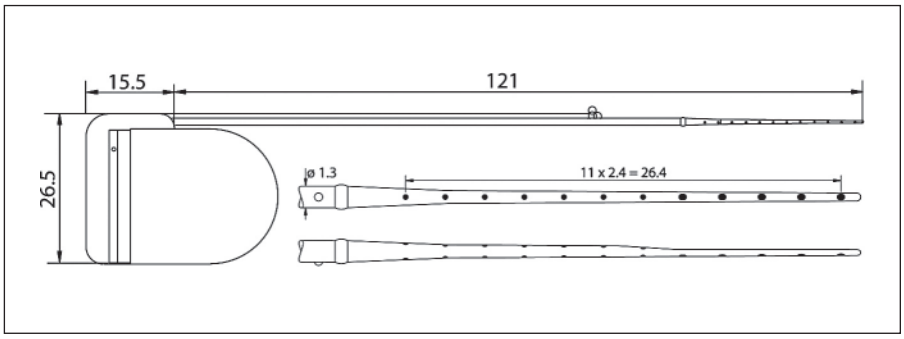

Fig. 1. The Med-El PULSAR$_{CI}^{100}$ Electrode array. The array is a wire bundle array with the configuration derived from that described in the citation in the text. The upper portion of the figure shows the array integrated to the internal processor and current driver package; the center image shows the placement of twelve electrode contacts on one side of the array; the bottom image depicts the placement of electrode contacts on both sides of the array. Dimensions are in millimeters. Taken from www.medel.com.

UCSF to Advanced Bionics

Robin Michelson and his coworkers began a series of studies in animals in the 1960s, resulting in technology transfer to the designers of cochlear implants, and then to human subjects [Michelson, 1985]. The UCSF arrays were made with 8 Pt-Ir (90% Pt-10% Ir) electrodes whose surfaces were formed into mushroom shapes, and whose carrier was molded to fit snugly into the human cochlea [Michelson and Schindler, 1981]. The device consisted of four paired electrodes of Pt-Ir, with four electrodes placed near the bony shelf of the cochlea and four placed near the modiolus [Rebscher et al., 1982]. The design took advantage of the direction of the peripheral processes of the auditory nerve, producing stimuli that followed along the lengths of the processes. The electrode array was built integral with its connector to the prosthesis' internal processor, the whole assembly being molded of silicone [Rebscher et al., 1982]. The technology was transferred from UCSF to Advanced Bionics in 1988, and later became the prototype of the Advanced Bionics electrode arrays, used in the Clarion® implant system. The array was wedded to a four-channel processor; the initial designs were to be driven as dipoles, developing fields that were at an acute angle, but not parallel to the peripheral processes of the nerve. The entire assembly was produced by hand.

Austria to Med-El

Erwin and Ingeborg Hochmair at the Technical University of Vienna developed a multi-channel, wire bundle electrode array with an approach that was different from that of UCSF, Cochlear Corp. and the French [Hochmair-Desoyer et al., 1983]. The array was built manually on a tapered silicone carrier with a basal diameter of 0.8 mm and an apical diameter of 0.5 mm. It employed eight Pt-Ir contacts arranged so that half were in a modiolar location and half were on the opposite side of the array. The array did not fill the scala tympani. The array was 16 mm long in the four-channel version, and was longer when it was produced in six-, eight- and twelve-channel models. All versions were tested in human subjects, and the longer arrays could be inserted surgically to a depth of 25 mm. The electrode was flexible and tractable for insertion. A newer version of the array was tested as a modiolar-hugging device that used a central fiber under tension to appose the electrodes to the modiolar wall [Jolly et al., 2000].

Med-El still produces its 24-electrode arrays manually, but may change that approach in the future (fig. 1, vide infra).

The French Prosthesis

Professor C.-H. Chouard and colleagues introduced a cochlear prosthesis in the 1970s. Their approach to electrode design that differed somewhat from that of the other arrays is described here. They used 12-contact Pt-Ir ball electrode contacts (0.3-mm spherical diameter) placed in indentations on a half-cylindrical silicone carrier for implantation in an unobstructed scala tympani. In the case of malformed cochleae, they inserted Pt-Ir ball electrodes into the scala via surgical fenestrations [MacLoed et al., 1985]. Cochlear prostheses with 15-contact arrays, based on the Chouard design, are currently produced in France by MXM Laboratories (Côte d'Azur, France).

The LAURA Cochlear Implant

The University of Antwerp introduced the LAURA cochlear implant in 1993 [Offeciers et al., 1998]. The effort was adopted by the Philips Corporation, but has not been sold worldwide. There are few details available on the LAURA electrode array. However, the designers of the LAURA implant proposed a new electrode array in 2003 [Deman et al., 2003]. The array is designed to occupy the entire scala tympani as a tapered, space-filling structure and has 48 contacts arranged with 24 contacts

to be placed near the basilar membrane and 24 on the opposite side of the device. The purpose is to achieve current flow in the radial direction of the cochlea. The contacts are stamped from platinum, attached to wires, and then the silicone substrate is injection molded to produce a spiral shape. Insertion tests in an acrylic model of the human cochlea produced forces appropriate for human use. The device has not been implanted in human subjects at the time of this writing.

Clark and Cochlear Corporation

Clark et al. [1975] reported on an electrode array that they introduced into human temporal bones from an opening drilled into the apex of the cochlea.

They described a more practical device in greater detail later, introducing the concept of a wire bundle array with cylindrical electrode contacts [Clark et al., 1983]. This novel array had the advantage that it did not require rotation to face the electrodes toward the modiolar wall of the cochlea. However, it had the disadvantage that current exits the electrodes in all radial directions. The electrodes were made of Pt-Ir rings that had widths of 0.3 mm and separations of 0.45 mm. The original design used a silicone tube with a uniform diameter of 0.64 mm. The arrays that have been adopted and which are manufactured by Cochlear Corporation are tapered along their lengths.

Cochlear's present array, the Contour Advance^{TM} Array, has 22 electrode contacts that are inserted into the scala tympani via the basal turn (fig. 2). The present array can be inserted to a depth of more than 20 mm. It apposes the modiolar wall by means of a premanufactured shape (fig. 2; www.cochlearamericas.com/Products/23.asp). To resist folding of the shaped array, it is inserted with a tool that straightens it during the surgery. The present array has rectangular rather than cylindrical electrode sites. Cylindrical sites are not required for radial symmetry because the spiral shape of the array places the contacts near the modiolar wall of the cochlea. Reducing the surface area of the electrode sites helps to concentrate the electric fields where they are needed to excite neurons. This array is manufactured by hand.

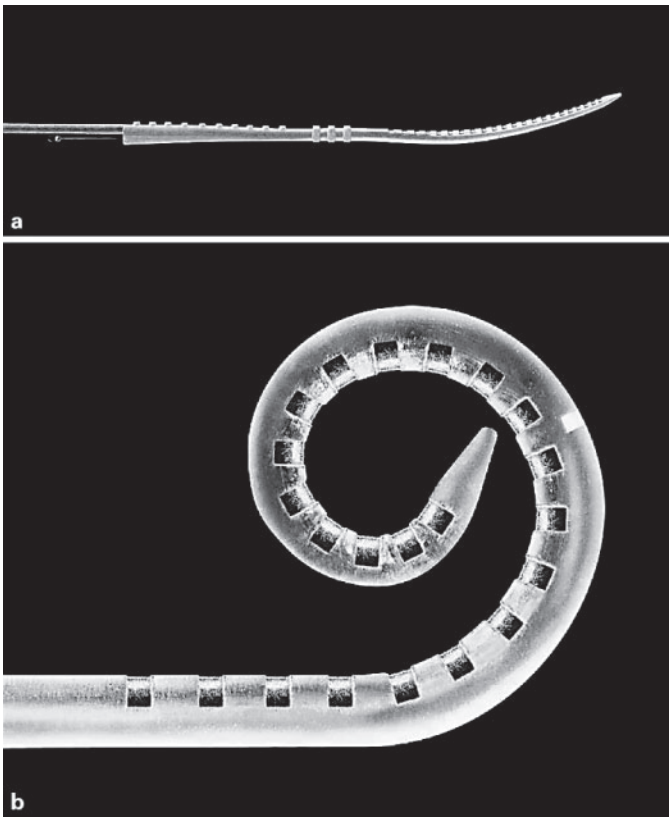

Fig. 2. The Contour Advance^{TM} electrode array of Cochlear Corporation. **a** The electrode array with a stilette inserted to straighten the device. The stilette can be seen at the left side of the figure. The active contacts are to the right of the rings that are visible in the center of the figure. The contacts to the left of the rings are for return current and are outside of the scala tympani. **b** Close-up image of the array with the stilette removed. The SofTip® is visible at the center of the spiral. The 22 active contacts are clearly seen in the figure. These images are courtesy of Cochlear Americas, Inc., C. van den Honert.

Materials Used

Substrates

Cochlear electrode arrays have used silicone rubber (dimethylsiloxanes) carriers, Pt-Ir electrode contacts, and Pt-Ir wires that are insulated with fluoropolymers. The contacts have been made of Pt for its durability and safety under the conditions of long-term pulsatile stimulation and Ir for its strength [Spelman, 1982]. Silicone rubber is used for its low toxicity, durability during long-term exposure to aqueous salt solutions and mechanical flexibility [Colas and Curtis, 2004].

Electrode Contacts

More recently, researchers have investigated the oxides of iridium as electrode contacts [Cogan et al., 2003a, b]. Iridium oxide electrodes were suggested earlier [Robblee and Rose, 1990]; no commercial arrays employ them at present, although the material is under active investigation by several groups. The oxides of iridium have

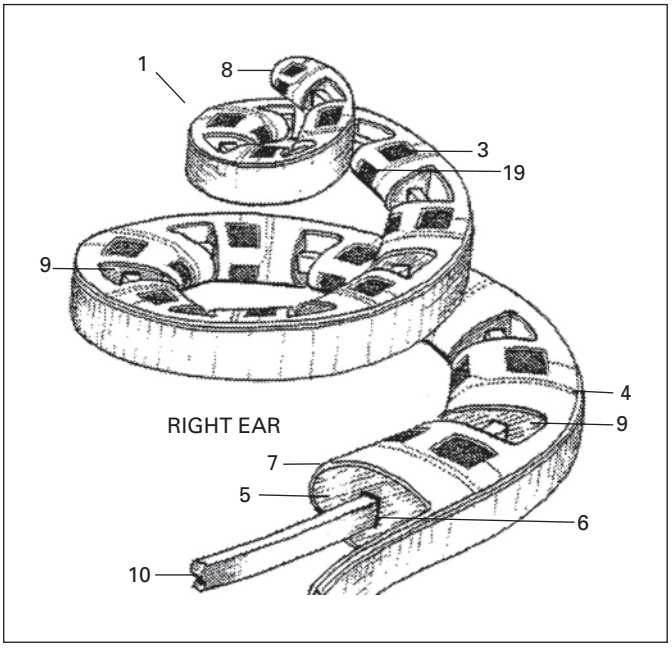

Fig. 3. Sketch of Berrang's electrode array design copied from U.S. Patent 6,374,143. The array is formed on a polymer substrate with a silastic core. The beam (10) in the center of the array provides the torque necessary to approximate the array to the modiolar wall of the cochlea.

charge storage capacities, that is, the ability to deliver electric currents over time, that are more than ten times those of Pt surfaces. Additionally, the oxides of iridium appear to be safe to use over long times in neural tissues [McCreery et al., 1992].

Manufacturing Techniques

The evidence offered above shows that present-day electrode arrays are built by hand. That approach requires highly skilled technicians to produce the arrays, long manufacturing times and high cost relative to devices that are manufactured automatically in large quantities. The idea of using integrated circuit techniques for artificial ears dates to the early 1970s [Sonn, 1972]. Sadly, nothing came of Sonn's work, although he covered several key points in detail: the use of polymeric substrates; sputtering metals onto plastics; feedlines; connectors; biocompatibility [Sonn, 1972].

Mercer and White [1978] designed monolithic electrode arrays and drove them into the auditory nerves of anesthetized cats. The arrays were designed first as gold-on-silicon and then developed as molybdenum or tungsten substrates with Pt electrodes. Mercer and White reported low threshold currents and reasonable recording from separate arrays that were placed in the inferior colliculus. The eight-contact arrays were robust when they were produced with the metallic substrates [Mercer and White, 1978]. Later, the Stanford group built electrode arrays on flexible polymers, choosing polyimide as a substrate and iridium as a contact. Titanium was deposited on spun polyimide, with a conducting layer of iridium evaporated on top of the titanium [Shamma-Donoghue et al., 1982]. The Stanford array never was used in human subjects. Some of the details of the techniques of deposition and difficulties encountered are found in the quarterly progress reports of the Stanford NIH Contract, N01-NS-0-2336, which was extant during the early 1980s.

A few years after Sonn proposed his device to Raytheon, van der Puije published a novel concept of an electrode array [van der Puije et al., 1989]. Van der Puije introduced several ideas, one of them the development of a cylindrical electrode array formed around a silicone core. He suggested the use of ring electrodes, already introduced by Clark [Clark et al., 1983]. However, van der Puije's array was based on a polyimide substrate, with a layer of titanium followed by an overcoating of platinum. Contacts, feedlines and wiring pads were sputter etched from the layered metal, using standard photolithographic techniques to distinguish the desired conductors from the substrate [van der Puije et al., 1989]. The surface of the array was insulated with another layer of polyimide. Using a special die, the flexible structure was rolled into a cylinder of 0.5-mm diameter whose central cavity was filled with silicone [van der Puije et al., 1989]. After the initial publication, no further work was reported on the electrode array, which never was implanted in human subjects.

More recently, Berrang et al. [2002b] have patented their design of a modiolar-hugging cochlear electrode array.

Figure 3 shows a sketch of the design, taken from a U.S. Patent for the device [Berrang et al., 2002b]. The array incorporates many of the desirable characteristics of a cochlear electrode array [Merzenich and White, 1977; Stypulkowski, 1984; van den Honert, 1984]. (1) The electrodes (numbers 3 and 19 in fig. 3) can be driven either as longitudinal sets or as radial bipolar pairs. (2) The array has a preferential direction of bending so that it approximates the cochlear spiral. (3) The array can be made to hug the modiolar wall because of the central beam (10 in fig. 3), and the backbone that lies on the side of the lateral wall of the cochlea. Berrang and Lupin [2002] patented an insertion technique for entry of the array into the cochlea. The Berrang array is designed to be a part of

a totally implantable cochlear implant [Berrang et al., 2002a]. Berrang's company, Epic Biosonics, was bought recently by Med-El. As of this writing, the Berrang array has not been used in human subjects.

Others have tried to automate the manufacture and production of cochlear electrode arrays. Two designs sought to both automate the manufacturing process and increase the number and density of electrode contacts. The first was a marriage of wire-based technology and automated manufacture in which tiny, insulated Pt-Ir wires were formed automatically into a layered spiral form with a central shape-memory core [Corbett et al., 1997; Spelman et al., 1998].

Insulation was removed with laser ablation, providing the potential of having more than 70 contacts of 1500 μm^2 and inter-contact separations of 0.1 mm. Prototypes were tested in preliminary studies in animals, demonstrating the potential of focusing fields on small groups of auditory neurons [Jolly et al., 1997]. As studies progressed, the investigators found that yield was small because the insulation on the wires developed pinholes that produced crosstalk between contacts.

Corbett et al. [2004] at Advanced Cochlear Systems (Snoqualmie, Wash., USA) developed a flexible, layered array on substrates of liquid crystal polymer. The array could be built with microcircuit techniques, which could be automated. To produce an array of 72 contacts, seven layers of 25-μm liquid crystal polymer were used, each separated by another layer (fig. 4). Traces were deposited on each layer, terminated in vias that were developed at the edge of the array. The vias were plated, and could be made of a variety of metals. The initial design specified iridium oxide contacts. Several limited prototypes with twelve gold or iridium oxide contacts were made for insertion into the first turn of the scala tympani of the cat. Experiments in the laboratory of Russell Snyder [pers. commun.] confirmed that it was possible to focus stimuli onto small groups of auditory neurons, confirming the results obtained by Middlebrooks and Bierer [Middlebrooks and Bierer, 2001, 2002; Bierer and Middlebrooks, 2002]. The animal data obtained with this array indicate that it should be possible to excite several independent groups of neurons simultaneously. Still, the array has not been incorporated into a clinical device.

Investigators at the Wireless Integrated MicroSystems Engineering Research Center at the University of Michigan are working to develop flexible, high-density electrode arrays for cochlear implants. Their most recent annual report briefly explains the design of a number of techniques that may permit the use of silicon substrates as platforms for cochlear implants. Arcand and Friedrich [2004] describe an articulated device that uses fluidics to achieve a spiral shape and to position the array against the modiolar wall of the cochlea. The device achieves a spiral shape of 1–2 turns, and looks promising. They do not mention either animal tests or insertion tests in cochlear models or temporal bones. However, in the same

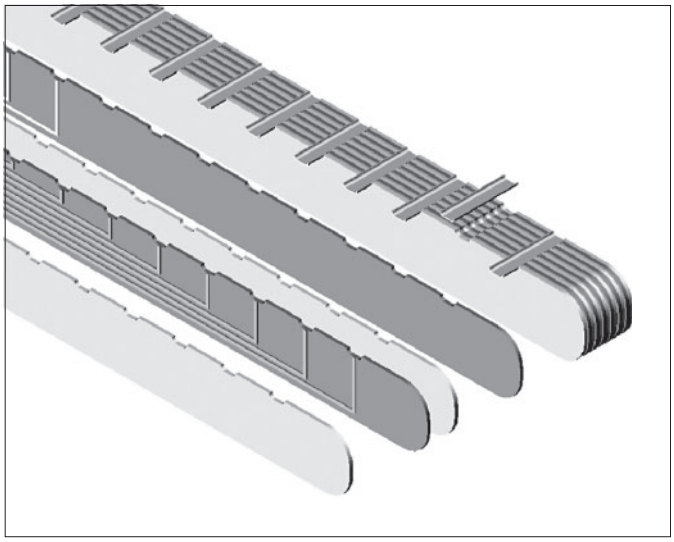

Fig. 4. Sketch of Corbett's multi-layered cochlear electrode array. For details, see text. Sketch courtesy of Scott S. Corbett, III, with permission.

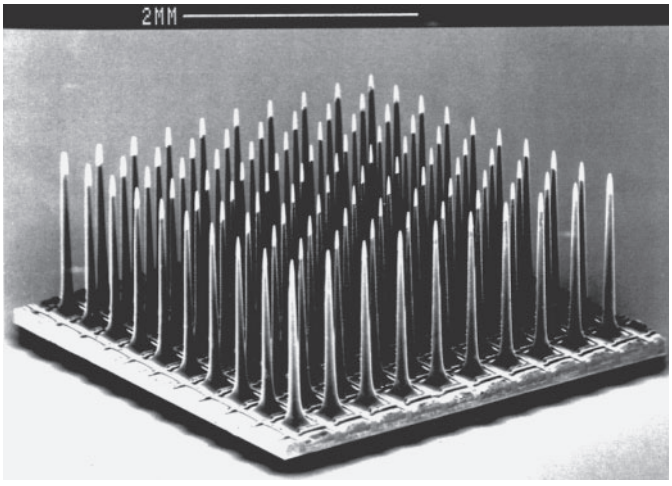

Fig. 5. Image of a prototype electrode array produced by the University of Utah to place in the modiolus of the cochlea. The array is designed to penetrate the auditory nerve. Taken from www.sci.utah.edu/~gk/abstracts/bisti03/img/array_bw.png.

organization, Bhatti et al. [2004] describe a high-density electrode array for the guinea pig. It employs contacts of 180-μm diameter that are spaced 250 μm center-to-center. The device is coupled to monolithic current generators and testing devices, and looks promising for insertion into the first turn of the guinea pig's cochlea.

The Michigan group is working toward a systems approach, with cochlear electrode arrays, positioning devices, force sensing devices and stimulators [Arcand and Friedrich, 2004; Bhatti et al., 2004; Tang and Aslam, 2004; Wang and Wise, 2004]. If they are successful, the goal of building a high-density, relatively inexpensive, precise cochlear electrode array may be achieved.

The Utah array can be manufactured automatically, using the techniques that are used to fabricate integrated circuits. It can support large numbers of contacts, although experimental work in vivo has been limited to 19 contacts [Hillman et al., 2003]. Arrays with 100 contacts have been fabricated and tested in vitro (fig. 5).

If human testing protocols can be perfected, this approach may provide promise to provide more independent channels of information than can be provided by scala tympani arrays. Still, sorting the tonotopic arrangement of the contacts in human patients may prove to be a daunting task.

Future Electrode Arrays

Future cochlear electrode arrays are likely to contain more contacts than the devices that are implanted currently. Scala tympani arrays will continue to be placed close to the modiolar wall of the cochlea in order to reduce thresholds and increase specificity. Whether the arrays will be manufactured by hand or automatically is unclear at this point. If the Michigan group is successful [Arcand and Friedrich, 2004], silicon arrays may well be placed in human ears. A human array that employs flexible circuit techniques [Berrang et al., 2002b; Corbett et al., 2004] has not been tested in human subjects. Technical issues, primarily related to longevity, still remain. However, developments in flexible circuits are rapid and exciting, demonstrating the possibility of printing conductors on flexible circuits and increasing the resolution at which the circuits are made [Chalamala and Temple, 2005].

The developers of electrode arrays will continue to attempt to produce devices that are manufactured automatically rather than by hand. The former technique offers precision and repeatability of electrode contacts, decreased cost to manufacture arrays and the potential of developing arrays with at least twice the number of contacts that is produced at present.

Hybrid arrays, containing silicon segments that can be manufactured within silicone substrates may overcome some of the difficulties of producing long silicon devices that are prone to shatter. More likely, polymeric substrates will be used if they can be made to retain their adhesion to metal conductors in the hostile environment of the inner ear.

Some investigators have suggested that arrays might release growth factors near or upon the electrode contacts, trying to lure the processes of the auditory neurons near the array. The Michigan Group has developed silicon tubes that might be integrated with a cochlear electrode array to make the technique possible [Li et al., 2004]. Some work has been done by Med-El to test the concept [Miller, pers. commun.]. Slow-release polymers, doped with growth factors may possibly work for the same purpose. There are anecdotal reports of such trials, but no published reports at this time.

Acknowledgements

Thanks are due to Scott S. Corbett, III, for his careful review and editing of the manuscript. This work was supported in part by NIH SBIR Grants DC005331 and DC04614.

References

Arcand B, Friedrich CR: An Articulated Package for a Cochlear Prosthesis. Ann Arbor, WIMS ERC, 2004, p 76.

Badi AN, Kertesz TR, et al: Development of a novel eighth-nerve intraneural auditory neuroprosthesis. Laryngoscope 2003;113:833–842.

Berrang PG, Bluger HV, et al: Totally implantable cochlear prosthesis. U.S. Patent Office. Epic Biosonics, 2002a.

Berrang PG, Bluger HV, et al: Modiolar hugging electrode array. U.S. Patent Office. Epic Biosonics, 2002b.

Berrang PG, Lupin AJ: Means for implanting a device in the canalis cochlaris. U.S. Patent Office. Epic Biosonics, 2002.

Bhatti PT, Pfingst BE, et al: A 128-site, 16-channel electrode array for a cochlear prosthesis. Ann Arbor, WIMS ERC, 2004, p 73.

Bierer JA, Middlebrooks JC: Auditory cortical images of cochlear-implant stimuli: dependence on electrode configuration. J Neurophysiol 2002;87:478–492.

Bierer JA, Middlebrooks JC: Cortical responses to cochlear implant stimulation: channel interactions. J Assoc Res Otolaryngol 2004;5:32–48.

Bilger RC, Black FO, et al: Evaluation of subjects presently fitted with implanted auditory prostheses. Ann Otol Rhinol Laryngol 1977; 86(suppl 38):1–176.
Chalamala BR, Temple D: Big and bendable. IEEE Spectrum 2005;42:50–56.
Clark GM, Hallworth RJ, et al: A cochlear implant electrode. J Laryngol Otol 1975;30:787–792.
Clark GM, Shepherd RK, et al: Design and fabrication of the banded electrode array. Cochlear prostheses: an international symposium, Ann N Y Acad Sci 1983;405:191–201.
Cogan SF, Troyk PR, et al: Characterization and variability of intracortical iridium oxide microelectrodes. 25 Annu Int Conf IEEE EMBS, Cancun, 2003a.
Cogan SF, Troyk PR, et al: Charge injection waveforms for iridium oxide (AIROF) microelectrodes. 25 Annu Int Conf IEEE EMBS, Cancun, 2003b.
Colas A, Curtis J: Silicone biomaterials: history and chemistry; in Lemons JE (ed): Biomaterials Science: An Introduction to Materials in Medicine. Amsterdam, Elsevier 2004, pp 80–86.
Corbett SS, Johnson T, et al: Method of making high contact density electrode array. U.S. Patent Office. Advanced Cochlear Systems, 2004.
Corbett SS, Swanson JW, et al: High density cochlear implant and method of manufacturing the same. U.S. Patent Office. BioElectric Corporation, University of Washington, 1997.
Deman PR, Kaiser TM, et al: Design, construction and mechanical optimisation process of electrode with radial current flow in the scala tympani. J Neurosci Methods 2003;128:143–150.
Geisler CD: From Sound to Synapse: Physiology of the Mammalian Ear. New York, Oxford University Press, 1998.
Greenwood DD: A cochlear frequency-position function for several species – 29 years later. J Acoust Soc Am 1990;87:2592–2605.
Hillman T, Badi AN, et al: Cochlear nerve stimulation with a 3-dimensional penetrating electrode array. Otol Neurotol 2003;24:764–768.
Hochmair-Desoyer IJ, Hochmair ES, et al: Design and fabrication of multiwire scala tympani electrodes. Ann N Y Acad Sci 1983;405:173–182.
House WF, Berliner KI: Cochlear Implants: from idea to clinical practice; in Cooper, H (ed): Cochlear Implants: A Practical Guide. San Diego, Singular Publishing Group, 1991, pp 9–33.
House WF, Urban J: Long term results of electrode implantation and electronic stimulation of the cochlea in man. Ann Otol Rhinol Laryngol 1973;82:504.
Jolly CN, Clopton BM, et al: Guinea pig auditory nerve response triggered by a high density electrode array. Med Prog Technol 1997;21 (suppl):13–23.
Jolly CN, Gstöttner W, et al: Principles and outcome in perimodiolar positioning. Ann Otol Rhinol Laryngol 2000;185(suppl):20–23.
Jolly CN, Spelman FA, et al: Quadrupolar stimulation for cochlear prostheses: modeling and experimental data. IEEE Trans Biomed Eng 1996;43:857–865.
Li Y, Bledsoe SCJ, et al: An Integrated Chemical Delivery Probe with In-Line Flow Measurement and On-Chip Signal Processing. Ann Arbor, WIMS ERC, 2004, p 88.
MacLoed P, Chouard CH, et al: French device; in Merzenich MM (ed): Cochlear Implants. New York, Raven Press, 1985, pp 111–120.
McCreery DB, Yuen TG, et al: Stimulation with chronically implanted microelectrodes in the cochlear nucleus of the cat: histologic and physiologic effects. Hear Res 1992;62:42–56.
Mercer HD, White RL: Photolithographic fabrication and physiological performance of microelectroded arrays for neural stimulation. IEEE Trans Biomed Eng 1978;25:494–500.
Merzenich MM, Michelson RP, et al: Neural encoding of sound sensation evoked by electrical stimulation of the acoustic nerve. Ann Otol Rhinol Laryngol 1973;82:486–504.
Merzenich MM, White MW: Cochlear implants. The interface problem; in Hambrecht FT, Reswick JB (eds): Functional Electrical Stimulation: Applications in Neural Prostheses. New York, Marcel Dekker, 1977, pp 321–340.
Michelson RP: Cochlear implants: personal perspectives; in Merzenich MM (ed): Cochlear Implants. New York, Raven Press, 1985, pp 9–12.
Michelson RP, Schindler RA: Multichannel cochlear implant. Preliminary results in man. Laryngoscope 1981;91:38–42.
Middlebrooks JC, Bierer JA: Cortical images of cochlear implant stimuli. 2001 Conf Implant Cochlear Prostheses, Pacific Grove, 2001.
Middlebrooks JC, Bierer JA: Auditory cortical images of cochlear-implant stimuli: coding of stimulus channel and current level. J Neurophysiol 2002;87:493–507.
NIH: NIH Consensus Statement: Cochlear Implants in Adults and Children. Bethesda, National Institutes of Health, 1995.
Offeciers FE, Govaerts P, et al: The LAURA Pediatric Cochlear Implant Program in Antwerp: what have we learnt in 5 years? Acta Otorhinolaryngol Belg 1998;52:105–109.
Patrick JF, Seligman PM, et al: Engineering; in Clark GM, Tong YC, Patrick JF (eds): Cochlear Prostheses. Edinburgh, Churchill Livingstone 1990, pp 99–125.
Rebscher SJ, Byers CL, et al: Development of Multichannel Electrodes for an Auditory Prosthesis. San Francisco, University of California, 1982, p 17.
Robblee LS, Rose TL: Electrochemical guielines for selection of protocols and electrode materials for neural stimulation; in Agnew WF, McCreery DB (eds): Neural Prostheses: Fundamental Studies. Englewood Cliffs, Prentice Hall, 1990, pp 25–66.
Rubinstein JT, Miller CA: How do cochlear prostheses work? Curr Opin Neurophysiol 1999;9: 399–404.
Rubinstein JT, Wilson BS, et al: Pseudospontaneous activity: stochastic independence of auditory nerve fibers with electrical stimulation. Hear Res 1999;127:108–118.
Rushton WAH: A physical analysis of the relation between threshold and interpolar length in the electric excitation of medullated nerve. J Physiol 1934;82:332–352.
Shamma-Donoghue S, May GA, et al: Thin-film multielectrode arrays for a cochlear prosthesis. IEEE Trans Elect Dev 1982;29:136–144.
Simmons FB: Electrical stimulation of the auditory nerve in man. Arch Otolaryngol 1966;84: 24–76.
Simmons FB, Mathews RG, et al: A functioning multichannel auditory nerve stimulator. A preliminary report on two human volunteers. Acta Otolaryngol 1979;87:170–175.
Simmons FB, Mongson CJ, et al: Electrical stimulation of the acoustic nerve and inferior colliculus in man. Arch Otolaryngol Head Neck Surg 1964;79:559.
Sonn M: An Artificial Cochlea for the Sensory Deaf: Presurgical Development. Portsmouth, Raytheon, 1972, pp 1–146.
Spelman FA: The cochlear prosthesis: a review of the design and evaluation of electrode implants for the profoundly deaf. CRC Crit Rev Bioeng 1982;8:223–253.
Spelman F: Cochlear prostheses; in Ratner BD, Hoffman AS, Schoen FJ, Lemons JE (eds): Biomaterial Science: An Introduction to Materials in Medicine. Amsterdam, Elsevier, 2004, pp 658–669.
Spelman FA, Clopton BM, et al: Cochlear Implant with Shape Memory Material and Method for Implanting the Same. U.S. Patent office, MicroHelix, 1998.
Spelman FA, Pfingst BE, et al: The effects of electrode configuration on potential fields in the electrically-stimulated cochlea: models and measurements. Ann Otol Rhinol Laryngol 1995;104(suppl 166):131–136.
Stypulkowski PH, van den Honert C: Physiological properties of the electrically stimulated auditory nerve. I. Compound action potential recordings. Hear Res 1984;14:205–223.
Tang Y, Aslam DM: Ultra-Sensitive Poly-C Sensors for Cochlear Prosthesis. Ann Arbor, WIMS ERC, 2004, p 75.
van den Honert CSP: Physiological properties of the electrically stimulated auditory nerve. II. Single fiber recordings. Hear Res 1984;14: 225–243.
van der Puije PD, Pon CR, et al: Cylindrical cochlear electrode array for use in humans. Ann Otol Rhinol Laryngol 1989;98:466–471.
Wang J, Wise KD: A Position Sensing and Control System for a Cochlear Prosthesis. Ann Arbor, WIMS ERC, 2004, p 74.
White MW, Merzenich MM, et al: Multichannel cochlear implants: channel interactions and processor design. Arch Otolaryngol 1984;110: 493–501.
White RL, Shamma SA, Cotter NE: First Quarterly Progress Report, NIH Contract N01-NS-0-2336. Development of Multi-Channel Electrodes for an Auditory Prosthesis. Stanford, Stanford University, 1982.
Wilson BS, Finley CC, et al: Better speech recognition with cochlear implants. Nature 1991;352: 236–238.

KARGER

able ability to sense the direction of an incident sound wave [Miles et al., 1995; Mason et al., 2001]. The fly's auditory system has evolved in such a way that it is ideally suited to hearing and localizing a cricket's mating call [Robert et al., 1992]. The parasitic female must find a specific host cricket on which to deposit her predaceous maggots. Hence, gravid female *O. ochracea* locate calling male crickets using auditory cues. The offspring are deposited on or near a cricket and ultimately consume it. Our initial efforts to study the fly's ears were on determining the mechanism by which these small animals localize the sounds from the cricket. It seemed surprising that such a small animal, roughly the size of a housefly, possessing auditory organs with eardrums separated by a few hundred microns, could be so adept at localizing sounds. Over the past decade, we have conducted a thorough mechanical and anatomical investigation of the ears of this animal [Robert et al., 1994, 1996; Miles et al., 1995, 1997].

In the following, we describe the mechanism for directional hearing in this animal. As will be apparent, these flies have evolved a unique mechanism for directional hearing, based on mechanical coupling of its eardrums. This 'invention' of nature has inspired a useful exercise in biomimicry, in which the physical acoustics of fly's ears serve as a basis for novel microphone design. The principles used for developing conventional directional microphones will be described along with a discussion of the evolution and performance possibilities of the current Ormia-inspired microphones. Because these new microphone designs are made possible by the use of new fabrication technologies, some of the challenges and opportunities for future advances in microphone constructions are discussed.

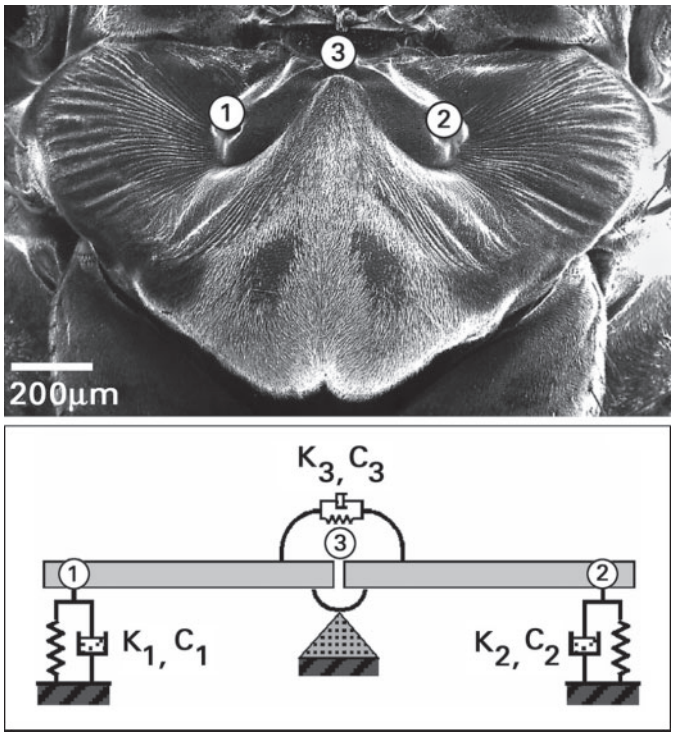

Fig. 1. The ears of *O. ochracea* and a mechanical model used to describe the directional sensitivity. The two tympana are the corrugated membranes that are mechanically connected through the intertympanal bridge, shown here with the numbers 1, 2, and 3. The central point (3) acts as a hinge. The sensory cells are connected to the tympanal pits (1 and 2). The mechanical model includes equivalent stiffnesses, K_1, K_2, and K_3 and equivalent viscous dashpots, C_1, C_2, and C_3 [Miles et al., 1995].

The Unusual Ears of *O. ochracea*

Laser vibrometric measurements of the mechanical response of the ears of *O. ochracea* indicate that when sound arrives from one side, the tympanum that is closer to the sound source responds with significantly greater amplitude than that which is further from the source. This occurs even though the two eardrums are very close together, both fitting in a space about 1 mm across. Because of the minute separation between the eardrums, the interaural differences in incident pressure are extremely small. The interaural difference in mechanical response is due to the coupling of the ears' motion by a cuticular structure that joins the two tympana, which we have named the intertympanal bridge, as shown in figure 1 [Miles et al., 1995]. This was the first report of the use of a mechanical link between a pair of ears to achieve directionally sensitive hearing, which had not been previously reported in any other animal.

We developed an analytical model of the ears of *O. ochracea* that accurately predicts the mechanical response of the eardrums when stimulated by sound from any incident direction [Miles et al., 1995]. An examination of this model shows that the system can be represented in terms of two independent resonant modes of vibration that are excited by a sound wave as shown in figure 2. This consists of a rocking mode, in which the two eardrums move in opposite directions, and a translational mode, in which the ears move in the same direction. The rocking mode is driven by the difference, or gradient, in pressure between the two exterior surfaces of the ears. The translational mode is driven by the average pressure

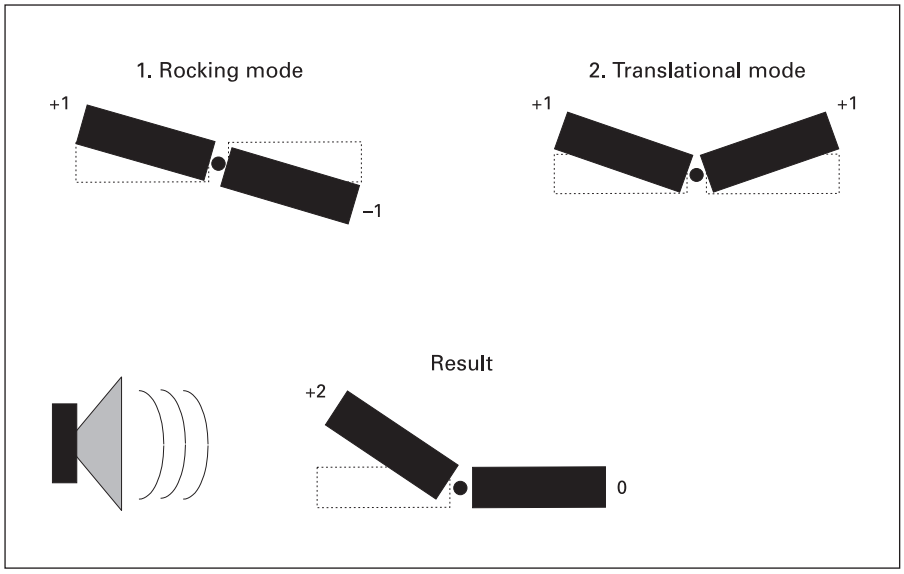

Fig. 2. The combination of a rocking mode and translational mode leads to directional sensitivity.

on the two ears. Operating under an appropriate set of mechanical properties for the ears, these two modes combine such that they add on the ear that is closer to the sound source and cancel on the ear that is further from the source. With the right choice of mechanical properties, this effect produces a directionally sensitive response in the fly's ears over a frequency range of about 5 kHz to over 25 kHz [Miles et al., 1995]. As shown in the lower schematic in figure 2, this mechanical coupling can generate a significant interaural difference in tympanal response, in the face of minute interaural difference cues in the sound field at the location of the ears. This difference in the amplitude of the motion at the two ears is due to very small differences in the phase of the incoming wave at the external surfaces of the tympana. One can view this system as a simple mechanical signal processor that combines the pressure gradient with the average pressure to achieve a directionally sensitive response [Miles et al., 1997].

This approach to sound source localization differs from what is used in most large vertebrate animals, like ourselves, in which two independent ears detect the sound and interaural differences in amplitude and time of arrival are processed by the central nervous system to determine the orientation of the sound source. Very little or no interaural processing takes place at auditory periphery, which is the 'secret' of the fly's ears. We exploit this mechanistic difference in device design below.

Comparison with Conventional Directional Acoustic Sensing

Any system that responds to sound pressure in a manner that depends on the direction of propagation of the wave must detect the spatial gradient in the pressure. The straightforward methods of creating a conventional pressure gradient sensor use either the difference in the response of two independent microphones (where the subtraction is accomplished by electronic circuitry or signal processing) or a pressure-sensitive membrane that responds due to the net (i.e. difference) pressure on its two sides.

The essence of what is special about the ears of *O. ochracea* is that miniscule pressure gradients in the sound field cause the pair of eardrums to rotate about a central anatomical pivot point in the rocking mode shown in figure 2. Essentially, the pressure gradient creates a net moment, producing rotation of the entire assembly about the pivot. Figure 3 shows a schematic of an Ormia-inspired pressure gradient diaphragm on the left and a conventional gradient diaphragm on the right. In the conventional diaphragm, the two pressures act on the top and bottom surface of a simple membrane. The membrane responds to the net force produced by these pressures, which is equal to the pressure difference because they act on opposite sides of the diaphragm. The use of an acoustic pressure gradient to produce a moment and hence a rotation of a diaphragm suggests a significant departure from previous approaches to directional acoustic sensing.

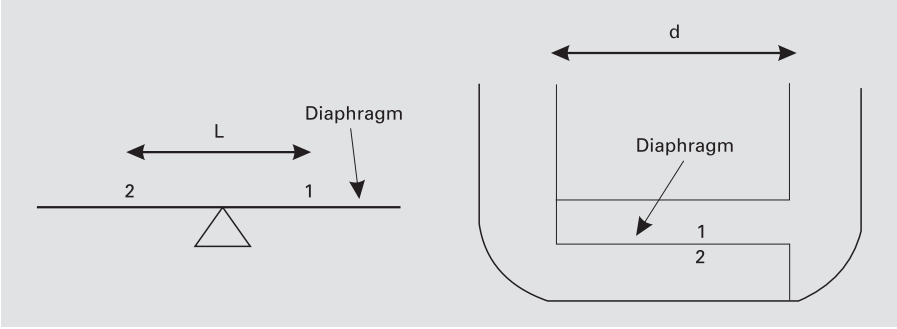

Fig. 3. Schematic of an Ormia-inspired pressure gradient diaphragm on the left and a conventional gradient diaphragm on the right. In the Ormia-inspired microphone diaphragm, the difference in sound pressure applied at points 1 and 2 produces a net moment, and hence a rotation of the entire assembly about a pivot. In the conventional diaphragm, the two pressures are sensed at the openings of two ports separated by the distance d as shown in the figure on the right. The microphone package then directs these pressures such that they act on the top and bottom surface (denoted by points 1 and 2) of a simple membrane. The membrane responds to the net force produced by these pressures, which is equal to the pressure difference because they act on opposite sides of the diaphragm.

This approach offers a host of design possibilities and the potential of radically improved performance.

Because nature conferred upon the small Ormia fly an unusual technique to detect pressure gradients, i.e. an auditory system that is severely constrained by size, it seemed appropriate that engineers interested in small, sensitive, and robust directional microphones should also examine the merits of this approach.

The Evolution of the Engineering Design – Biomimetic Directional Microphone

Because the materials and fabrication processes that are available preclude simply 'copying' of the design of Ormia's ear, our approach has been to mimic, or borrow, the essential ideas rather than create a high fidelity replica. This becomes the starting point of an extensive engineering design process. The analysis and design of the mechanical diaphragm structure involved engineering evolution. The earliest design consisted of a membrane, or thin plate, supported along its perimeter and stiffened and tuned with masses in order to emphasize the response to the difference in pressure [Gibbons and Miles, 2000; Miles et al., 2001; Yoo et al., 2002]. Lessons learned from the analysis and fabrication of this structure led to the realization that a considerably more compliant (and hence more responsive to sound) diaphragm could be constructed if it was fashioned out of a stiffened plate and supported by carefully designed hinges as shown in figure 4 [Miles et al., 2001; Tan et al., 2002]. In this design, rather than attempt to construct a diaphragm that possesses both the rocking and translational modes of Ormia's ear (as shown in figure 2), we sought the more modest goal of constructing a pressure gradient microphone that responds primarily with the rocking mode; the stiffness of the structure was designed so that the natural frequency of the translational mode of figure 2 was above the frequency range of interest (approximately 40 kHz). The materials and fabrication constraints thus led to a significant departure from the morphology of the fly's ear but the essential principle of differential sensing is still employed. In order to achieve the effect of the in-phase mode, one can add another nondirectional microphone and combine the signals to obtain any of the directivity patterns that are possible with a first-order directional sensor.

Differential Microphone Acoustic Performance

In this section, predicted results for the sensitivity and noise performance of the Ormia differential microphone (fig. 4) are compared with that of a conventional design (such as depicted in the right panel of figure 3). The performance of several specific designs are compared to illustrate some of the advantages of the present approach. Since our goal is to develop very small acoustic sensors, we deliberately used silicon microfabrication techniques.

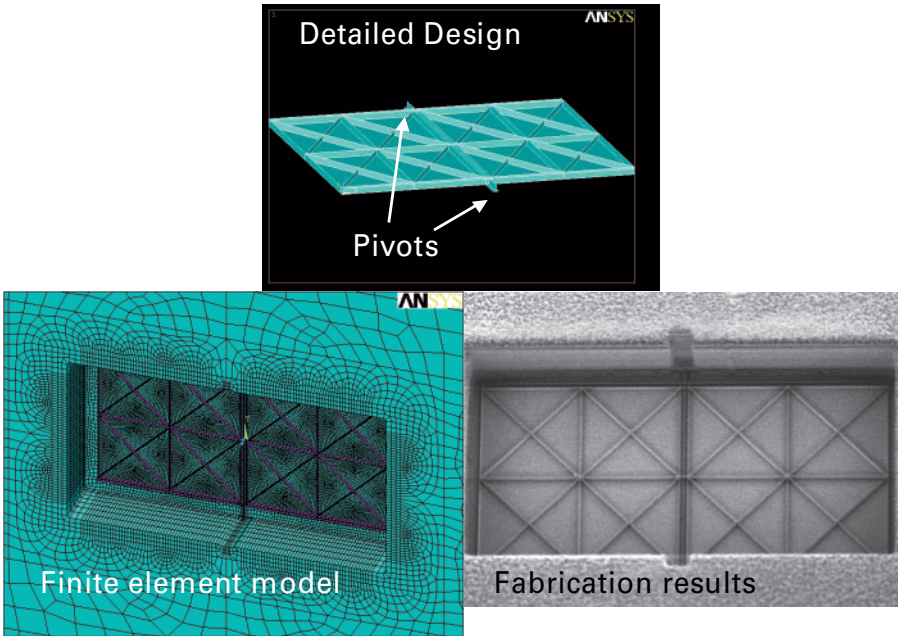

Fig. 4. Ormia-inspired differential microphone diaphragm. This diaphragm is supported only on carefully designed pivots. A slit separates the diaphragm from the surrounding substrate everywhere except at the pivots. A finite element model of the diaphragm is shown at the top, and a mesh of a model used to examine stresses is shown in the lower left. A scanning electron micrograph of a diaphragm fabricated out of polycrystalline silicon is shown on the lower right. The rectangular diaphragm has dimensions 1 × 2 mm.

In order to facilitate the design process, it is important to use a computationally efficient means of estimating the acoustic sensitivity of the diaphragm. Because of the complexity of the diaphragm structures that can be fabricated in silicon, it is appropriate to use the finite element method to model the dynamic response. Based on the detailed finite element models, we have established that the design behaves much like a rigid body that rotates about the pivots shown in figure 4. This is determined by predicting the resonant mode shapes and natural frequencies of the structure. In our typical design, the rocking mode (as illustrated in the upper left of fig. 2) has a resonant frequency between 1 and 2 kHz, while the translational mode has a resonant frequency between 30 and 40 kHz. The translational mode is thus above the frequency range of human hearing in these designs.

With the assumption that the diaphragm structure behaves like an ideal rigid body, with a response that is dominated by the rocking mode, we can estimate the response to sound by calculating the moment applied to the diaphragm by a plane acoustic wave that is incident at an angle Φ relative to the direction normal to the plane of the diaphragm. The analysis of this simplified lumped-parameter representation of the diaphragm requires knowledge of the equivalent stiffness of the pivots and of the mass moment of inertia about the pivots. These quantities may be readily determined by using the detailed finite element model. We have shown that this lumped-parameter model, where the parameters are identified by the finite element method, yields accurate predictions of the response of the diaphragms to sound [Tan et al., 2002].

A similar approach can be taken to estimate the sensitivity of a differential microphone that is fashioned out of a conventional diaphragm as in the right panel of figure 3. The diaphragm can be modeled as a flexible plate with fixed boundaries. In this comparison, the sound field is assumed to enter the microphone through the two openings separated by the distance d in the right side of figure 3. The difference in the pressures on the top and bottom sides of the diaphragm (labeled 1 and 2 in the figure) produce a net force on the diaphragm. In both of these microphones, it is assumed that the wavelength of sound is significantly longer than the distances L or d in figure 3. We will assume that capacitive sensing is used to obtain an electronic signal from the microphones.

The sensitivities of the differential microphone concepts shown in figure 3 may be estimated from:

$$S_o = \frac{V_b 2si\omega (L/2)^3 \cos(\phi)/(cIh)}{\omega_o^2 - \omega^2 + i\omega 2\zeta_o\omega_o}$$

and

$$S_c = \frac{V_b}{h} \frac{s\alpha^2 i\omega \frac{d}{c}\cos(\phi)/m_c}{\omega_c^2 - \omega^2 + i\omega 2\omega_c\zeta_c},$$

where the subscripts *o* and *c* denote the Ormia and conventional concepts shown on the left and right of figure 3, respectively. S_o and S_c are the sensitivities of the microphones in volts/Pascal, $i = \sqrt{-1}$, c is the sound speed, Φ is the angle of incident sound, ω_c and ω_o are the resonant frequencies of the conventional and ormia directional microphone, respectively,

$$\omega_c = \sqrt{\frac{k}{m_c}}, \quad \omega_o = \sqrt{\frac{k_t}{I}},$$

and ω is the driving frequency.

The dimensions of the microphones are assumed to both be 1 × 2 mm, and the structures are constructed out of 1-μm-thick polysilicon. Both microphones thus have the same area *s*. For the Ormia microphone, the total mass, obtained from our finite element model is $m = 0.975 \times 10^{-8}$ kg, the mass moment of inertia about the axis through the supports is $I = 3.299 \times 10^{-15}$ kgm^2. The resonant frequency of the rotational mode ω_o is predicted to be 1409 Hz. For the conventional microphone, the mass is $m_c = 0.46 \times 10^{-8}$ kg, the resonant frequency of the diaphragm ω_c is found to be about 10 kHz. The bias voltage $V_b = 1$ V and the distance between the diaphragm and the backplate electrode is $h = 3$ μm. The damping constants in each design are selected to achieve critical damping, i.e. $\zeta_c = \zeta_o = 1$. The parameter α is equal to 0.69. This parameter is computed by taking the inner product of the first vibrational mode shape of the clamped plate with the uniformly distributed acoustic pressure.

Predicted acoustic responses for the two microphone diaphragm designs show that the Ormia microphone has approximately 20 dB greater sensitivity of the conventional microphone over the audible frequency range [Tan et al., 2002].

Along with the acoustic sensitivity, it is also very important to examine the lowest sound levels that can be measured with a given microphone. This is limited by the self-noise of the microphone [Gabrielson, 1993]. Noise performance of microphones is usually characterized by using the A-weighted overall equivalent sound pressure due to the noise. In order to construct a fair comparison of the noise performance of candidate designs, a compensation filter is utilized so that the signals from the microphones are adjusted to have identical frequency responses. The compensation filter for each microphone signal was applied to achieve a flat frequency response from 250 Hz to 8 kHz. The noise of the microphone results from energy dissipation in the system that can be thought of as being due to equivalent dashpots that are distributed over the diaphragm surface. The microphone self, or thermal noise in dBA may be estimated from

$$N = 135.2 + 10 \log_{10} P_{sd},$$

where P_{sd} is the white noise power spectrum due to thermal noise, $P_{sd} = 4\ k_b TR/s^2$ [Gabrielson, 1993]. k_b is Boltzmann's constant, $k_b = 1.38 \times 10^{-23}$ *J/K*, T is the absolute temperature, s is the area over which the dashpots act, R is the equivalent dashpot constant. In this comparison the value of R has been taken such that each design is critically damped so that the damping ratio is unity, i.e. $\zeta_c = \zeta_o = 1$. It is found that the predicted thermal noise floor of the conventional microphone is 40.4 dBA while that of the Ormia differential microphone is 20.8 dBA [Tan et al., 2002].

The significant reduction in thermal noise of the Ormia differential microphone results from the fact that the compliance of the diaphragm can be made to be very high. This high compliance is achieved by careful design of the pivot supports.

Our approach enables us to create almost any desired stiffness (or compliance) of the diaphragm through the proper design of the support at the pivot. The only ways to adjust the stiffness of a conventional diaphragm, being essentially a plate or membrane, are to adjust its thickness, or change its initial tension. The reduction of the diaphragm thickness introduces a host of fabrication difficulties and raises concerns over the device's durability. The frequency response of the diaphragm will also suffer as its thickness is reduced because unwanted resonances will appear in the frequency range of interest. Because our design consists of a stiffened plate supported on a carefully designed hinge, we are able to design it so that any unwanted resonances are well above the frequencies of interest.

Current Challenges and Future Opportunities

Based on the predicted results described above, there are significant benefits to the use of a rather unconventional microphone diaphragm that would be very difficult to realize without the precision that is available through silicon microfabrication. Silicon microfabrication enables the use of novel diaphragm constructions that are likely to lead to significant performance benefits as this technology matures.

Fabrication Issues

In order for any promising microphone concept to have an impact on the hearing impaired, it is essential that great care be taken at the outset to ensure it ultimately can be fabricated in a cost-effective way. Silicon microfabrication has great potential to provide devices that can be manufactured using a minimum of human labor and, subsequently, low cost. The promise of low-cost devices has been a primary motivation in nearly all research on silicon microphones and it has proven an intoxicating lure for a number of microphone manufacturers. Despite these efforts, however, much more needs to be done to develop microphone designs that can be fabricated with a sufficiently high yield to make this approach cost-effective.

It is widely accepted that by far the biggest challenge in fabricating microphones out of silicon (or other materials used in microfabrication) is the reduction of the influence of stress on the structural integrity and dynamic properties of the microphone diaphragm [Pedersen, 2001; Loeppert, 2001]. Unfortunately, due to the micromechanical properties of the materials, the fabrication process typically results in a significant amount of stress in the diaphragm that can be sufficient to result in fracture of a significant percentage of the devices before the fabrication is complete. In addition, the stress is strongly dependent on fine details of the fabrication process that are almost impossible to control sufficiently. Since the typical microphone diaphragm consists of a very thin plate, stress (either tensile or compressive) can have a marked influence on the dynamic response. Stress nearly always has significant detrimental effects on microphone performance.

Myriad approaches have been developed to reduce the effects of stress on silicon microphones including the use of corrugations and stress relieving supports [see for example Scheeper et al., 1994; Bergqvist and Rudolf, 1994; Zhang and Wise, 1994; Jennan, 1990; Cunningham and Bernstein, 1997; Spiering et al., 1993].

By incorporating a diaphragm as shown in figure 4 that, by design, has significant bending stiffness, in-plane stresses due to fabrication have substantially less impact. It is also important to note that the overall compliance of the diaphragm is determined by the design of the pivot supports, not the thickness or stress in the diaphragm as in conventional approaches. As a result, our design approach avoids many of the difficulties caused by stress in silicon microphones.

Performance Limitations due to Capacitive Sensing

Capacitive sensing, either through the use of a charged electret or a biased back-plate, is employed in the vast majority of miniature microphones that have sufficiently low noise and high sensitivity to be candidates for use in hearing aids. It is well known, however, that the use of capacitive sensing places significant design limitations on the microphone diaphragm that adversely impacts the electronic noise performance. In addition, due to the viscosity of air, the use of a biased electrode in close proximity to the diaphragm introduces a significant source of microphone self-noise. A major breakthrough in microphone performance may be achievable through the use of alternative sensing methods, such as optical sensing, by eliminating many of these design limitations.

To illustrate the limitations imposed on the noise performance of the read-out circuitry used in a capacitive sensing scheme, consider a simple model of a conventional (nondirectional) pressure-sensitive microphone. Suppose the buffer amplifier used to convert the change in microphone capacitance to an electronic signal has a white noise spectrum given by N volts/$\sqrt{\text{Hz}}$. If the effective sensitivity of the capacitive microphone is S volts/Pascal then the input-referred noise will be N/S Pascals/$\sqrt{\text{Hz}}$. In a conventional (nondirectional) capacitive microphone, the sensitivity may be approximated by $S = V_bA/(hk)$ where V_b is the bias voltage, A is the area, h is the air gap between the diaphragm and the back plate, and k is the mechanical stiffness of the diaphragm. Here we have assumed that the resonant frequency of the diaphragm is beyond the highest frequency of interest. The input referred noise of the buffer amplifier then becomes $N/S = Nhk/(V_bA)$ Pascals/$\sqrt{\text{Hz}}$. Based on this result, one is tempted to reduce this noise by increasing the bias voltage, V_b, or by reducing the diaphragm stiffness, k.

Unfortunately, one is not free to adjust these parameters at will because the forces that are created by the biasing electric field can cause the diaphragm to collapse against the back plate. In a constant-voltage (as opposed to constant charge) biasing scheme, the maximum voltage that can be applied between the diaphragm and the back plate is called the collapse voltage given by

$$V_{collapse} = \sqrt{\frac{8}{27}\frac{kh^3}{\varepsilon A}},$$

where ε is the permittivity of the air in the gap. Diaphragms that have low equivalent mechanical stiffness, k, will thus have low collapse voltages. To avoid collapse,

one must have $V_b << V_{collapse}$. The above equation clearly shows that the collapse voltage can be increased by increasing the gap spacing, h, but this comes at the cost of reducing the microphone capacitance (and electrical sensitivity), which is inversely proportional to the nominal spacing, h. Since miniature microphones (and particularly silicon microphones) have very small diaphragm areas, A, the capacitance tends to be rather small, on the order of a pF. The small capacitance of the microphone challenges the designer of the buffer amplifier because of parasitic capacitances and the effective noise gain of the overall circuit. For these reasons, the gap, h, used in silicon microphone designs tends to be small, on the order of 5 μm.

The use of a gap that is as small as 5 μm introduces yet another limitation on the performance that is imposed by capacitive sensing. As the diaphragm moves in response to fluctuating acoustic pressures, the air in the narrow gap between the diaphragm and the back-plate is squeezed and forced to flow in the plane of the diaphragm. Because h is much smaller than the thickness of the viscous boundary layer (typically on the order of hundreds of μm), this flow produces viscous forces that damp the diaphragm motion [Skvor, 1967; Bergqvist, 1993; Homentcovschi and Miles, 2004, 2005]. It is well known that this squeeze film damping is a primary source of thermal noise in silicon microphones [Gabrielson, 1993]. By eliminating the constraints imposed by capacitive sensing along with the constraints of conventional diaphragm design approaches, microphone designs will be able to break through significant performance barriers.

In order to decouple the design of the diaphragm's compliance from the requirements of the sensing scheme, we are developing optical methods that do not require the use of significant bias voltages [Hall and Degertekin, 2002; Cui et al., 2006]. Preliminary calculations indicate that this sensing approach can achieve noise floors less than 20 dBA, rivaling those of large precision microphones.

Improvements in Fabrication Technology Will Lead to Improved Designs

While there have been numerous efforts to fabricate silicon microphones, thus far very few have led to successful commercial products. The technology of fabricating silicon sensors is still relatively immature, particularly compared to the very mature and highly successful electret microphones as currently used in hearing aids. Nonetheless, because silicon fabrication technology permits the creation of extremely precise and complex microstructures, it opens up a new world of possibilities in sensor design.

When a revolutionary technology arrives, its primary advantages may not be initially appreciated by designers. As an example, the earliest transistor circuits quite naturally bore a strong resemblance to vacuum tube circuits with the transistors replacing the function of the tubes. When designers learned more about the advantages of transistors, entirely new circuit topologies were created, making integrated circuits possible.

This effect has also occurred in the development of silicon accelerometers. While the initial designs resembled conventional accelerometers that were reduced in size, current silicon accelerometer designs utilize complex structures for their proof-mass and microscopic interdigitated comb fingers for capacitive sensing of the motion of the proof mass [see for example Xie et al., 2004]. These new sensor designs have evolved to take advantage of what can be accomplished with silicon microfabrication.

With very few exceptions, existing attempts to fabricate silicon microphones amount to a dramatic miniaturization of the same sorts of structures that are used in conventional microphones. They consist of a thin diaphragm supported around its perimeter, and a back plate a small distance away to permit capacitive sensing [see for example Bergqvist and Rudolf, 1995]. It is likely that the real advantages of silicon microfabrication for microphones have yet to be discovered. When they are, a revolution in microphone technology may occur.

We believe that one example of this technology 'coming of age' is the development of the differential microphone diaphragm we have developed. This structure takes advantage of what can be accomplished using silicon microfabrication and would be particularly difficult to realize using conventional fabrication methods.

Acknowledgement

This work is supported by NIH grant 1R01DC005762-01A1, Bioengineering Research Partnership to RNM.

References

Bergqvist J: Finite-element modeling and characterization of a silicon condenser microphone with a highly perforated backplate. Sens Actuators 1993;39:191–200.

Bergqvist J, Rudolf F: A silicon condenser microphone using bond and etch-back technology. Sens Actuators 1994;45:115–124.

Bergqvist J, Rudolf F: Process for the manufacture of integrated capacitive transducers. United States Patent 5,404,731, 1995.

Bilsen FA, Soede W, Berkhout AJ: Development and assessment of two fixed-array microphones for use with hearing aids. J Rehabil Res Dev 1993;30:73–81.

Cui W, Bicen B, Hall N, Jones SA, Degertekin FA, Miles RN: Optical sensing in a directional MEMS microphone inspired by the ears of the parasitoid fly, *Ormia ochracea*. Proc IEEE Int Conf Micro Electro Mech Sys, Istanbul, January 2006.

Cunningham B, Bernstein J, Wide Bandwidth Silicon Nitride Membrane Microphones, SPIE Micromachining and Microfabrication Process Technology III. Austin, September 29–30, 1997.

Gabrielson T: Mechanical-thermal noise in micromachined acoustic and vibration sensors. IEEE Trans Electron Devices 1993;40:903–909.

Gibbons C, Miles RN: Design of a Biomimetic Directional Microphone Diaphragm. Proc Int Mech Eng Congr Expo, Orlando, November 2000.

Hall NA Degertekin FL: An integrated optical interferometric detection method for micromachined capacitive acoustic transducers. Appl Phys Lett 2002;80:3859–3861.

Homentcovschi D, Miles RN: Modeling of viscous damping of perforated planar microstructures. Applications in acoustics. J Acoust Soc Am 2004;116:2939–2947.

Homentcovschi D, Miles RN: Viscous damping of perforated planar micromechanical structures. Sens Actuators 2005;199:544–552.

Jennan JH: The fabrication and use of micromachined corrugated silicon diaphragms. Sens Actuators 1990;A21–A23:988–992.

Loeppert PV: Scaling issues in a submillimeter MEMS microphone (abstract). J Acoust Soc Am 2001;110:2645.

Mason A, Oshinsky ML, Hoy RR: Hyperacute directional hearing in a microscale auditory system. Nature 2001;410:686–690.

Miles RN, Robert R, Hoy RR: Mechanically coupled ears for directional hearing in the parasitoid fly *Ormia ochracea.* J Acoust Soc Am 1995; 98:3059–3070.

Miles RN, Sundermurthy S, Gibbons C, Hoy R, Robert D: Differential Microphone. United States Patent application filed August 1, 2001, serial number 09/920,664.

Miles RN, Tieu TD, Robert D, Hoy RR: A mechanical analysis of the novel ear of the parasitoid fly *Ormia ochracea*; in Lewis ER, et al. (eds): Proceedings: Diversity in Auditory Mechanics. Singapore, World Scientific, 1997, pp 18–24.

Pedersen M: Challenges for the commercialization of acoustic sensors using microfabrication technologies (abstract). J Acoust Soc Am 2001; 110;2646.

Ricketts TA: Impact of noise source configuration on directional hearing aid benefit and performance. Ear Hear 2000a;21:194–205.

Ricketts TA: Directivity quantification in hearing aids: fitting and measurement effects. Ear Hear 2000b;21:45–58.

Robert D, Amoroso J, Hoy RR: The evolutionary convergence of hearing in a parasitoid fly and its cricket host. Science 1992;258:1135–1137.

Robert R, Miles RN, Hoy RR: Directional hearing by mechanical coupling in the parasitoid fly *Ormia ochracea*. J Comp Physiol 1996;98: 3059–3070.

Robert D, Read MP, Hoy RR: The tympanal hearing organ of the parasitoid fly *Ormia ochracea* (Diptera, Tachinidae, Ormiini). Cell Tissue Res 1994;275:63–78.

Scheeper PR, Olthuis W, Bergveld P: The design, fabrication, and testing of corrugated silicon nitride diaphragms. J Microelectromech Syst 1994;3:36–42.

Sessler G, West J: Electret Microphone. United States Patent 3,118,022, 1964.

Spiering VL, Bouwstra S, Fluitman JHJ: Realization of mechanical decoupling zones for package-stress reduction. Sens Actuators A 1993; 37–38:800–804.

Tan L, Miles RN, Cui W, Miller RA, Su Q, Weinstein MG: Response of a Biologically Inspired MEMS Differential Microphone Diaphragm. Proc SPIE AeroSense, Orlando, 2002.

Xie H, Fedder GK, Pan Z, Frey W: Integrated Monolithic Micromachined Accelerometer. United States Patent Application Publication US 2004/0231420 A1, 2004.

Yoo K, Yeh JLA, Tien NC, Gibbons C, Su Q, Miles RN: Fabrication of biomimetic 3-D structured diaphragms. Sens Actuators A 2002;97–98: 448–456.

Zhang Y, Wise KD: Performance of non-planar silicon diaphragms under large deflections. IEEE J Microelectromech Syst 1994;3:59–68.

KARGER

take advantage of the so-called tonotopic organization in the cochlea, namely, the apical part of the cochlea encodes low frequencies while the basal part encodes high frequencies. These implants, therefore, all have implemented a bank of filters to divide speech into different frequency bands, but they differ significantly in their processing strategies to extract, encode, and deliver the right features. Current CI technology can provide 22 electrodes per implant, as in the Nucleus 24 model, available from Cochlear (Cochlear, Lane Cove, Australia).

Although having flexible programmability [McDermott, 1998; Zeng, 2004], hearing enhancement devices based on digital signal processor technology are expensive, costing typically $30000 for CIs, and require relatively large and expensive microelectronic chipsets that consume large amounts of power, typically 50–750 mW for a CI. Consequently, the devices require large body-worn battery packs and accessories to produce the electrical signals needed for the deaf to hear. Furthermore, the battery life is limited to less than a week or just a few hours in many cases, requiring frequent recharging of the devices. The use of digital signal processors introduces latency in the audio signal of up to tens of milliseconds. Since the signal must be encoded and then transmitted via a wireless connection to electronics beneath the skull, only a limited number of channels (e.g., up to 22) can be processed. The expense, inconvenience, and frequent recharging requirement of current technology means that the majority of the hearing-impaired population cannot or choose not to fully benefit from the technology [Tyler et al., 2004]. The current market penetration rate for CIs is less than about 5% [Zeng, 2004].

Apart from practical and cosmetic concerns about speech processor-based CIs, there is a concern regarding hearing quality. Most speech processor algorithms encode temporal cues about the waveform envelope to aid the patient in interpreting speech [Saunders and Kates, 1997; Loizou, 1997, 1998]. While this is effective in distinguishing the spoken word (at least for Indo-European languages in quiet conditions), it provides little help in enabling the patient to hear true musical pitch for the appreciation of music or the understanding of tonal languages [Zeng, 2004]. Recent work has indicated that such temporal-based algorithms are unlikely to succeed – the source of tone transduction is truly tonotopic in the cochlea [Oxenham et al., 2004]. Properly positioning more electrodes in the cochlea, and properly stimulating them, is the most likely means for restoring tonal sense.

An alternate approach to cochlear implants and speech coding is the ambitious goal of building an artificial cochlea that truly mimics the behavior of the natural cochlea. Such a device could be used for research aid for understanding cochleas (e.g., for developing mathematical models), or eventually as a front-end transducer for an electrode system.

Some progress has been made in this area already. Researchers have demonstrated the ability to build fluid-filled, 1:1 scale models of the human cochlea and have demonstrated that they respond to sound in a manner similar to the known response of the mammalian cochlea [Ohyama and Koike, 1999; Lim et al., 1999; White and Grosh, 2005]. Most recently, the team of White and Grosh [2005] demonstrated the ability to use silicon micromachining technology in order to build their cochlea model. This is significant because the batch micromachining process used to fabricate the system will allow future integration of sensing elements into the structure to economically produce low-power, micromechanical, cochlear-like sensor filters. The devices built thus far are primarily for research purposes and to aid in understanding the mechanism of the cochlea.

In this same spirit, a second type of artificial cochlea may be constructed by building a mechanical bank of resonators designed to respond in a manner similar to the cochlea. A mechanical filter bank acts in a passive way to perform sub-band filtering, reducing power requirements. Furthermore, an array of such resonators may work in parallel to produce a large number of frequency bands simultaneously, reducing latency. By controlling the shape and composition of the resonators, one may design simple to complex resonances into the system, depending on the requirements of the cochlear design. The traveling wave phenomena of the cochlea may be included by lightly coupling the resonators together. A mechanical bridge version of this was demonstrated by Haronian and MacDonald [1995]. Their design employed a large array of thin bridges micromachined in silicon with lengths that were increased exponentially. This formed an array of resonators, each with a characteristic frequency. In some cases, the spacing between bridges was small enough to couple neighboring bridges (by the viscosity of air) so that the device behaved similarly to a cochlea. In addition, the viscosity of air served to dampen the resonances so that the device exhibited low Q, a desirable feature for an artificial cochlea. Apart from a single conference paper in 1995, no other work appears to be published on this research.

Japanese researchers Tanaka et al. [1998] also demonstrated a variation of this concept by fabricating an ingenious device that they called a 'fishbone' resonator. Their

device, fabricated from silicon, consisted of an array of mechanical beams connected to a single torsional beam at their centers, making it appear as a 'fishbone'. The resonators in this device were coupled by the central beam making it behave as an acoustic transmission line. This construction enabled the device to mimic a cochlea. The device was not directly instrumented – the researchers used external optical instrumentation to monitor the movement of the oscillators.

A third type of artificial cochlea can be built based on electronic circuitry designed to convert an input signal into multiple outputs that mimic the cochlea. Banks of band-pass filters have been built [Loulou, 2004], as well as the so-called 'silicon cochlea', an electronic transmission line (filter cascade) designed to mimic the cochlear function [Kuszta, 1998]. The filter cascade model seems to hold great promise. By tapping in to the cascading series of filters one can achieve a large number of outputs that appear to closely mimic the gain, filtering and dynamic range characteristics of the cochlea [Lyon and Mead, 1988, 1998; Lyon, 1998]. Moreover, such a device has been built with 117 outputs over the range of 100 Hz to 10 kHz, 61 dB dynamic range, with small size (less than 3 × 3 mm) and low power consumption (0.5 mW) [Sarpeshkar et al., 1998; Sarpeshkar, 1999]. This is a tremendous feat that may well signal the next generation of artificial cochleas.

Whether fluidic, mechanical or electrical, the development of a small, low-power, analog, multiresonator system that can mimic the cochlea would be a major step toward developing a completely implantable bionic ear that can provide true, quality hearing.

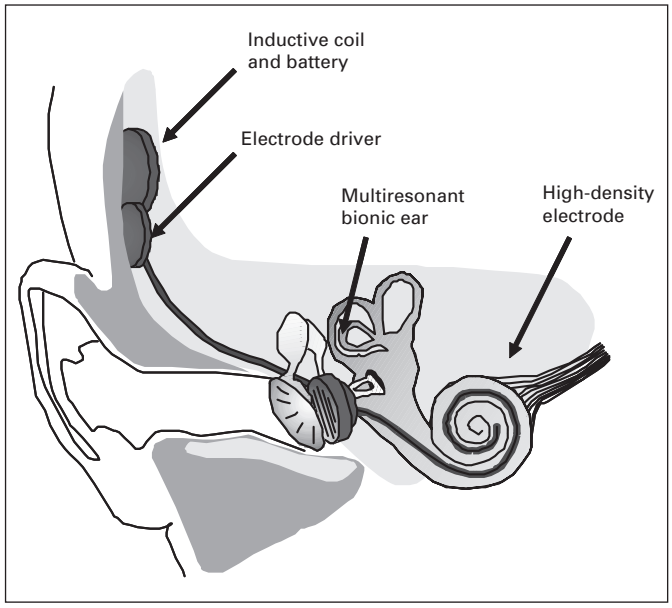

Fig. 1. Illustration of bionic ear concept. A multiresonant transducer receives acoustic energy and splits into frequency bands that mimic the tonotopic distribution of the cochlea. An electrode driver amplifies the signal and sends current to an implanted electrode in the cochlea.

Micromachined Multiband Transducer

We are developing a low-power micromachined multiband transducer, small enough to be implanted in the head, which we believe could ultimately alleviate the need for a speech processor. Power requirements for a system using this technology could be much less than conventional systems, enabling it to be run by rechargeable, implanted battery system. By doing so, we may envision a fully implantable bionic ear that can restore human hearing. The microphone consists of an array of micromechanical resonators, each tuned to a different center frequency, and each instrumented to an individual amplifier. The output from the device is a number of independent channels, each carrying an electrical signal representing a particular frequency sub-band of the original acoustic signal. We have built and tested two versions of this device. One used optical readout [Xu et al., 2004], the second used capacitive readout.

An illustration of the optical microphone is shown in figure 1. It consisted of an array of suspended polymer cantilevers, each one at a different length, ranging from 2 to 7 mm. The cantilevers were rectangular cross section, 100 μm in width and 40 μm in height, made from epoxy using modern micromachining techniques for polymer [Xu et al., 2002]. The cantilevers were suspended over an etched cavity in silicon, allowing them freedom to vibrate. A second rectangular epoxy channel was fabricated to meet the cantilever at its distal end, stopping short of contact, leaving a 20-μm air gap. A 635-nm laser was directed down the cantilevers, and the light intensity was monitored at the exit end of the second epoxy channel. The transparent polymer channels acted as excellent light pipes, so that light was efficiently guided from the laser, through the channel and cantilever, through the second channel to the photodetectors at the end. When the cantilever vibrated, the cantilever was temporarily misaligned with its mating channel reducing the efficiency of light to pass across the 20-μm air gap. This was seen as a reduction in light intensity at the photodetector. In this

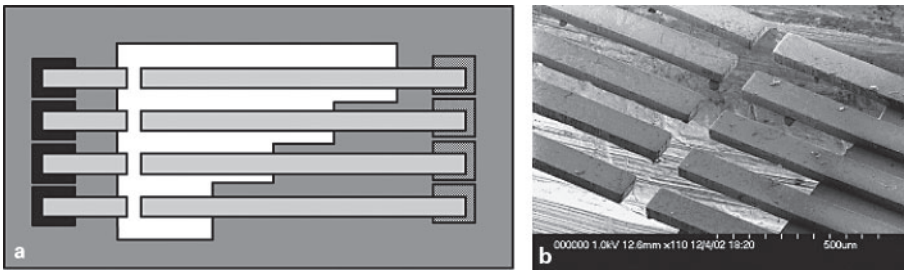

Fig. 2. a Illustration of four-channel multiresonant microphone showing cantilevers of different lengths suspended above an etched open cavity. **b** Scanning electron microscope image of cantilevers showing air gap between resonators and receiving light pipes.

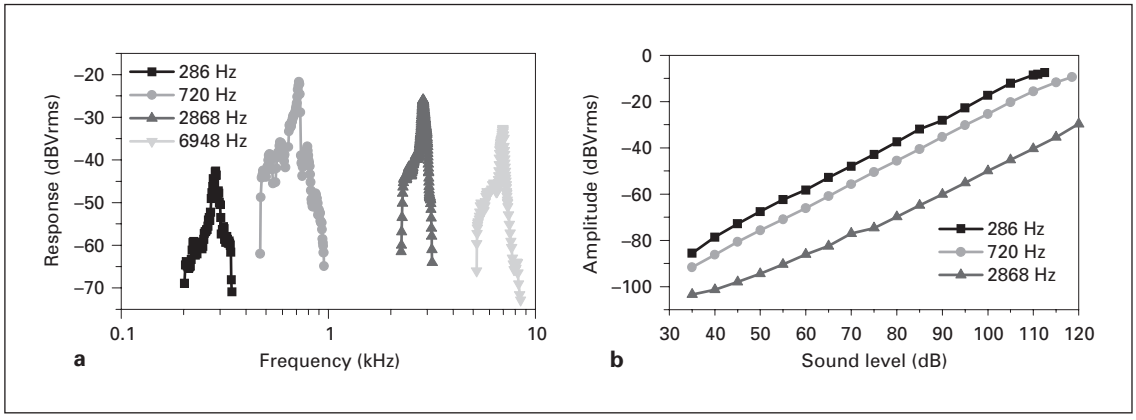

Fig. 3. Frequency response and dynamic response for multiresonant transducer. **a** The Q10 values of these cantilevers are 9.38, 10.11, 11.56, and 14.01 for resonant frequencies at 286, 720, 2868, and 6948 Hz, respectively. Measurements were made at 70 dB (SPL). **b** The polymeric cantilever array has a linear dynamic range of 80 dB for sound inputs between 35 and 115 dB (SPL). Measurements were made at each cantilever's resonance. The fourth cantilever is not shown in the right figure because it was destroyed during handling between measurements.

manner, the movement of the cantilever, and hence, the sound energy could be monitored (fig. 2).

Several variations of the optical device were built to demonstrate different fabrication methodologies. Fabrication methods included using UV patternable high-definition epoxy (SU-8), performing laser machining on polymer films, and performing microinjection molding. The details of the injection molding manufacturing process which produced the results presented here, have been detailed elsewhere [Xu et al., 2004].

We tested a four-resonator device by placing it under a speaker connected to an amplified tone generator. Signal was collected from the resonators and analyzed using standard data acquisition instrumentation. Frequency response, dynamic response, and directionality were recorded. The preliminary data, shown in figure 3, are very encouraging. Cantilever response shows specific peak frequencies at 286, 720, 2868, and 6948 Hz, respectively, well within human hearing range. Q10 values (peak frequency divided by the bandwidth 10 dB below the peak) are similar to mammalian basilar response [Robles and Ruggero, 2001]. Dynamic response is linear from 35 to 115 dB SPL. While linear response is an excellent characteristic for a microphone, for cochlear stimulation, dynamic compression may need to be performed using appropriate amplification circuitry.

We have observed similar results with cantilevers prepared for capacitive readout. In those devices, the cantilevers were coated with a thin (100-nm) layer of gold on their underside forming a capacitor between each cantilever and a ground plane directly beneath each cantilever. A bias of 45 V was placed on the cantilever making it a capacitor. Vibration of the cantilever resulted in changes in the capacitance, and thus modulated an induced current across the capacitor. The small signal was amplified by a JFET and recorded using conventional microphone

Table 1. Summary of differences between optical and electronic cantilevers

Optical readout	Electrical readout
Low noise floor	Noisy due to electromagnetic interference – good shielding required
Low bias	High bias preferred (45 V) or electret
Moderate power requirement due to light coupling losses (5–10 mW)	Low power (<1 mW)
Difficult integration with electronics	Easy integration with electronics
Good sensitivity and dynamic range	Good sensitivity and dynamic range

amplifiers and instrumentation. Ultimately, the capacitor (or even electret) readout is preferred over the optical readout because it is easier to integrate with conventional electronics and consumes considerably less power. However, the electrical system is more suspect to noise and must be carefully shielded, whereas the optical system demonstrated clear signal with almost no noise. Differences between electrical and optical readout are indicated in table 1.

The multiband transducer works because the individual cantilevers have been designed to exhibit resonances at frequencies within the range of human hearing. For a simple cantilever, the natural frequency is given by

$$f_k = \frac{1}{4\pi}\,\frac{n_k^2}{\sqrt{3}}\,\frac{T}{L^2}\sqrt{\frac{E}{\rho}}$$

where E = Young's modulus in pascals, T = thickness in meters, L = length in meters, ρ = density in kg/m^3, and n_k = 1.875, 4.694, 7.855, … (n_k is mode number). When energized by acoustic energy, the cantilever will respond with maximum amplitude at the natural frequency, as given by the well-known Lorentzian formula,

$$A(f) \propto \frac{\frac{\Gamma}{2}}{(f - f_0)^2 + \left(\frac{\Gamma}{2}\right)^2}$$

Here, Γ is the 'linewidth' or full width and half maximum. For discussion, we prefer to use the 'quality factor' value Q10, which is peak frequency divided by the bandwidth 10 dB below the peak, or Q10 = $f_0/3\Gamma$. Thus, high quality factors correspond to narrow resonances. The human cochlea is also a resonator and typically responds with Q10 values under 10, relatively low quality factors [Geisler, 1998]. Second and higher order modes will also be excited, but these are typically much lower in amplitude.

Traditional micromachining materials, namely silicon, ceramics and metals, characteristically exhibit large Young's modulus and low damping [Petersen, 1982]. This results in large natural frequencies (for example, a silicon cantilever, 1 mm × 5 μm, resonating at about 5 kHz) and high quality factors. These are desirable qualities for fabricating mechanical resonators, such as those used in miniature accelerometers and gyroscopes, but this is not satisfactory for mimicking the response of the cochlea. If the device can be built small enough, air may be used to dampen the oscillations [e.g., Haronian and MacDonald, 1995].

Polymers have more suitable material properties, exhibiting high damping and low modulus, typically 50 times less than metal. As a result, the natural frequencies of polymer cantilevers can be designed to be in the range of a few hundred Hz to 10 kHz for microphone size under 1 cm. Polymers have certain problems, however. Polymers cannot conduct electricity, requiring the addition of a thin metal layer if electrical transduction is desired. Polymers are difficult to fabricate at the small sizes required for this transducer. Polymers may exhibit long-term plastic deformation, or may develop stress from thermal processing. Indeed, our own microfabrication efforts required a special annealing step to reduce residual stress and straighten out the resonators (for microinjection molded cantilevers). Nevertheless, many engineered polymers exist that have been demonstrated as useful in critical applications, for example, polyester and polyimide.

Because natural frequency is so directly related to length (for a cantilever) it is easy to design multiband devices of arbitrary frequency distribution. Furthermore, since the signal from each cantilever is amplified, each channel's gain may be adjusted independently. In this manner, we can enable the design of a microphone with any arbitrary frequency range and response. We can imagine designing a transducer that can correctly compress and map electrical signals to all regions of the human cochlea.

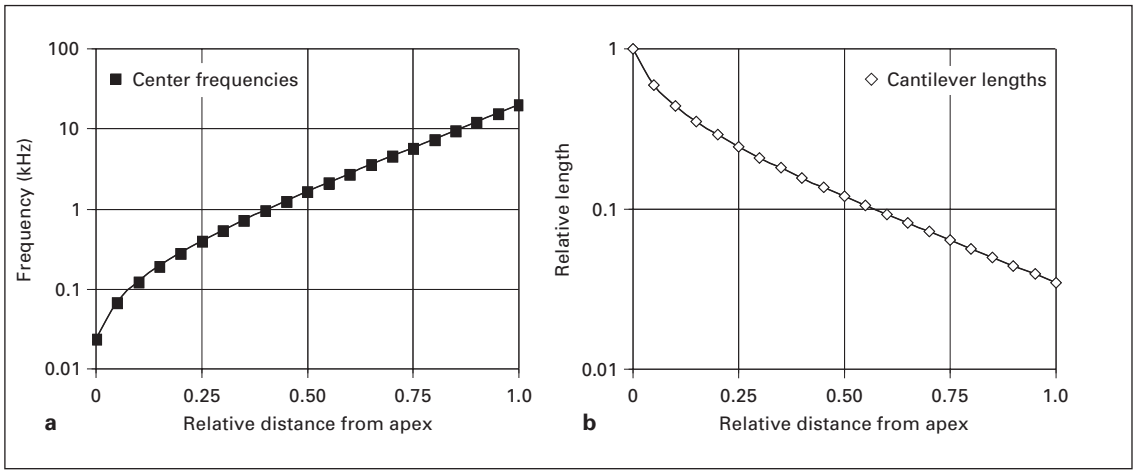

Fig. 4. a Tonotopic mapping of the human cochlea showing center frequency as a function of distance from the apex of the cochlea. **b** Relative lengths for a cantilever-based multiresonator that can reproduce natural frequencies that coincide with the center frequencies.

The mammalian cochlea has a tonotopic response to frequencies [Moore, 1997]. This relationship between center frequency and position along the basilar membrane has been mapped for several mammals and generally follows a relationship of

$$CF = A\,(10^{ax} - k),$$

where CF is center frequency in kHz, x is the relative distance from the apex, $k \sim 0.85$ and $a \sim 1.2$ for most mammals [Greenwood, 1961, Greenwood, 1990, Robles and Ruggero, 2001]. The constant A determines the range of center frequencies (20 Hz–20 kHz in humans). This relationship indicates a logarithmic compression of frequencies at the high frequency range. A typical implantable electrode array is likely to produce electrodes at equally spaced separations, indicating that our resonator design should follow a similar compression in frequency. Cantilever resonators designed to mimic this frequency are readily fabricated using lithographic or UV cutting methods. Figure 4 shows the required cantilever lengths for electrodes destined to be placed at different regions in the cochlea. The cantilever length is given as a relative number since the physical length for a given center frequency also depends on the material and thickness of the cantilever, which can be adjusted according to design criteria.

Although this discussion assumes simple straight cantilevers, one is by no means limited to designing a system of uniform cantilevers only. One can achieve complex resonance profiles by assuming more complex shapes and mass distributions in the resonators. For example, resonators may employ torsional or meander springs, patterned mass areas, or material combinations in order to produce a desired response. For low-frequency response it would make more sense to increase the mass at the end of a cantilever rather than extend the length, enabling the transducer to remain small (fig. 5). In complex designs, the mechanical analysis is more sophisticated and finite element modeling is required. In many cases, bridge or ribbon structures may be preferred to cantilevers, particularly in the case of capacitive readout devices where

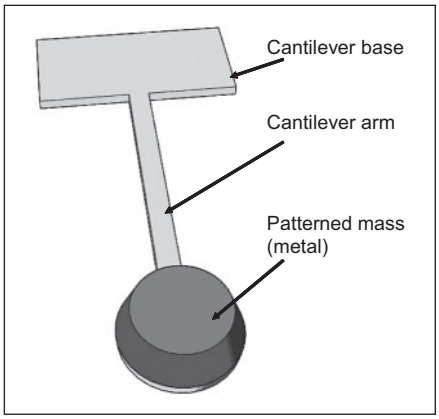

Fig. 5. Illustration showing method for decreasing natural frequency while still maintaining short cantilever length by adding additional mass at the end of the cantilever.

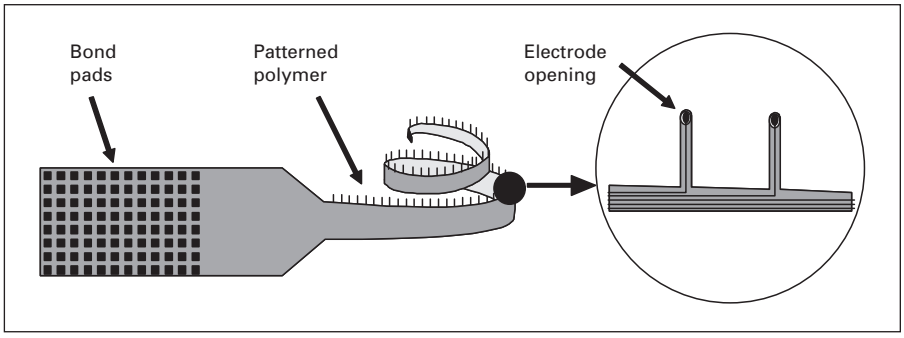

Fig. 6. Illustration of a high-density electrode concept. The polymer material and electrical traces may be completely defined by lithography, resulting in a large number of fine 'hairs' that contain electrodes. At the tip of each hair, the electrode is exposed allowing the electrode to penetrate close to the site of the hair cells, minimizing cross talk (and possibly threshold voltage) through the conductive cochlear fluid.

a small controlled gap between the resonator and the ground plane is required. A ribbon device can maintain tight gap tolerance, whereas any residual stress in a cantilever will result in bending, which will compromise the gap tolerance. Traveling wave phenomena may be mimicked by lightly coupling adjacent resonators through micromachined tethers or springs.

High-Density Microelectrode Arrays

The strategy of this and other technologies is to try to accurately mimic the response of the human cochlea so that one may artificially stimulate the cochlea in the way it was designed to be stimulated. It is unlikely, however, that true hearing can be restored unless the electrode density is made large. Small numbers of electrodes, blunt and ill-positioned, are likely to miscode and blend the spectral information of sound resulting in an unintelligible sensation. Electrode density is limited by practical concerns (manufacturability, power consumption), as well as by physical limitations – current lines tend to overlap for adjacent electrodes when the electrodes are far from their target, reducing the ability to stimulate specific sites. Thus, electrode design must also include a mechanism for the electrical contacts to be highly localized. The benefit of the micromechanical resonator is that a large number channels can be simultaneously filtered at low power and low latency, in a small package. Advanced, high-density electrodes are needed to complement this technology to deliver high-fidelity signals to the auditory nerves.

High-density electrodes may be manufactured using micromachining techniques similar to those used for building the resonator array. Figure 6 shows a hypothetical electrode array that can be manufactured in thin polymer membrane. The device consists of lithographically defined electrodes built up in platinum, passivated by ceramic or polymer (e.g., parylene), and encapsulated in a flexible polymer carrier, such as polyimide. Each electrode juts out in lithographically defined 'hair', 20–100 μm in width and several hundred micrometers in length. At the tip of each electrode hair is an opening in the passivation layer that exposes the platinum to the environment. Such hairs could enable the electrodes to make close contact with the basilar membrane and, presumably, minimize cross talk among nearby electrodes. One may wish to design multiple electrode hairs per electrical trace, and the hairs themselves may include hooks, dendrites, and other special geometries to improve electrical performance. Delamination of polymers may occur due to swelling from fluid exposure, failure of adhesives, or electrochemical effects such as cathodic delamination. As with any implantable device, materials reliability will be a critical factor for success.

Assuming the electrodes are 10 μm wide, with 10 μm interspacing (smaller electrical traces can be manufactured), one can trace out 50 electrodes in a single side of plastic, 1 mm in width. This suggests that an electrode capable of delivering all 88 keys on the piano should require a strip of plastic 1 mm in width, patterned on both sides with electrical traces. Since the electrode can be fabricated using conventional micromachining technology, one can imagine having each electrode strip custom produced to fit each patient's cochlea.

Smaller electrodes will result in higher resistances, increasing the driving power per electrode. The resistance of a 3-cm platinum electrode, 10×0.1 μm, will be nearly 3 kΩ. This will necessitate the use of smaller currents to reduce power consumption. Such a strategy can only work if smaller currents can still produce threshold voltages at the dendrites. One can anticipate that the hairlike electrodes indicated in figure 6 may experience lower thresholds because they are in such close proximity to the

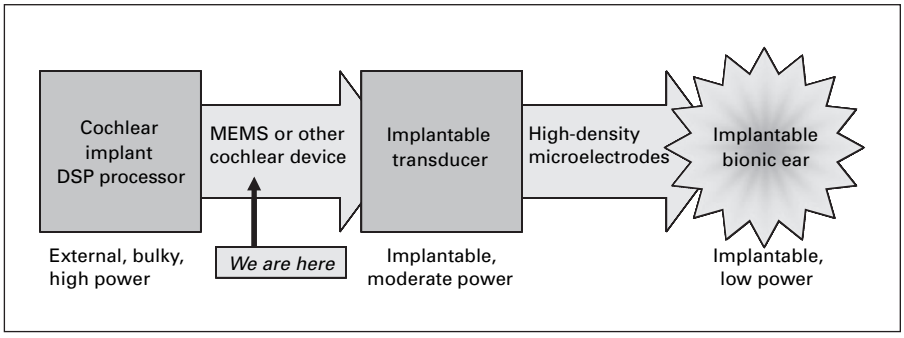

Fig. 7. Road map to bionic ear technology. Researchers are currently tackling the problem of building a miniaturized cochlear device. System insertion issues and, most importantly, high-density microelectrodes are critical developments for a successful bionic ear.

nerve sites, and less energy is wasted in the region between electrodes. This has not been experimentally verified, however, and more work is needed in this area to confirm design strategies.

System Packaging

A complete system can be expected to consist of a multiband microphone, amplification electronics, electrode driver, a high-density electrode array, small rechargeable battery, and a recharge coil. (The system might be copackaged with a traditional CI system as an optional secondary implant choice.) A significant engineering problem for such a system will consist of packaging for the microphone. There are several major issues that need to be addressed, namely (1) electrical packaging to make electrical connections from the microphone to the electronics, (2) mechanical packaging to mount the microphone in an appropriate location, (3) environmental packaging to seal and protect the microresonators from fluids, and (4) radio frequency packaging to shield the device from electrical noise.

The resonator array must be mounted so that a large number of resonators can make electrical contact to a microelectronic chip that performs the appropriate amplification for each channel. This may represent a large number of bond points, possibly hundreds of electrical connections may need to be made. High density bumpbonding, or even postprocessing of the microfabrication directly on the die are possible solutions to this problem. Since the fabrication method can be designed to be performed at low temperature, one may consider building the microresonators directly on the electronic die.

Direct connection of the resonators to the mechanical substrate can degrade performance of the microphone. Vibrations of the mechanical package can be readily picked up by the transducer, typically introducing broadband response where narrow band may be desired. This is a well-known problem for microphone designers. One may need to design damping systems or a vibration isolation mechanism into the packaging or into the microdevice itself.

Sealing the device against fluid leakage is a particularly difficult task because the protective package will introduce an acoustic barrier and impedance mismatch which will degrade the performance of the transducer. One approach is to follow the example of the reptilian middle ear and use a columella (a stiff rod) to connect the ear drum to a membrane opening (analogous to the oval window) in the packaged device. By choosing the size of the window appropriately, one may be able to match the acoustic impedances.

For most electrical transducers (e.g., capacitive, magnetic), interference from external electromagnetic sources is very problematic and greatly increases the noise in the signal. All condenser and electret microphones are heavily shielded against electromagnetic interference through metal packages and grills. One may hope that the presence of conductive fluid in the ear chamber and head can help provide natural shielding for the microphone. If not, then conductive casing will need to be placed around the transducer, grounding the system to the electrical potential of the patient.

Summary

We describe a micromachined multiresonator technology for building an artificial human cochlea that allows flexible design and good integration with electronic circuitry. The use of polymer material is recommended for low Q characteristics. An array of resonating cantilevers, each built with a different natural frequency, allows a device to perform a mechanical Fourier transform at

the front end of a bionic ear system. The channels may be mechanically coupled together, if desired. Furthermore, by controlling the amplification gain and the composition and geometry of the resonators, one may achieve sophisticated frequency profiles for each sub-band channel. The sub-band signals can be used to directly stimulate the cochlea according to its tonotopic arrangement. A mechanical bank of resonators can only be considered for this application if the resonators are very small, so that the device can be implanted in the ear cavity of a patient. Miniaturization methods, developed for electronic and sensor applications, can now be directed to make such small resonators.

A number of technologies are being explored by researchers to build artificial human cochleas, ranging from microfluidic devices, micromechanical devices, and electronic devices. A possible roadmap to a bionic ear is shown in figure 7. A miniaturized cochlear device is not enough, however. A critical development for the implant to be useful is the technology to build high-density electrode arrays that can efficiently bring the many sub-band signals to the appropriate nerve endings. System engineering issues, such as electronic integration, power sources, and sophisticated packaging also need to be studied and understood.

Ultimately, the goal for this type of technology is to simulate the response of the human cochlea. Any analog approach, whether fluidics, mechanics or analog electronics will lack the flexibility of digital programming. Analog strategies are likely to be most successful when combined with digital control electronics to provide a measure of programmability for each individual patient.

References

Geisler CD: From Sound to Synapse. London, Oxford University Press, 1998.

Greenwood D: Critical bandwidth and the frequency coordinates of the basilar membrane. J Acoust Soc Am 1961;33:1344–1356.

Greenwood D: A cochlear frequency-position function for several species – 29 years later. J Acoust Soc Am 1990;87:2592–2605.

Haronian D, MacDonald NC: A microelectromechanics based artificial cochlea (MEMBAC). Proc Transducers (Stockholm) 1995;2:708–711.

Lim KM, Fitzgerald AM, Steele CR, Puria S: Building a physical cochlea model on a silicon chip; in Wada H, Takasaka T, Ikeda K, Ohyama K, Koike T (eds): Developments in Auditory Mechanics. Teaneck, World Scientific, 1999, pp 223–229.

Loizou PC: Signal processing for cochlear prosthesis: a tutorial review. Proc Midwest Symp Circuits Syst (MWSCAS'97), Sacramento, 1997, pp 200–204.

Loizou PC: Mimicking the human ear. IEEE Signal Process Mag 1998;5:101–130.

Loulou M, Neji K, Mabrouk C, Fakhfakh A, Fakhfakh M, Masmoudi N: New Approach to a Digitally Programmable Analogue VLSI Cochlea Prosthesis and its Implementation with SI Technique. 16th Int Conf Microelectronics, Tunis 2004, pp 604–607.

Lyon RF: Filter cascades as analogs of the cochlea; in Lande TS (ed): Neuromorphic Systems Engineering. Amsterdam, Kluwer Academic, 1998, pp 3–18.

Lyon RF, Mead CA: A CMOS VLSI cochlea. Acoust Speech Signal Process 1988;4:2172–2175.

Lyon RF, Mead C: An analog electronic cochlea. IEEE Trans Acoust 1998;36:1119–1134.

McDermott H: A programmable sound processor for advanced hearing aid research. IEEE Trans Rehab Eng 1998;6:53–59.

Moore BCJ: An Introduction to the Psychology of Hearing. New York, Academic Press, 1997.

Ohyama K, Koike T (eds): Recent Developments in Auditory Mechanics. Teaneck, World Scientific, 1999, pp 223–229.

Oxenham AJ, Bernstein JGW, Penagos H: Correct tonotopic representation is necessary for complex pitch perception. Proc Natl Acad Sci USA 2004;101:1421–1425.

Petersen KE: Silicon as a mechanical material. Proc IEEE 1982;70:420–457.

Rauschecker JP, Shannon RV: Sending sound to the brain. Science 2002;295:1025–1029.

Robles L, Ruggero MA: Mechanics of the mammalian cochlea. Physiol Rev 2001;81:1305–1352.

Sarpeshkar R: Energy efficient adaptive signal decomposition: the silicon and biological cochlea. Circuits Syst 1999;5:70–73.

Sarpeshkar R, Lyon RF, Mead CA: A low-power wide-dynamic-range analog VLSI cochlea. Analog Integr Circuits Signal Process 1998;16:245–274.

Saunders GH, Kates JM: Speech intelligibility enhancement using hearing-aid array processing. J Acoust Soc Am 1997;102:1827–1837.

Shannon RV, Otto SR: Psychophysical measures from electrical stimulation of the human cochlear nucleus. Hear Res 1990;47:159–168.

Simmons FB: Cochlear implants. Arch Otolaryngol 1969;89:61–69.

Tanaka K, Abe M, Ando S: A novel mechanical cochlea 'Fishbone' with dual sensor/actuator characteristics. IEEE/ASME Trans Mechatron 1998;3:98–105.

Tyler R, Witt S, Dunn C: Tradeoffs between better hearing and better cosmetics. Am J Audiol 2004;13:193–199.

Volta A: On the electricity excited by mere contact of conducting substances of different kinds. R Soc Philos Trans 1800;90:403–431.

White RD, Grosh K: Microengineered hydromechanical cochlear model. Proc Natl Acad Sci USA 2005;102:1296–1301.

Xu T, Bachman M, Zeng FG, Li GP: Polymeric micro-cantilever array for auditory front-end processing. Sens Actuators A 2004;114:176–182.

Xu T, Li GP, Bachman M, Lai Z, Yang Y: A novel vacuum filling process for polymeric optical waveguide fabrication. Proc Optic Fiber Commun Conf, Anaheim 2002, pp 17–18.

Zeng FG: Trends in cochlear implants. Trends Amplif 2004;8:1–34.

KARGER

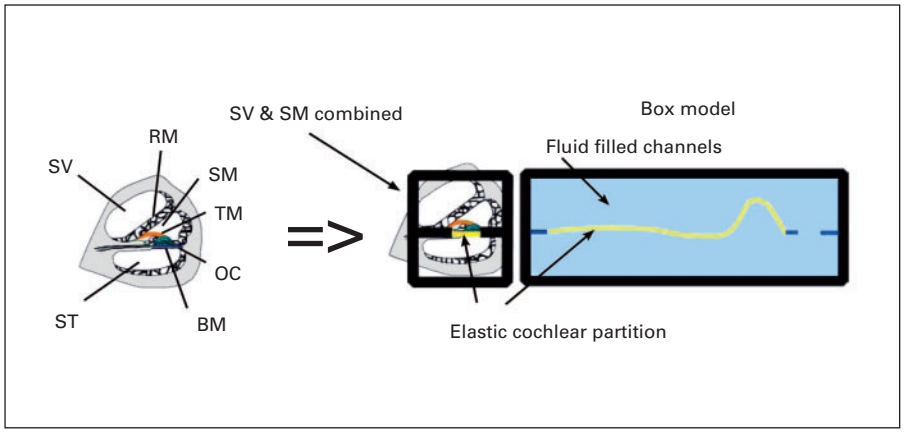

Fig. 1. Box model of the cochlea. Simplified drawing of the cross-section of the cochlea showing the organ of Corti (OC), scala vestibuli (SV), scala media (SM), scala tympani (ST), Reissner's membrane (RM), tectorial membrane (TM), and basilar membrane (BM). The three fluid-filled channels are reduced to two channels. Reissner's membrane has small stiffness and the SV and SM are combined as a single channel. The organ of Corti and basilar membrane are combined as a flexible cochlear partition separating the two fluid (saline)-filled channels.

duces scaling questions. The model of Zhou et al. [1993] is the first with life-sized dimensions for the basilar membrane. However, the basilar membrane thickness was not controlled, a fluid viscosity 20 times that in the cochlea was used, and the fabrication is not easily extended to include other features.

Advances in micromachining equipment have enabled the development of models that can be extended to include more detailed features of the cochlea with life-sized dimensions, as by Hemmert et al. [2002] and White and Grosh [2005]. Work in the area of sensor and actuator development for atomic force microscopy [Manalis et al., 1996; Grow et al., 2002] has provided additional reasons to pursue physical modeling using microfabrication methods. Utilizing atomic force microscopy techniques, a model with active mechanisms could be developed.

Why study the passive cochlea response since the cochlea has been demonstrated to have active mechanisms? With any complex problem it is important to understand the underlying mechanisms. In the case of the cochlea, the macro mechanics of the passive basilar membrane must be studied in detail first in order to establish a basis for how the active mechanisms work.

Modeling

The cochlea consists of three fluid-filled channels: scala vestibuli, scala media, scala tympani. Separating the scala vestibuli from the scala tympani is the organ of Corti which runs the full length of the spiraled cochlea. The connection to the cochlea from the middle ear ossicles is through the oval window at the stapes footplate. The round window is open to the middle ear cavity.

Box Model

This physical cochlear model is intended as a research tool. Simplifications to the design are made to focus on important features of the cochlear function. The basic response of the cochlea is examined by studying the passive behavior of an elastic cochlear partition separating two fluid channels. This is referred to as the 'box model' (fig. 1). One of the distinct deviations from the actual coiled geometry is the use of straight channels. A straight channel is easier to model mathematically and reduces the complexities in the fabrication process. Calculations by Loh [1983] and Steele and Zais [1985] showed no significant differences between straight and coiled models of a guinea pig cochlea. The fluid channels are rectangular (2×2 mm) and filled with saline. Saline was chosen as the fluid since it has similar viscous properties as perilymph. The channels were machined from plexiglas using conventional machining methods.

Cochlear Partition Design

A critical part of the box model design is the cochlear partition. The more elastic portion represents the basilar membrane. For humans, the basilar membrane has a length of approximately 35 mm and is tapered in width from approximately 100 μm at the base to 500 μm at the apex [Wever, 1949]. The width variation of the basilar membrane is the primary contributor to the stiffness gradation along the length.

Iurato [1962] and Cabezudo [1978] describe the basilar membrane as consisting of a supporting layer made up of collagen filaments arranged in a transverse direction. This fiber arrangement leads to direction dependent properties for the basilar membrane. This was demonstrated by the measurements of Naidu and Mountain

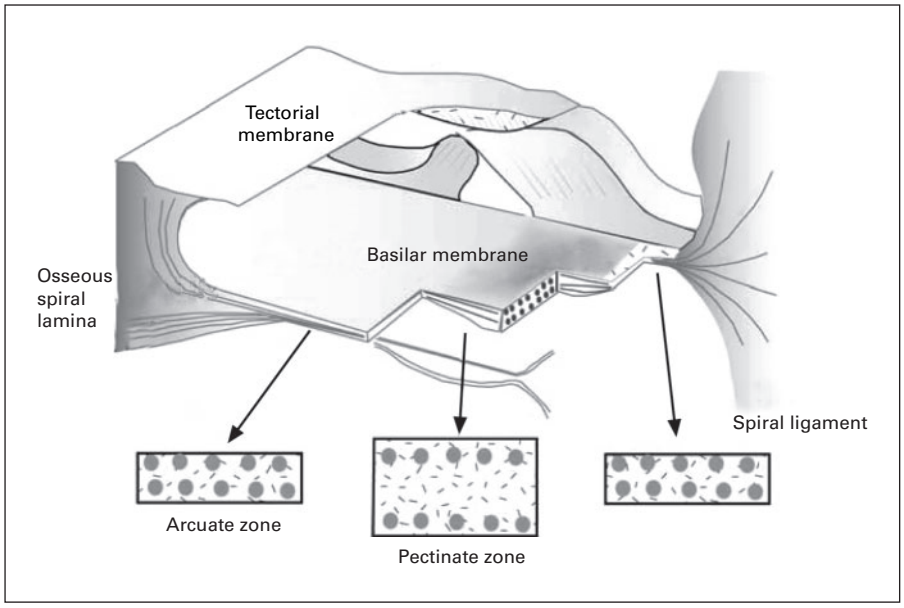

Fig. 2. Organ of Corti [after Iurato, 1962]. The basilar membrane consists of circular bundles of fibers arranged in a matrix. In the arcuate zone, the fibers are closely spaced. In the pectinate zone, the fibers are separated which results in a greater bending stiffness compared to the arcuate zone.

[2000]. Developing a design with this feature is important to the dynamic response of the cochlear partition. A sketch of the organ of Corti is shown in figure 2. In the pectinate zone, the fibers are widely spaced. In the arcuate zone and at the spiral ligament, the fibers are closely packed. This distribution of the fibers will lead to a variation in radial stiffness.

An approximation to the variation in radial stiffness is achieved in the model by creating a composite material consisting of a base material and discrete ribs (fig. 3). The ribs terminate prior to the boundary to give a change in the radial stiffness. Each rib has a width of 1.5 μm and the spacing between ribs is 2.5 μm. The thickness of the base material and height of the ribs were constant for a specific design, but several variations were fabricated as described in the results section.

Stapes Simulator

The primary excitation method for the cochlea is motion of the stapes footplate. A system of excitation which is similar to the stapes is highly desirable, so a coil magnet system was developed. A magnet suspended in silicone acts like the stapes footplate. One side of the magnet interfaces with the fluid (fig. 3). A sinusoidally varying current in the coil creates a varying magnetic field which causes the magnet to oscillate. Motion of the magnet creates a wave in the fluid at the desired frequency. The wave in the fluid interacts with the cochlear partition causing a traveling wave on the partition.

Mathematical Modeling

The cochlea is a complex fluid-structure interaction problem because the geometric parameters and material properties for the elastic cochlear partition are not constant. Additionally, the presence of the boundary layer in the viscous fluid increases the mesh resolution needed for a direct numerical method. Combined with the variable elastic partition properties, the number of degrees of freedom becomes overwhelmingly large. With such a large model the significant features and trends become difficult to see with limited parameter studies. Asymptotic expansion procedures offer simple, efficient, and reasonably accurate approximate solutions in contrast to finite element method or other large scale model methods. The asymptotic solution approach starts with the mathematical representation of the 3-D fluid using a Newtonian fluid model. This results in the Navier-Stokes equations. The elastic cochlear partition is modeled as a tapered plate. Details of the method can be found in Steele and Taber [1979].

Methods

Micromachining Methods

Micromachining is a method of fabricating devices with features as small as a few microns and dimensions to several hundred microns. Typical devices are pressure sensors, accelerometers, actuators, and microsystems such as polymerase chain reaction devices. The tools are shared with those developed for the microelectronic integrated circuit industry. The strength of the technology is

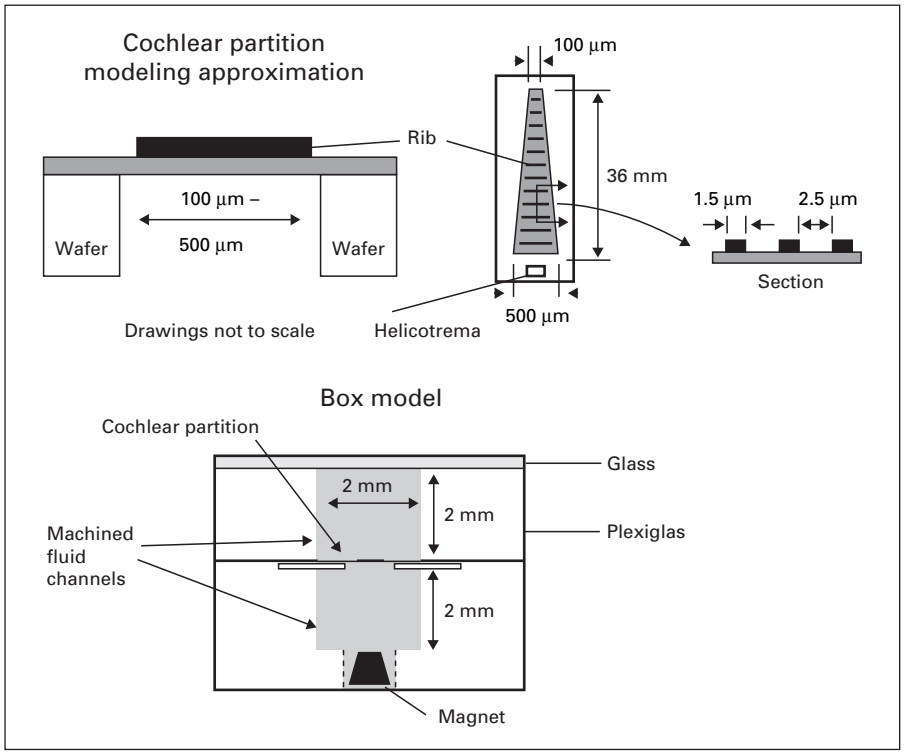

Fig. 3. Modeling approximation for the cochlear partition is shown on a silicon wafer section. The basilar membrane is modeled with a thin layer of polyimide and discrete ribs. The discrete ribs are used to create orthotropic (direction-dependent) material properties similar to the circular bundles. The ribs terminate prior to the wafer section to provide a stiffness variation across the width which is similar to the arcuate and pectinate zones. The width of the elastic portion varies linearly from 100 to 500 μm over the 36-mm length. The ribs have a width of 1.5 μm and spacing of 2.5 μm. Also shown in the drawing is the cochlear partition in the box model. Each saline filled channel is 2 × 2 mm. The magnet used to represent the stapes footplate is identified.

the ability to simultaneously fabricate many devices on a single wafer and to combine mechanical devices with integrated circuits. However, a limitation is 2-D planar processing, which makes it difficult to achieve 3-D structures. Kovacs [1998] provides an overview of micromachined transducers, but cautions of the need to understand both strengths and weaknesses of the technology before committing to a fabrication approach. Information on the basics of integrated circuit processing can be found in Plummer et al. [2000]. Fundamentals of micromachining are covered in Madou [2002]. An overview of design methods related to microelectromechanical systems are found in Senturia [2001] and Maluf [2000].

The basic methods of micromachining involve selection of a substrate, materials, and micromachining methods. A common substrate is silicon, but other materials are used depending on the properties needed for the device. Standard wafer diameters are 100, 200, and 300 mm. Thicknesses range from 450 to 2500 μm and can be custom made. Materials are selectively added to the substrate in thin layers. Typical layers are from 0.1 to 1 μm, but can be as large as 10s of microns for certain materials.

Through the use of photolithography, patterns are created on the thin layers using photoresist. The materials are selectively removed using surface etching. Etching is a chemical reaction that is performed either as a 'wet' or 'dry' process. The development of deep reactive ion etching tools have enabled devices to be fabricated by bulk etching through the thickness of the substrate.

For the cochlear partition, a material with a Young's modulus close to that of the biological material is desirable. A polymer, Pyralin® PI2610 series polyimide from HD Microsystems, was selected as the base material for its properties (Young's modulus 6.6 GPa) and handling durability. Aluminum (~70 GPa) was selected for the discrete ribs. A summary of the fabrication method is given in figure 4. A thin layer (several microns) of the polymer (polyimide) was spun and cured on a 100-mm silicon wafer. Aluminum was sputter deposited, patterned with photolithography, and dry etched to form the discrete ribs. The tapered plate was patterned on the backside and was released by bulk etching through the wafer thickness using deep reactive ion etching.

Measurement Methods

The cochlear model is evaluated by measuring the response of the cochlear partition to a stapes-simulated input. A He-Ne laser vibrometer (Polytec CLV 700 with HLV 1000 controller) was used to measure the velocity (fig. 5). The laser was mounted on a surgical operating scope for the stapes magnet measurements and mounted on an adjustable table for X-Y positioning during the cochlear partition measurements. Locations along the length are measured. A glass cover slide was used over the fluid chamber to improve the laser signal to noise ratio. A hydrophone [Puria, 2003] was used to measure pressure in the fluid chamber. The frequency range of excitation was 100 Hz to 25 kHz using stepped tones.

Results

Microfabrication Results

Fabrication of the cochlear partition was performed in a class 100 clean room at the Stanford Nanofabrication Facility. Samples with base thickness from 1 to 5 μm were

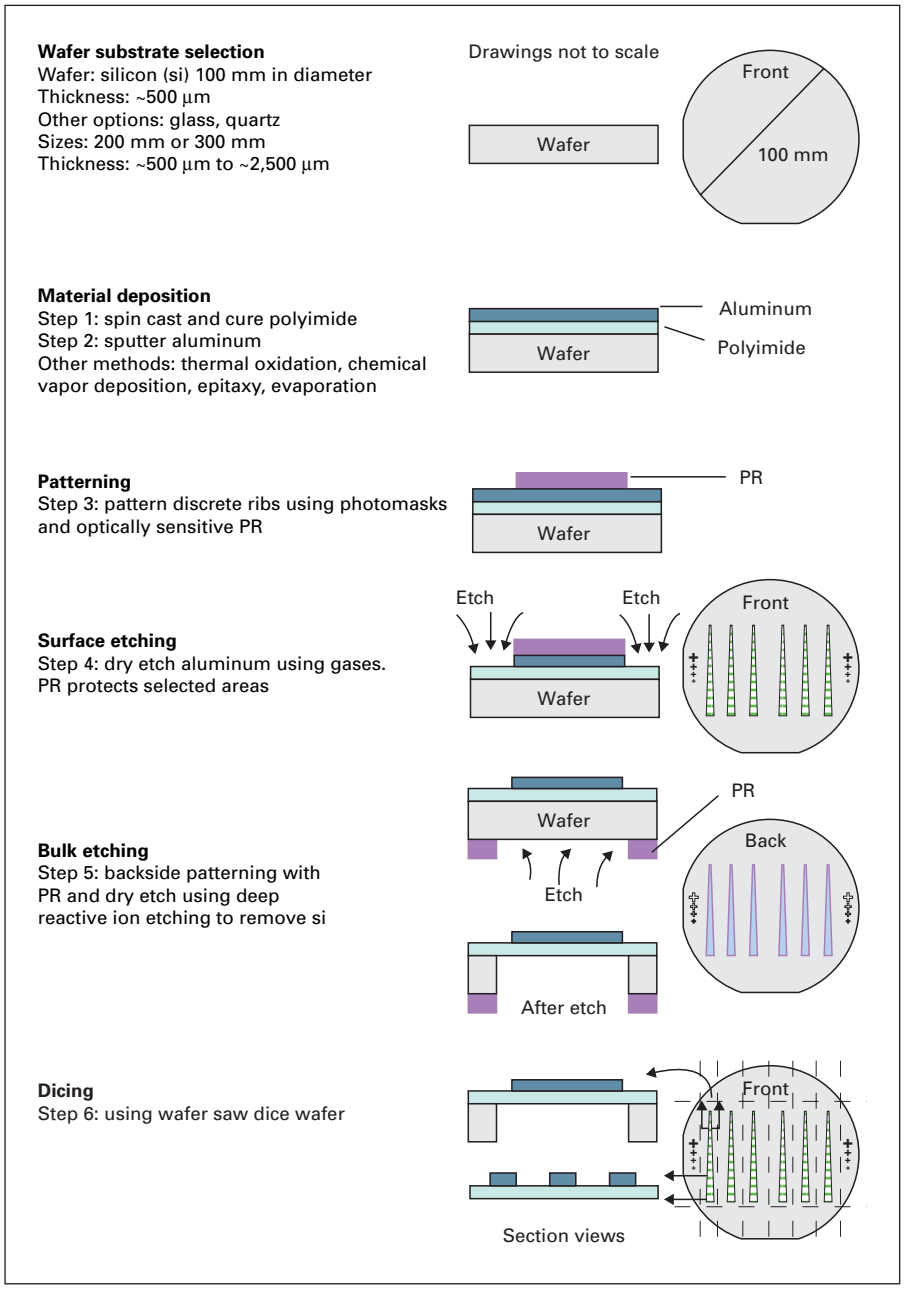

Fig. 4. Micromachining methods for creating a cochlear partition. Selection of a substrate material is followed by deposition of thin layers of material. Patterns are formed in photoresist (PR) using optical photolithography. Materials are selectively removed using etching methods. A wafer saw is used to dice the wafer into individual devices.

fabricated. Rib height ranged from 0.1 to 1.0 μm, but were constant for a particular design. A sample cochlear partition is shown in figure 6. Over the 36 mm length, there are approximately 9000 discrete aluminum ribs. The figure shows a scanning electron microscope image of the aluminum ribs on the polyimide. The specific sample shown in the sections which follow had a thickness of 4.75 μm with a rib height of 0.2 μm.

Measurement Results

The measurement results can be examined in several ways. The first way is to examine a single location for multiple frequencies. The response of interest is the velocity of the elastic portion of the cochlear partition. The velocity of the wafer portion is several orders of magnitude lower (not shown). Normalized plots of the partition velocity are shown in figure 7. Two locations, 0.035 m and 0.023 m from the base location, are plotted in the

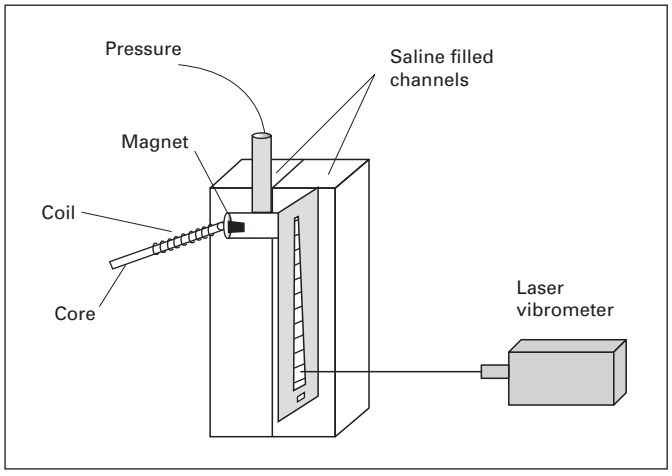

Fig. 5. Measurement system. Cochlear partition separating two fluid (saline)-filled channels. A coil magnet system provides the input. The magnet is suspended in silicone. One side of the magnet interfaces with the fluid. A sinusoidally varying current through the coil creates a varying magnetic field which causes the magnet to oscillate. The oscillating magnet creates a wave in the fluid at the desired frequency. A He-Ne laser vibrometer is used to measure the response. Additionally, the pressure near the input source is measured.

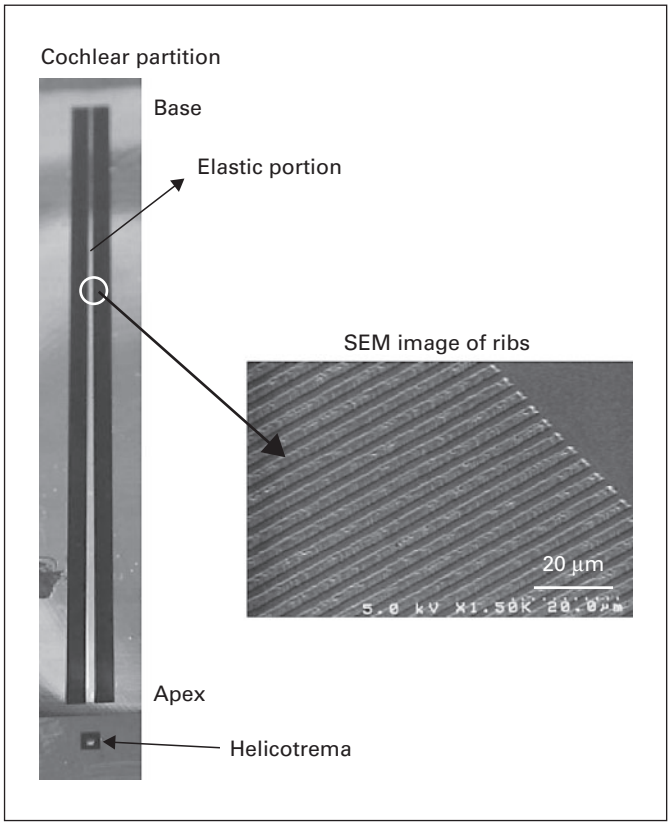

Fig. 6. Conventional photograph of cochlear partition with elastic portion and helicotrema identified. Scanning electron microscope (SEM) image shows details of the discrete ribs. Scale bar length is 20 μm. Width of a rib is 1.5 μm. The spacing between each rib is 2.5 μm. There are approximately 9000 ribs along the length of the partition.

figure. The peak response for the 0.035 m location occurs near 7.5 kHz. Beyond this frequency the amplitude rolls off into the noise level. The 0.023 m location gradually builds up in response and peaks near 18 kHz. The phase is also shown. The point further away from the stapes input shows a larger build up of phase.

Another way to examine the results is a spatial representation. For a single frequency, the measured response at multiple points is plotted. A 9-kHz response is shown in figure 8 and exhibits a gradual build-up in response to a peak location which is dependent on the frequency of excitation. A change in wavelength is also apparent. This is typical for a dispersive wave.

Discussion and Conclusions

The physical model demonstrated several important features which are also observed in mammalian cochleas: traveling waves, tuning, frequency to place tonotopic organization, and roll off beyond the characteristic place. The physical model demonstrates a traveling wave which peaks at a characteristic place with a gain of 2.4 at 0.029 m and a phase lag of $\sim 3\ \pi$ for 9-kHz input.

The calculations based on the design specifications reasonably approximate the measured responses (fig. 7). However, the measured responses showed some variation. The variations could have been due to geometry or material property nonuniformity. High magnification images indicate some geometric variability resulting from the processing. Variability in width dimensions as small as 5–10 μm can lead to measurable changes in the stiffness profile. To quantify the effect of the processing variations and to account for the possibility of material nonuniformity, an approach was needed to validate the stiffness.

The stiffness of the cochlear partition in the fluid chamber can be estimated using low frequency excitation. For this comparison, the velocity was divided by the frequency of excitation, ω, to give an equivalent displacement. The displacement was divided by the pressure at

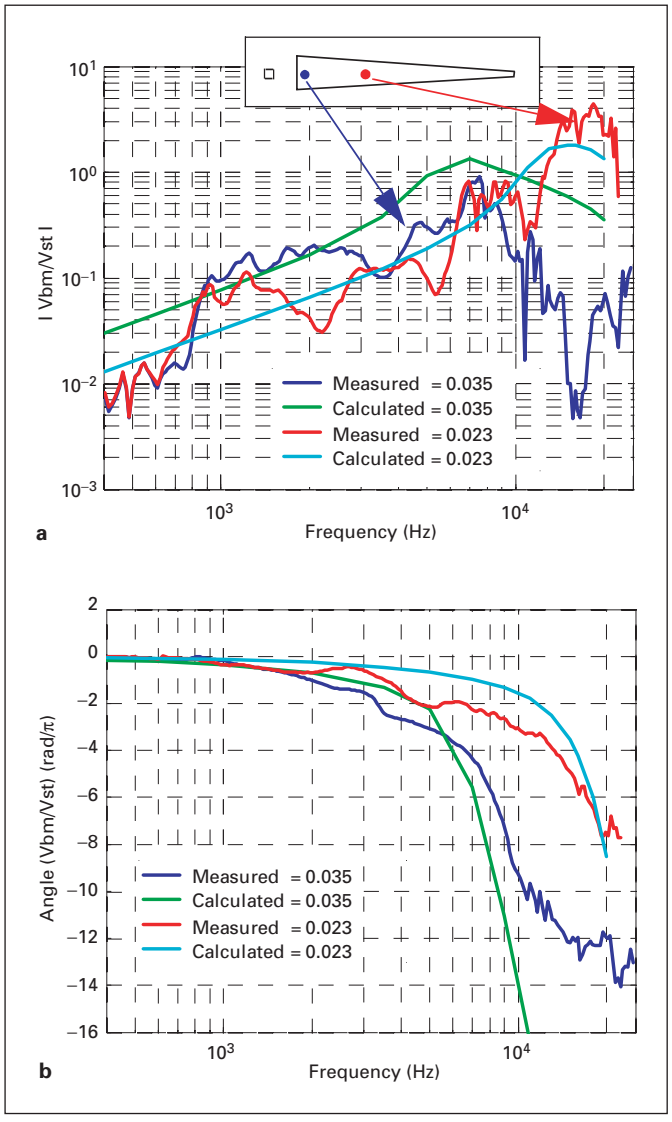
I Vbm/Vst I
Frequency (Hz)
Measured = 0.035
Calculated = 0.035
Measured = 0.023
Calculated = 0.023
a
Angle (Vbm/Vst) (rad/π)
Frequency (Hz)
Measured = 0.035
Calculated = 0.035
Measured = 0.023
Calculated = 0.023
b

7

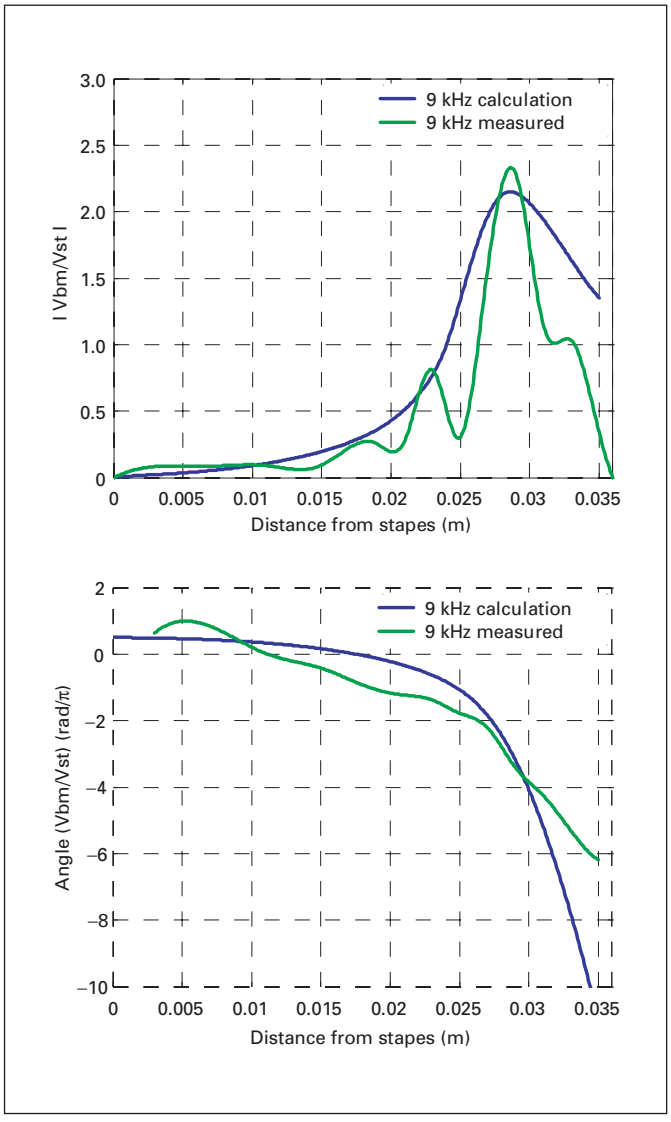
I Vbm/Vst I
Distance from stapes (m)
9 kHz calculation
9 kHz measured
Angle (Vbm/Vst) (rad/π)
Distance from stapes (m)
9 kHz calculation
9 kHz measured

8

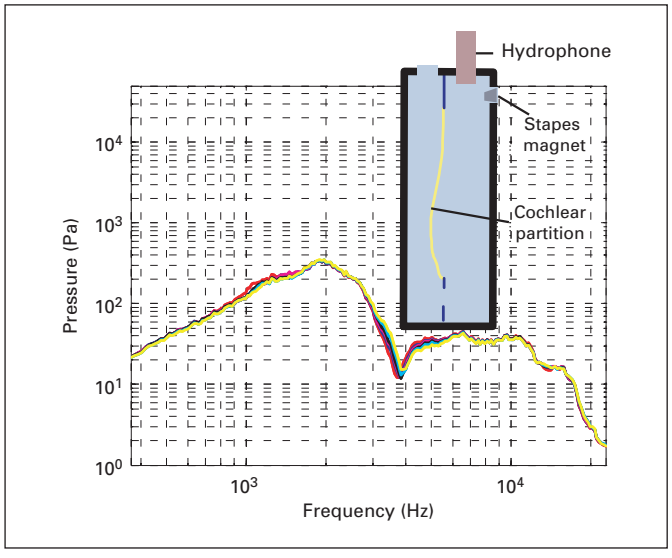
Hydrophone
Stapes magnet
Cochlear partition
Pressure (Pa)
Frequency (Hz)

9

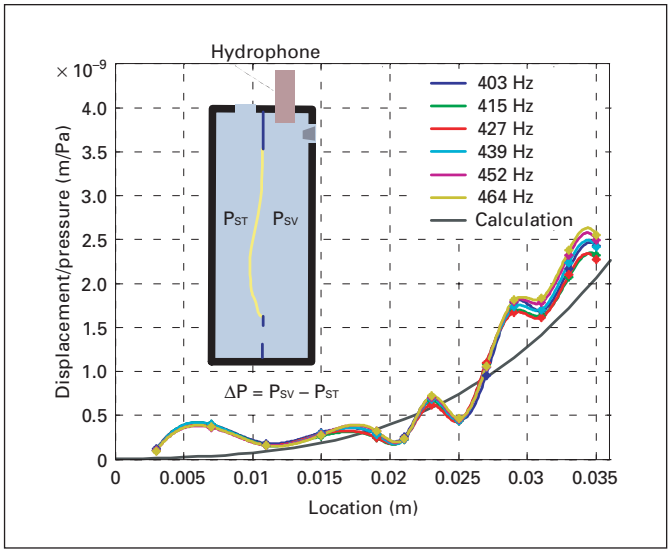
Hydrophone
403 Hz
415 Hz
427 Hz
439 Hz
452 Hz
464 Hz
Calculation
PST
PSV
ΔP = PSV – PST
Displacement/pressure (m/Pa)
Location (m)

10

the location. Since the pressure was only measured at the stapes source (fig. 9), an approximation of the net pressure ($\Delta P = P_{SV} - P_{ST}$) at the measurement location was calculated based on the assumption of a linear profile. Using the calculated net pressure on the elastic partition, the displacement divided by net pressure is given in figure 10. The variation in the compliance is reasonably consistent with the dynamic response shown in figure 8. A next step for the computations would be the use of the compliance results in an updated vibration response calculation.

The usefulness of physical and mathematical models lies in their ability to describe accurately the significant physical processes. Their ability to provide useful information for understanding cochlear mechanics is dependent on using parameters which are physiologically realistic. Initial efforts have shown biological-like responses can be achieved with a physical model. It is a first step toward models with more complicated features. Microfabrication with polyimide and aluminum has been shown to give responses which can be validated with a mathematical model. Modifications to the base material thickness and height of the ribs can be made to produce a model with a frequency range closer to that of human.

Fig. 7. Measurements are normalized to the stapes magnet input velocity. Magnitude (**a**) and phase (**b**) are shown for locations 0.035 and 0.023 m from the base on the cochlear partition. Corresponding calculations using nominal design geometry and an asymptotic solution method are also shown. The amplitude builds up to a peak at a certain frequency and then rolls off. Measured values show deviation from the calculated response due to deviations in geometry and material properties.

Fig. 8. Spatial response of the cochlear partition to an oscillatory input of 9 kHz. Magnitude and phase are shown along the centerline of the cochlear partition. Distance is shown relative to the stapes input. Calculation is based on the nominal design geometry.

Fig. 9. Six pressure measurements using a hydrophone near the stapes magnet location in the physical model scala vestibuli. The pressure builds in magnitude until 2 kHz as a result of the stapes input profile. A dip in pressure occurs near 4 kHz as a result of a resonance.

Fig. 10. Compliance evaluation using low frequency velocity data. The net pressure on the partition ($\Delta P = P_{SV} - P_{ST}$) is computed based on the hydrophone measurement. The displacement is determined using the velocity and frequency. A range of frequencies (403–464 Hz) are plotted to show the data are consistent in that region. A calculation for the expected compliance based on nominal geometry is also shown.

Research Tool and Front End Processor

Using a physical cochlear model, the effect of basilar membrane orthotropy on the sharpness of tuning can be studied by varying the rib height. In the current physical model, the osseous spiral lamina and spiral ligament were designed to be nearly rigid compared to the elastic partition. By modifying the supporting conditions with different thicknesses for the supports, the effect of a more compliant boundary can be assessed experimentally.

A problem of clinical relevance which can be investigated with either the physical model or mathematical model is the effect of a short electrode cochlear implant. A short electrode implant is used for high frequency excitation in cases when the lower frequency range is functioning adequately. The electrode is placed in the scala tympani and occupies significant volume. How is the mechanical response of the basilar membrane affected by the presence of the electrode? In addition to being a research tool for cochlear mechanics, a physical model might serve as a front end processor for cochlear implants. Current cochlear implants bypass the mechanical auditory pathway and directly stimulate portions of the auditory nerve. The next generation cochlear implants may take advantage of micromachining technology to create a totally implantable cochlear system [Zeng, 2004]. Development of an array of cantilever beams for this purpose was demonstrated by Xu et. al. [2004]. While the physical model presented in this work demonstrates cochlear-like capabilities, there is still much development work needed before it could be used in a cochlear implant device.

Acknowledgements

Work supported in part by grants F31 DC05454 and R29 DC03085 from the NIDCD of NIH and a grant from the Human Frontier Science Program (HFSP).

References

Cabezudo LM: The ultrastructure of the basilar membrane in the cat. Acta Otolaryngol 1978; 86:160–175.

Cancelli C, D'Angelo S, Masili M, Malvano R: Experimental results in a physical model of the cochlea. J Fluid Mech 1985;153:361–388.

Grow RJ, Minne SC, Manalis SR, Quate CF: Silicon nitride cantilevers with oxidation-sharpened silicon tips for atomic force microscopy. IEEE J Microelectromech Syst 2002;11:317–321.

Helle R: Beobachtungen an hydromechanischen Modellen des Innenohres mit Nachbildung von Basilarmembran Corti-Organ und Deckmembran. Technische Universität München, München, 1974.

Hemmert W, Durig U, Despont M, Drechsler U, Genolet G, Vettiger P, Freeman DM: A life-sized, hydrodynamical, micromechanical inner ear; in Gummer AW (ed): Biophysics of the Cochlea. Teaneck, World Scientific, 2002.

Iurato S: Functional implications of the nature and submicroscopic structure of the tectorial and basilar membranes. J Acoust Soc Am 1962;34: 1386–1395.

Kovacs GTA: Micromachined Transducers Sourcebook. San Francisco, WCB/McGraw-Hill, 1998.

Lechner T: A hydromechanical model of the cochlea with nonlinear feedback using PVF2 bending transducers. Hear Res 1993;66:202–212.

Loh CH: Multiple scale analysis of the spirally coiled cochlea. J Acoust Soc Am 1983;74: 94–103.

Madou M: Fundamentals of Microfabrication: The Science of Miniaturization, ed 2. Boca Raton, CRC Press, 2002.

Maluf N: An Introduction to Microelectromechanical Systems Engineering. Boston, Artech House, 2000.

Manalis SR, Minne SC, Quate CF: Atomic force microscopy for high speed imaging using cantilevers with an integrated actuator and sensor. Appl Phys Lett 1996;68: 871–873.

Naidu RC, Mountain DC: Longitudinal coupling within the basilar membrane and recticular laminae; in Wada H, Takasaka T, Ikeda K, Ohyama K, Koike T (eds): Recent Developments in Auditory Mechanics. Teaneck, World Scientific, 2000, pp 123–129.

Puria S: Measurements of human middle ear forward and reverse acoustics: implications for otoacoustic emissions. J Acoust Soc Am 2003; 113:2773–2789.

Senturia SD: Microsystems Design. Boston, Kluwer Academic, 2001.

Steele CR, Taber LA: Comparison of WKB calculations and experimental results for three-dimensional cochlear models. J Acoust Soc Am 1979;65:1007–1018.

Steele CR, Zais JG: Effect of coiling in a cochlear model. J Acoust Soc Am 1985;77: 1849–1852.

von Békésy G: Experiments in Hearing. New York, McGraw-Hill, 1960.

Wever EG: Theory of Hearing. New York, Wiley, 1949.

White RD, Grosh K: Microengineered hydromechanical cochlear model. Proc Natl Acad Sci USA 2005;102:1296–1301.

Xu T, Bachmann M, Zeng FG, Li GP: Polymeric micro-cantilever array for auditory front-end processing. Sens Actuators A Phys 2004;114: 176–182.

Zeng FG: Trends in cochlear implants. Trends Amplif 2004;8:1–34.

Zhou G, Bintz L, Anderson DZ, Bright KE: A life-sized physical model of the human cochlea with optical holographic readout. J Acoust Soc Am 1993;93:1516–1523.

KARGER

trical pulses for direct stimulation of the vestibular nerve. Della Santina et al. [2005] recently described a multichannel vestibular prosthesis employing commercial off-the-shelf microelectromechanical system (MEMS) gyro transducers and demonstrated responses to prosthetic stimulation in vestibular-deficient animals.

Here we describe development of a MEMS-based, vestibular prosthesis prototype. The core technology is a customized silicon chip that is 5 × 5 mm in size and includes three gyroscopes and three linear and angular accelerometers [Shkel and Howe, 2002]. We envision using the MEMS gyroscope as the input and then to adapt the cochlear implant technology for signal processing and electric stimulation. The combined MEMS and integrated circuit technologies should significantly shrink the sensor size, reduce the fabrication cost, and integrate the sensing-processing-stimulating functions on the same silicon chip for a 'balance on-a-chip' system.

We first briefly summarize the function and structure of the vestibular system. We then describe the system level design and functional blocks of the proposed vestibular prosthesis. Third, we present an engineered prototype of a unilateral vestibular prosthesis and compare the prototype performance to the physiological data recorded in the vestibular nerve of squirrel monkeys. Finally, we discuss both the opportunities and challenges facing the development of a totally implantable vestibular prosthesis.

Vestibular Function and Structure

The vestibular system is responsible for maintaining balance and spatial orientation while allowing the head and body to move freely [Goldberg and Fernandez, 1975; Highstein et al., 2005; Minor, 1998]. The vestibular system accurately senses and processes position and motion information. The brain then acts on the information by using the vestibulo-ocular reflex to stabilize gaze and the vestibulo-spinal reflex to control posture and balance. The sensing unit of the vestibular system consists of three semicircular canals and two otolith organs. The three semicircular canals are orthogonal to each other and can detect rotational movements of the head by sensing angular acceleration. The two otolith organs are the saccule and utricle that detect linear movements of the head, with the saccule being sensitive to gravity and the utricle being sensitive to linear accelerations in all planes.

All vestibular organs have small sensory hair cells, which convert motion into action potentials in the vestibular nerve. Each hair cell has a resting potential and its associated nerve has a spontaneous firing rate. The mean spontaneous rate is 91 spikes/s (SD = 36) in the squirrel monkey [Goldberg and Fernandez, 1971]. The firing rate increases when a semicircular canal responds to rotation in one direction, and decreases in the other direction. The firing rate changes in the opposite direction for vestibular nerve fibers innervating the contralateral semicircular canal in the same plane. Adaptation and small nonlinearities also occur in response to constant angular acceleration [Fernandez and Goldberg, 1971]. The average sensitivity is 0.3–0.7 spike/s, per 1°/s in rats and guinea pigs [Curthoys, 1982].

The perceptual threshold for rotation detection in humans has been measured to be between 0.1°/s and 2°/s [Benson et al., 1989]. Montandon [1954] found that the acceleration threshold is $1°/s^2$ in normal healthy individuals, but greater than $6°/s^2$ in patients with vestibular dysfunction. It should be noted that the perceptual threshold is likely to be different for different rates of acceleration and highly dependent upon individuals. Nevertheless, these reported electrophysiological and behavioral data have formed the basis on which the sensing and pulse generating units are built in the proposed vestibular prosthesis.

System Design

We initially focus on a semicircular canal prosthesis to restore rotational sensibility. The prosthesis should sense motion with sufficient precision and deliver electric stimulation to the central nervous system that mimics the dynamic vestibular function. Figure 1a contrasts the natural and prosthetic systems, with both having three main functional units – a sensing unit, a pulse generator, and a stimulator. Figure 1b shows a functional block diagram for the circuit components of a vestibular prosthesis [Liu et al., 2003]. The sensing unit includes a gyroscope, a low-pass filter and a differentiator. The input is rotational motion while the output is an analog voltage that is proportional to angular acceleration along the sensing axis. The pulse generator consists of a transfer function unit and a voltage-to-frequency converter. It generates monophasic voltage pulses based on a mathematical model describing biomechanics of the vestibular organ. The current source converts the monophasic voltage pulses into biphasic, charge-balanced, cathodic-first, current pulses that can be used to safely stimulate the vestibular nerve.

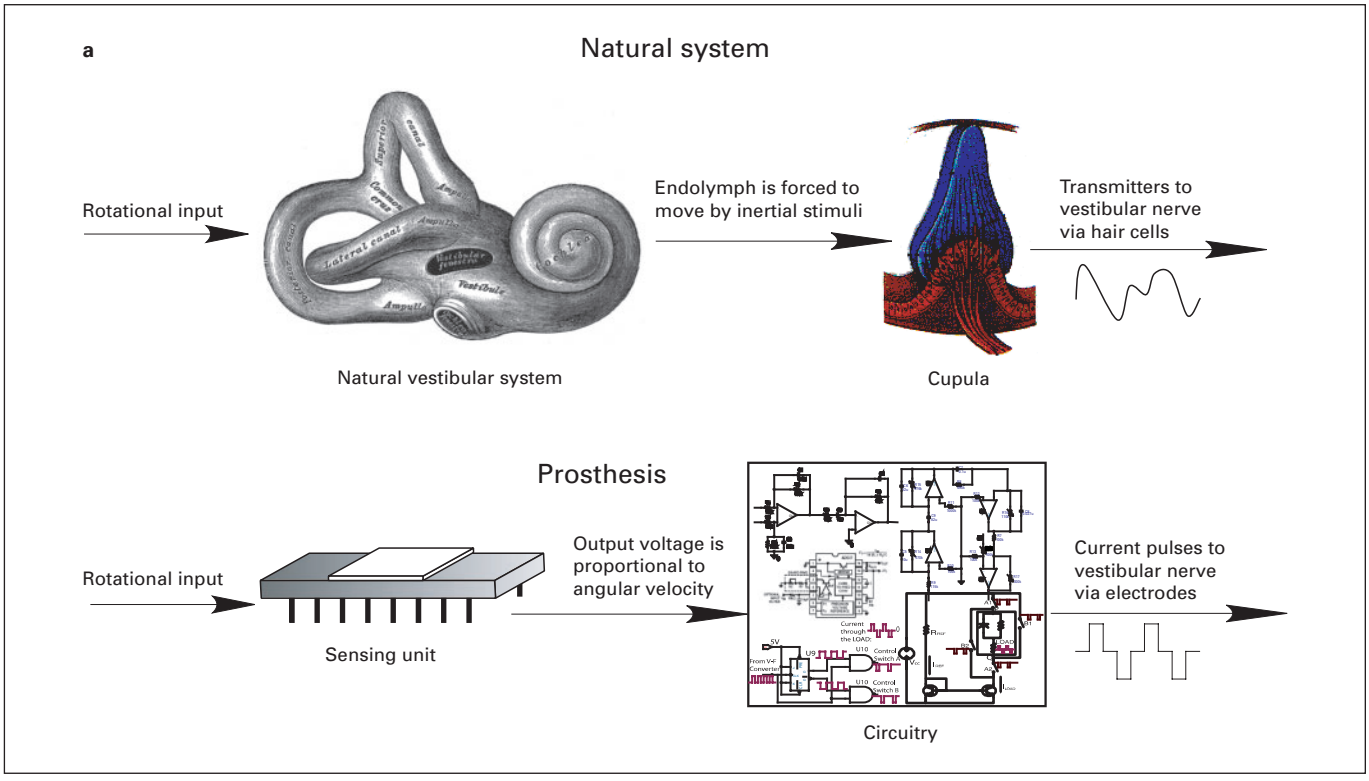

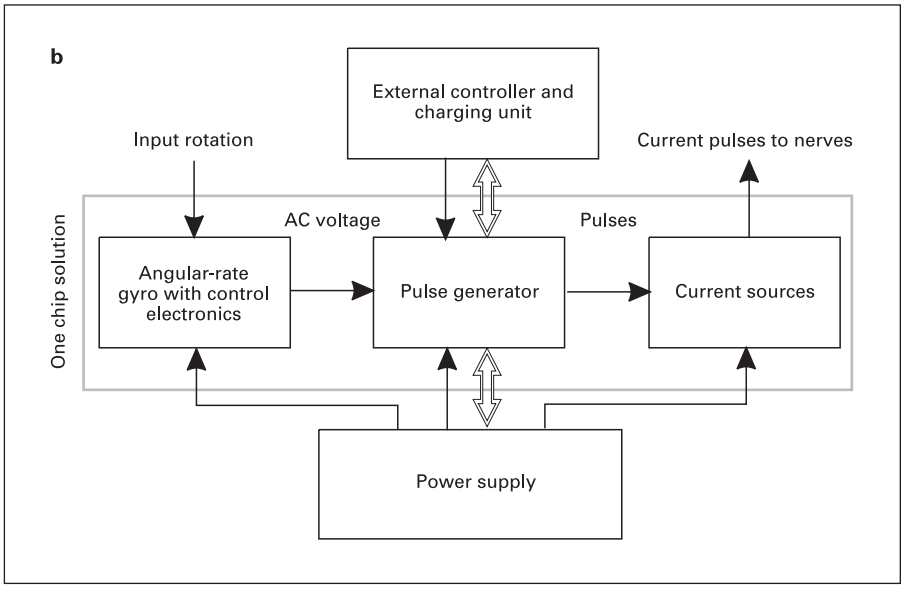

Fig. 1. a Comparison of the natural and prosthetic vestibular systems. **b** The functional block diagram of a MEMS-based vestibular prosthesis mimicking the dynamic function of the natural vestibular system.

Sensing Unit

The prosthesis utilizes a custom-made single-axis MEMS gyroscope, developed by UCI Microsystems Laboratory [Shkel, 2001]. Figure 2 shows a scanning electron micrograph of a MEMS gyroscope prototype. The gyroscope is approximately 2 × 2 mm^2 in size with a minimum feature of 5 μm. The MEMS gyroscope consumes ~10 mW power, which compares favorably with ~30 mW/rotational axis for the piezoelectric and MEMS sensors by Murata and Analog Devices Inc., respectively.

The micromachined gyroscope uses a vibrating element to measure rotational velocity based on the Coriolis

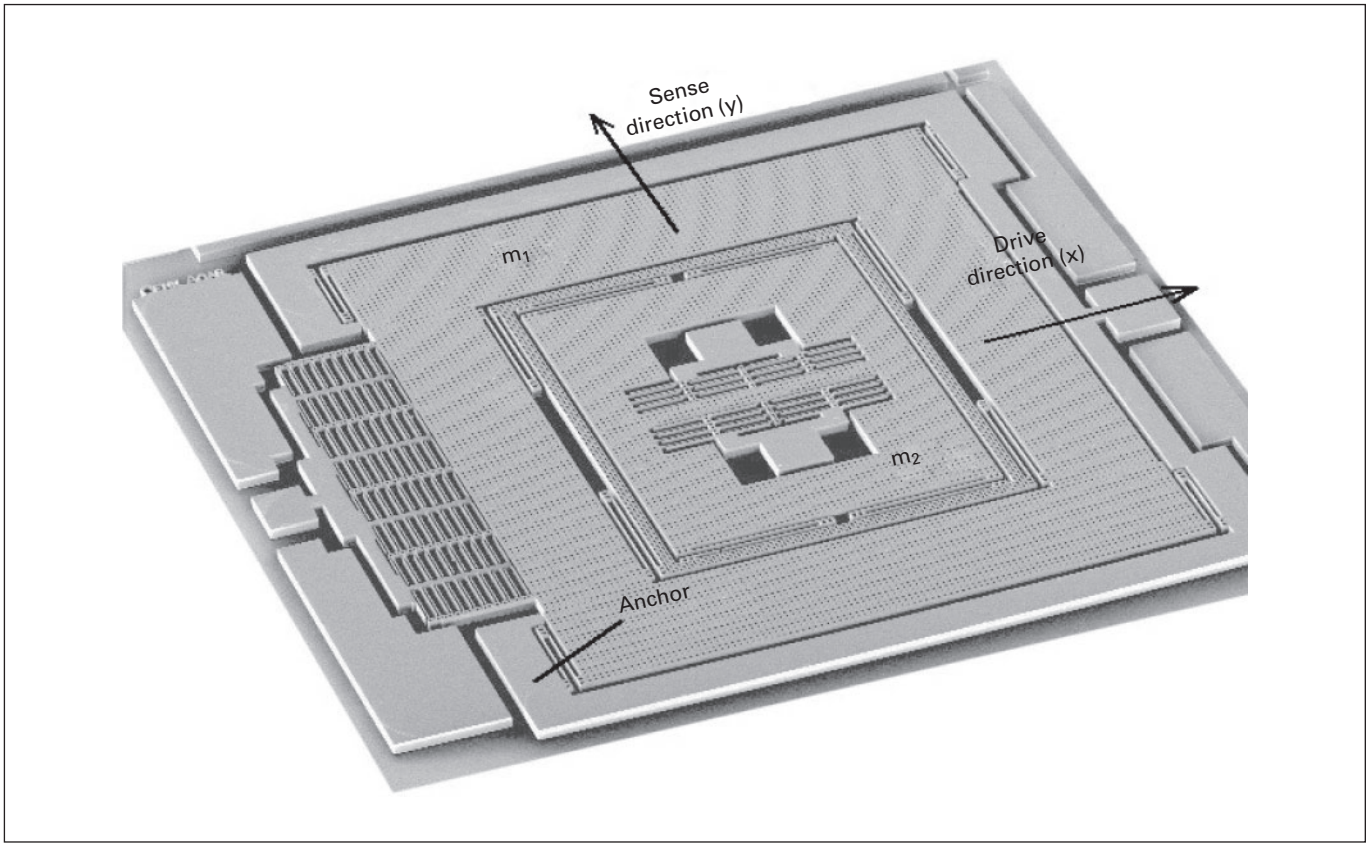

Fig. 2. Scanning electron micrograph of a prototype MEMS gyroscope.

principle [Greiff et al., 1991; Shkel et al., 2005]. The proof mass, which constitutes the active portion of the sensor, is driven by an oscillator circuit at a precise amplitude, X_D, and a relatively high frequency, ω_n, so that $x(t) = X_D \sin(\omega_n t)$. When subject to a rotation with angular velocity Ω, the proof mass will be subject to the Coriolis force. The resultant Coriolis force is perpendicular to both the input rate and the instantaneous radial velocity in the drive direction. This force produces a motion of the proof mass, $y(t)$, in a direction perpendicular to its initial oscillation:

$$\| y(t) \| = \frac{2X_D \Omega Q}{\omega_n} \quad (1)$$

This equation shows that the output deflection is proportional to the input angular velocity. The gyroscope response is also directly proportional to quality factor Q (i.e., the sharpness of the resonance) of the device. To improve performance of the MEMS gyroscope, the device has to be vacuum packaged to achieve high-amplitude response in the sensing direction. Detection of the Coriolis response is also challenging, requiring measurements of picometer scale oscillations in the sense mode, with the proof mass oscillating with tens of micrometers amplitude in the drive mode. The synchronous demodulation technique is commonly used to tackle this problem. A high-frequency carrier signal is imposed on the structure. An array of differential capacitors is used to detect picometer scale deflections due to the Coriolis-induced motion. The difference of the outputs of the differential amplifiers is amplitude demodulated at the carrier signal frequency, yielding the Coriolis response signal at the driving frequency.

We have also developed alternative vibratory gyroscopes with rate-integrating capabilities [Shkel et al., 2005]. Here we consider the design principle and specifications for a single-axis MEMS gyroscope employing a unique architecture that comprises a drive mode oscillator and a sense mode oscillator. This architecture improves sensitivity while maintaining robust operation

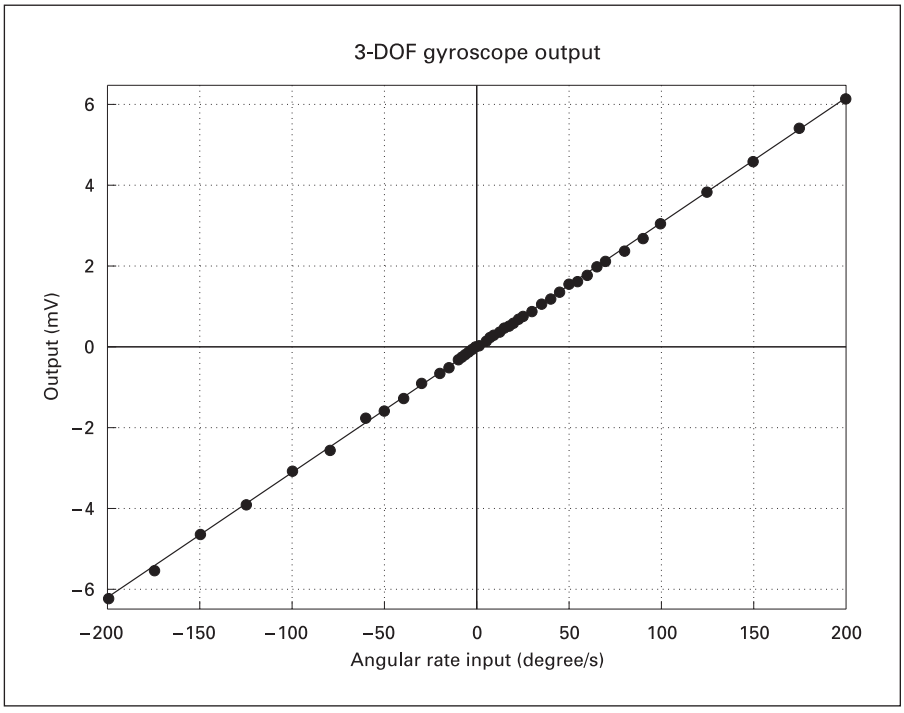

Fig. 3. A MEMS gyroscope's voltage output as a function of angular rate input.

characteristics. The device operates in air and does not require vacuum packaging. Figure 3 shows this MEMS gyroscope's linear response in DC voltage as a function of the angular rate input. The gyroscope has a sensitivity of 0.0694 mV/degree/s and a noise floor of 0.211 mV/$\sqrt{}$Hz at a 50-Hz bandwidth, yielding a resolution of 3.05°/s/$\sqrt{}$Hz at the same bandwidth.

The MEMS gyroscope can sense any type of angular rotation (constant or nonconstant rotational rate), while the natural vestibular organ only responds to the angular acceleration. To mimic the natural organ, a circuit differentiates the output voltage of the gyroscopes to produce a signal proportional to the angular acceleration. To minimize the effect of high-frequency noise without affecting the input motion signal, which is usually less than 10 Hz, a 3030-Hz low-pass filter is used prior to the differentiator [Liu et al., 2003].

Pulse Generator

The pulse generator consists of a transfer function unit emulating the dynamics of the natural vestibular organ. It uses a high-order transfer function, described by two zeros and three poles, to encode angular acceleration by increasing or decreasing the firing rate from the spontaneous rate of the vestibular nerve. The transfer function is modeled as a linear torsion-pendulum system [Steinhausen, 1931; von Egmond et al., 1949]. In this model, the cupula and endolymph are treated as a heavily damped, second-order linear system, where the cupula angular deflection $\varepsilon(t)$ is related to angular acceleration $\alpha(t)$ by the following differential equation:

$$\Theta\frac{d^2\varepsilon(t)}{d^2t}+\Pi\frac{d\varepsilon(t)}{dt}+\Delta\varepsilon(t)=\Theta\alpha(t) \quad (2)$$

where $\tau_1 = \Pi/\Delta$ and $\tau_2 = \Theta/\Pi$ are two time constants defined by morphology and material properties of the vestibular end-organ [Groen, 1956].

Furthermore, the relationship between the input angular acceleration and the overall change in firing rate of neurons is described by:

$$H(s)=\frac{\tau_A s}{1+\tau_A s}\frac{1+\tau_L s}{(1+\tau_1 s)(1+\tau_2 s)} \quad (3)$$

where τ_1 and τ_2 are time constants of the pendulum model described above, τ_A is related to the level of neuron adaptability, and τ_L is the dynamical-electrical time constants. Fernandez and Goldberg [1971] estimated: τ_1 = 5.7 s, τ_2 = 0.003 s, τ_A = 80 s, and τ_L = 0.049 s.

We use three operational amplifiers in serial to implement the transfer function relating the input angular acceleration to the firing rate of the vestibular nerve fibers. The input to the pulse generator is the voltage signal cor-

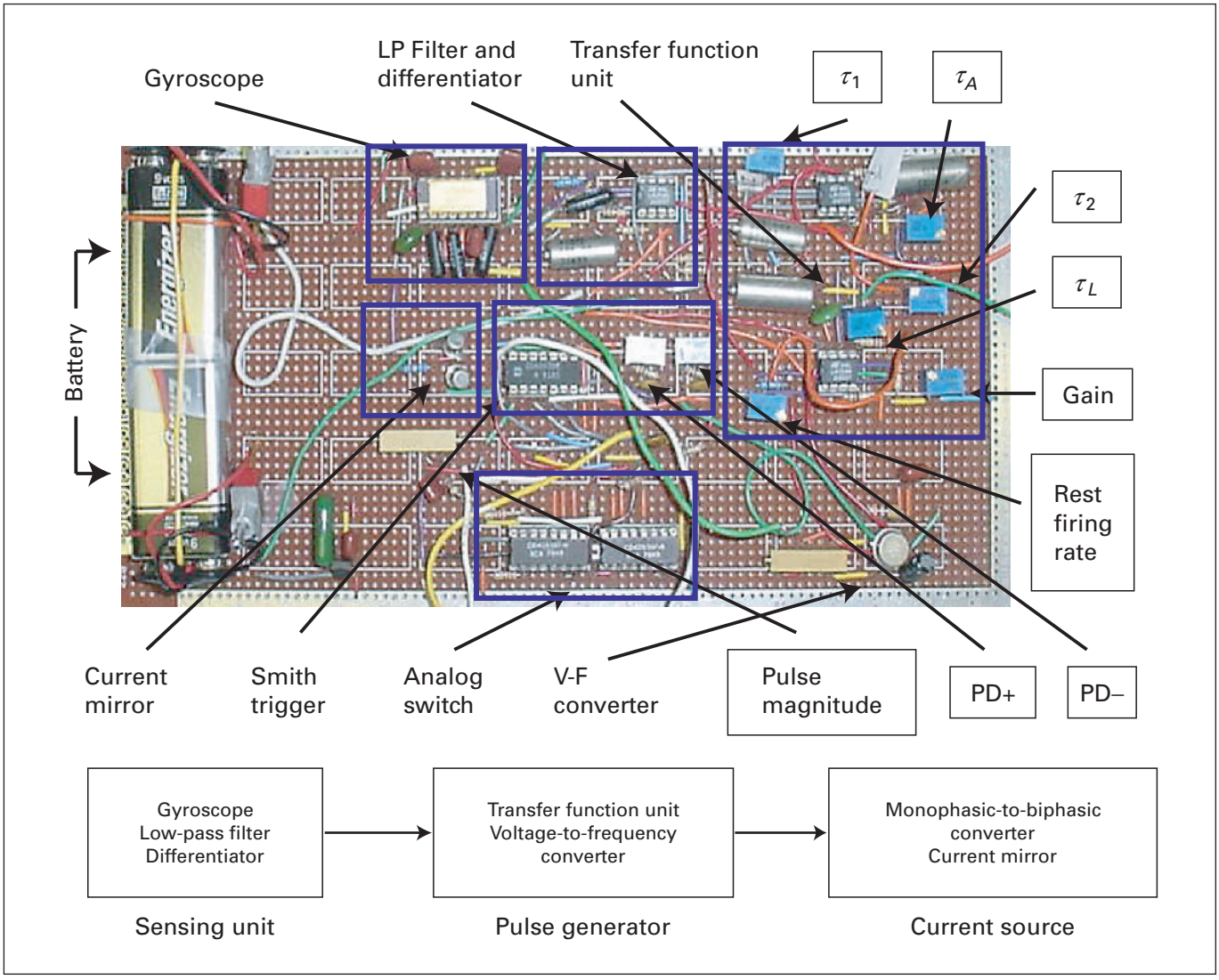

Fig. 4. A printed circuit board prototype of the electronic unilateral semicircular canal prosthesis. The dimension is ~12 × 24 cm^2.

responding to angular acceleration, and the output is the pulse train with its rate being equal to the firing rate estimated from the animal model.

Current Source

To provide effective and safe electric stimulation, the monophasic voltage signal has to be converted into a biphasic current signal [McCreery et al., 1990; Scheiner et al., 1990]. Similar to cochlear implants, the vestibular implant will likely have great individual variability in threshold and dynamic range [Zeng and Galvin, 1999]. Therefore, the electric parameters, including pulse rate, pulse amplitude, and pulse duration, have to be dynamically and individually adjusted. In our implementation, the shortest pulse duration is set at 1 ms. Therefore, the maximum rate can be set close to 500 Hz, doubling the maximum rate of 250 Hz used in a previous study [Gong and Merfeld, 2002].

Printed Circuit Board Prototype

Figure 4 shows such a vestibular prosthesis prototype implemented in a printed circuit board. The sensing unit is a z-axis gyroscope, followed by a low-pass filter and a differentiator. The pulse generator includes a transfer

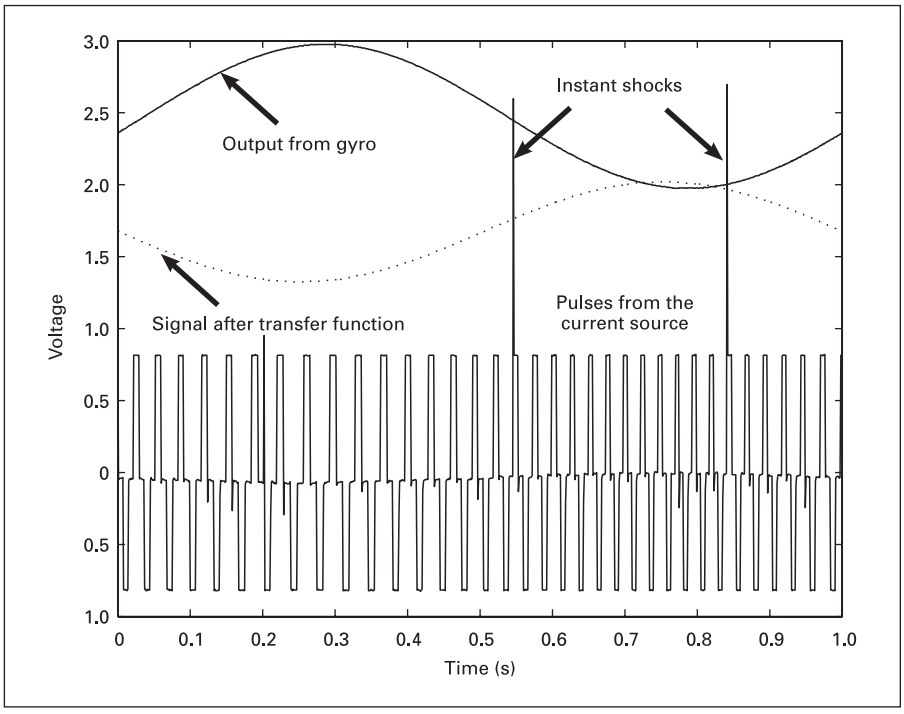

Fig. 5. Electronic evaluation of the vestibular prosthesis. The solid line shows the output of the MEMS gyroscope. The dotted line shows the output of the pulse generator. The pulses are the current source's output, corresponding to the output of the pulse generator (note the greater inter-pulse interval between 0.2 and 0.3 s than between 0.7 and 0.8 s).

function unit and a voltage-to-frequency converter. The current source includes Smith triggers, analog switches and a current mirror. Two 9-volt batteries are used as a power supply for the prototype circuitry and the sensor. Nine potentiometers are utilized to adjust for the resistance parameters, including four time constants in the transfer function (τ_1, τ_2, τ_A, and τ_L), the gain of the transfer function, spontaneous firing rate, pulse amplitude, and duration of both positive and negative phases for the biphasic pulses.

Electronic Evaluation

We have evaluated electronic performance of the vestibular prosthesis prototype against the experimentally obtained results in a squirrel monkey model [Fernandez and Goldberg, 1971]. In their experiment, the animal was mounted in a structure so that the center of the head was coincident with the axis of rotation and the horizontal canal was in the horizontal plane. Sinusoidal rotations with a frequency of 0.1–8 Hz were sequentially applied and responses of the vestibular nerve in terms of the firing rate were monitored and recorded. In our experiment, the prosthesis prototype was placed on a rate table, moving under the same rotational conditions as those reported in Fernandez and Goldberg [1971].

Figure 5 shows a segment of the prosthesis response to inertial stimuli in real time. The continuous line (top trace) is the output of the sensing unit (gyroscope), which accurately reflects the sinusoidal rotation input of the rate table. In this example, the rotation input frequency is 1 Hz and acceleration amplitude is 250°/s^2. The dotted line (second trace) is the analog signal reflecting the output of the transfer function in the pulse generator. The value of this analog signal is used to generate a corresponding pulse rate. Note the apparent phase difference between the gyroscope's output and the pulse generator's output. In this example, the biphasic current pulses generated by the prosthesis dynamically varied from a maximum of 50 spikes/s to a minimum of 30 spikes/s, with a spontaneous rate of 40 spikes/s. We should note that both the spontaneous firing rate and the sensitivity (setting the maximum and the minimum firing rates) can be easily adjusted, should this adjustment be needed to accommodate individual differences. Finally, occasional instant shocks on top of the pulses may occur as a result of conversion of a digital signal to an analog signal. While adding a capacitor parallel to the load can minimize the potential effect of such shocks on the electrode and tissue, more sophisticated circuit design may be required to eliminate them.

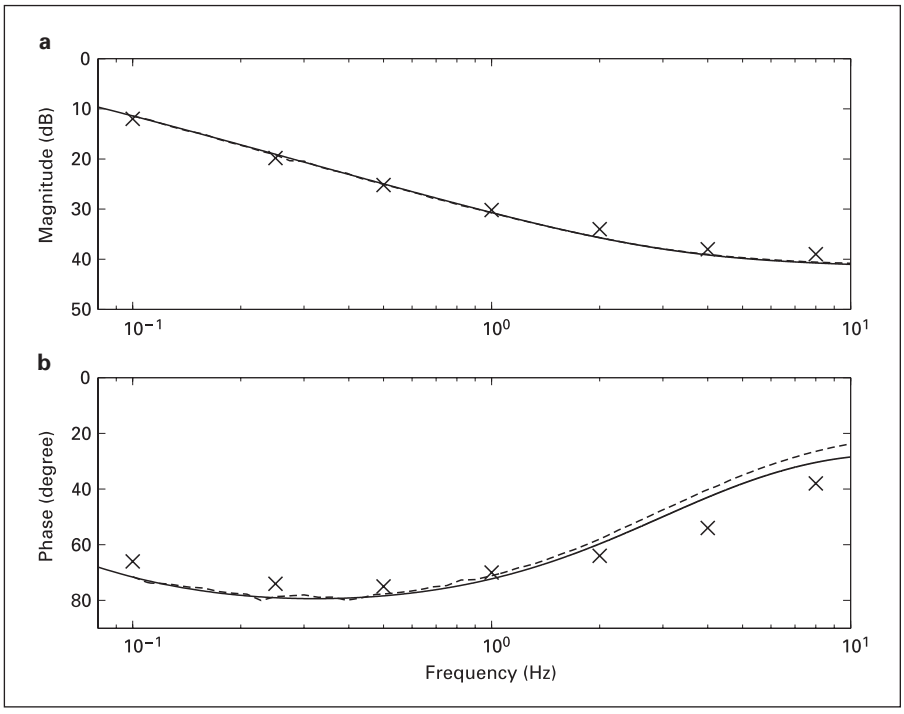

Fig. 6. Magnitude (**a**) and phase (**b**) responses to a sinusoidal stimulus from the actual vestibular nerve fibers in squirrel monkeys [Fernandez and Goldberg, 1971] (crosses), the mathematical model prediction (dashed lines), and the measured output of the present prototype (solid lines). The dashed line is not visible in the magnitude response because the mathematical model prediction totally overlaps with the prototype output.

Figure 6 compares the magnitude (panel a) and phase (panel b) responses for the experimentally obtained data in squirrel monkeys [Fernandez and Goldberg, 1971] (symbols), the mathematical model prediction (dashed lines), and the output of the vestibular prosthesis prototype (solid lines). The dashed line in the magnitude response is not visible because the model prediction is virtually identical to the prototype's output. A comparison is performed for the harmonic angular acceleration with frequencies between 0.1 and 8 Hz. The gain response matches closely for all three sets of data, but the phase response differs slightly, particularly at higher frequencies, reaching 5 degrees between the physiological data and the prototype output at 8 Hz, and 12 degrees between that physiological data and the model prediction at the same frequency. Higher-order models or even nonlinearities simulating the biomechanics of the vestibular end-organ are required to remove this phase difference.

Future Direction

This paper describes the design, implementation and evaluation of an electronic prosthesis mimicking the dynamic function of a unilateral semicircular canal. The encouraging preliminary results have demonstrated the technical feasibility of combining MEMS gyroscopes and analog circuits to reproduce a natural vestibular system's dynamic response to unilateral rotational movement.

The present architecture enables the use of the surface mount hybrid techniques, which can reduce the size of the overall system and potentially implement them on a single chip. Power consumption can also be reduced using the custom-integrated MEMS gyroscope and low-power analog circuitry. Figure 7 shows the conceptual design of a totally implantable version for the next generation of the vestibular prosthesis. A three-axis MEMS gyroscope will be integrated with control and signal conditional electronics on a silicon substrate encapsulated in a vacuum environment (panel a). The same silicon structure will support a stimulating electrode at each end and provide multiple feedthroughs (panel b). Wireless communication capabilities, wireless gain adjustment capabilities, and wireless power supply will be integrated and housed in a glass capsule. The glass capsule will be electrostatically bonded to the substrate to provide hermetic sealing for protection of the receiver circuitry, sensor, and hybrid elements from body fluids.

We should also note that successful implementation of the vestibular prosthesis not only requires innovative engineering solutions but also novel surgical approaches.

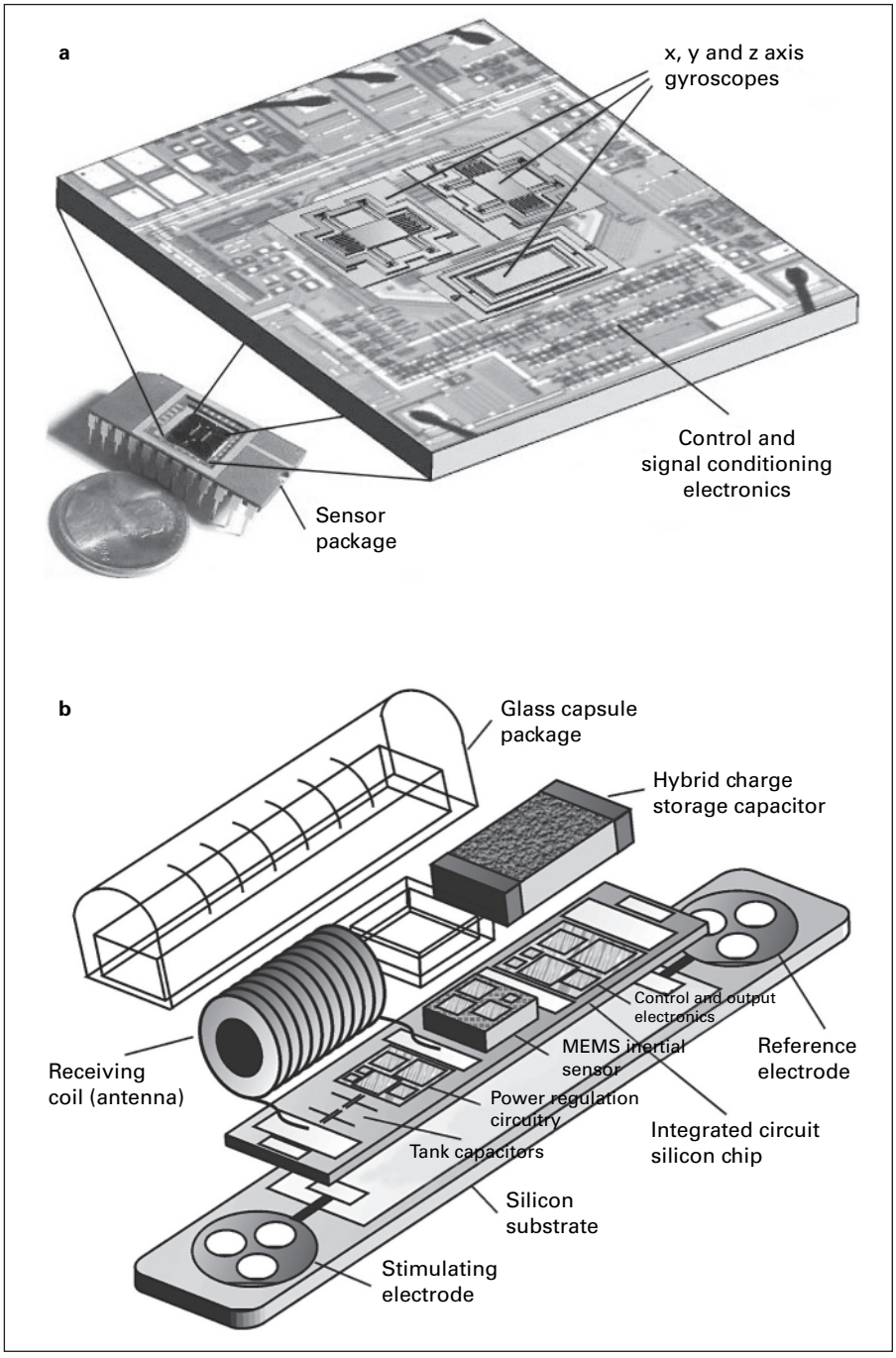

Fig. 7. a Conceptual illustration of the final inertial measurement unit with integrated electronics. **b** Structure of the totally implantable vestibular prosthesis showing the silicon substrate, receiver circuitry, 6-DOF inertial sensors, vacuum packaging cup, and glass capsule.

The implantation procedures and interface with vestibular nerves should minimize the risk of injury to and stimulation of the adjacent facial nerves. In addition, vestibular implantation should not interfere with hearing. An important next step is to demonstrate both the technical and surgical feasibilities of the present vestibular prosthesis prototype in a live animal model.

Acknowledgments

The authors would like to acknowledge Cenk Acar for his contribution in the development of the MEMS gyroscope and Jiayin Liu for her work on the implementation of the pulse generator and current source. We thank Hongbin Chen, Abby Copeland, and two anonymous reviewers for their helpful comments on an earlier version of the manuscript. This project was partially supported by NSF CAREER award CMS-0449442 and NIH RO1 DC002267.

References

Benson AJ, Hutt EC, Brown SF: Thresholds for the perception of whole body angular movement about a vertical axis. Aviat Space Environ Med 1989;60:205–213.

Curthoys IS: The response of primary horizontal semicircular canal neurons in the rat and guinea pig to angular acceleration. Exp Brain Res 1982;47:286–294.

Della Santina CC, Migliaccio AA, Patel AH: Electrical stimulation to restore vestibular function – development of a 3-D vestibular prosthesis. Proc 27th Annu IEEE Eng Med Biol Conf, Shanghai, September 2005.

Fernandez C, Goldberg JM: Physiology of peripheral neurons innervating semicircular canals of the squirrel monkey. II. Response to sinusoidal stimulation and dynamics of peripheral vestibular system. J Neurophysiol 1971;34:661–675.

Gauchard GC, Gangloff P, Jeandel C, Perrin PP: Physical activity improves gaze and posture control in the elderly. Neurosci Res 2003;45:409–417.

Goldberg JM, Fernandez C: Physiology of peripheral neurons innervating semicircular canals of the squirrel monkey. I. Resting discharge and response to constant angular accelerations. J Neurophysiol 1971;34:635–660.

Goldberg JM, Fernandez C: Vestibular mechanisms. Annu Rev Physiol 1975;37:129–162.

Gong W, Merfeld DM: Prototype neural semicircular canal prosthesis using patterned electrical stimulation. Ann Biomed Eng 2000;28:572–581.

Gong W, Merfeld DM: System design and performance of a unilateral horizontal semicircular canal prosthesis. IEEE Trans Biomed Eng 2002;49:175–181.

Greiff P, Boxenhorn B, King T, Niles L: Silicon monolithic micromechanical gyroscope. Tech Dig 6th Int Conf Solid-State Sensors Actuators (Transducers '91), San Francisco, June 1991.

Groen JJ: The semicircular canal system of the organs of equilibrium. I. Phys Med Biol 1956;1:103–117.

Highstein SM, Rabbitt RD, Holstein GR, Boyle RD: Determinants of spatial and temporal coding by semicircular canal afferents. J Neurophysiol 2005;93:2359–2370.

Lewis RF, Gong W, Ramsey M, Minor L, Boyle R, Merfeld DM: Vestibular adaptation studied with a prosthetic semicircular canal. J Vestib Res 2002;12:87–94.

Liu J, Shkel AM, Nie K, Zeng FG: Circuits with adjustable parameters mimicking the function of the natural vestibular end-organ. Proc 1st Int IEEE EMBS Conf Neural Eng, Capri Island, March 2003.

McCreery DB, Agnew WF, Yuen TG, Bullara L: Charge density and charge per phase as cofactors in neural injury induced by electrical stimulation. IEEE Trans Biomed Eng 1990;37:996–1001.

Minor LB: Physiological principles of vestibular function on earth and in space. Otolaryngol Head Neck Surg 1998;118:S5–S15.

Minor LB: Intratympanic gentamicin for control of vertigo in Meniere's disease: vestibular signs that specify completion of therapy. Am J Otol 1999;20:209–219.

Montandon A: A new technique for vestibular investigation. Acta Otolaryngol 1954;39:594.

Patla AE: Strategies for dynamic stability during adaptive human locomotion. IEEE Eng Med Biol Mag 2003;22:48–52.

Rubinstein JT, Della Santina CC: Development of a biophysical model for vestibular prosthesis research. J Vestib Res 2002;12:69–76.

Scheiner A, Mortimer JT, Roessmann U: Imbalanced biphasic electrical stimulation: muscle tissue damage. Ann Biomed Eng 1990;18:407–425.

Shkel AM: Micromachined gyroscopes: challenges, design solutions, and opportunities. SPIE Annu Int Symp Smart Structures Materials, Newport Beach, March 2001.

Shkel AM, Acar C, Painter C: Two types of micromachined vibratory gyroscopes. Int IEEE Sensors Conf, Irvine, 2005.

Shkel AM, Howe RT: Micro-Machined Angle-Measuring Gyroscope. Oakland, University of California Regents, 2002.

Steinhausen W: Über den Nachweis der Bewegung der Cupula in der intakten Bogengangsampulle des Labyrinthes bei der natürlichen rotatorischen und calorischen Reizung. Arch Ges Physiol 1931;228:322–328.

von Egmond AA, Groen J, Jongkees LBW: The mechanics of the semicircular canal. J Physiol 1949;110:1–17.

Wall C 3rd, Merfeld DM, Rauch SD, Black FO: Vestibular prostheses: the engineering and biomedical issues. J Vestib Res 2002;12:95–113.

Weiland JD, Liu W, Humayun MS: Retinal prosthesis. Annu Rev Biomed Eng 2005;7:361–401.

Zeng FG: Trends in cochlear implants. Trends Amplif 2004;8:1–34.

Zeng FG, Galvin JJ: Amplitude mapping and phoneme recognition in cochlear implant listeners. Ear Hear 1999;20:60–74.

KARGER

ability of the material and the magnetization $M = m/V$ is the magnetic moment (m) per volume of material. All materials are magnetic to some extent and are classified by their susceptibility (χ) to an external magnetic field, where $M = \chi H$. The uniform dispersal of SNP in aqueous solutions is dependent on the magnetic field, susceptibility to that field and also is related to the zeta potential of the particles. For in vivo applications, organic coatings surrounding SNP are used to insure dispersion and prevent aggregation of particles, which would impede transport across cell membranes.

Steric stabilization of SNP solutions can be achieved by polymeric encapsulation. Poly (D,L,-Lactide-co-glycolide, PLGA) is one such (biodegradable) polymer, which can also bind therapeutic moieties [Panyam et al., 2003; Aubert-Pouessel et al., 2004; Bala et al., 2004; Funhoff et al., 2004; Jeong et al., 2004; Jiang et al., 2004; Kumar et al., 2004a, b; Panyam et al., 2004; Prabha and Labhasetwar, 2004; Gupta and Gupta, 2005; Yamamoto et al., 2005]. One procedure used to encapsulate PLGA involves a double-emulsion technique, a water-in-oil emulsion being created, followed by this emulsion being dispersed in water [Gupta and Gupta, 2005]. Previous examples using this technique have been described; however, water-dispersible SNP were used that, in general, seem to have poor SNP dispersion in the polymer. Based on fundamental colloid chemistry principles, an oil-dispersible SNP should have much better dispersion.

Mechanical forces imposed on SNP by external magnetic fields have been used to manipulate tissues in which they reside or are attached [Puig-De-Morales et al., 2001]. Silica-encapsulated SNP chronically implanted into the middle ear epithelium of guinea pigs respond to a sinusoidal electromagnetic field and can oscillate the ossicular chain at displacements comparable to hearing levels [Dormer et al., 2005]. Implantable middle ear hearing devices in various stages of development directly drive the ossicular chain for hearing amplification using piezoelectric, motor or electromagnetic actuators [Dormer, 2003]. However, otologic biomechanical applications of SNP have not yet been made.

Nanotechnology also may prove useful in inner ear medicine with recent better understanding of the pathologies of noise- [Kopke et al., 2002], toxin- [Ravi et al., 1995; Song et al., 1997], inflammatory-, viral- and immune-mediated injury [Adams, 2002; Ryan et al., 2002] and cell death processes [Huang et al., 2000] leading to new treatment approaches [Kopke et al., 2002; Seidman and Van de Water, 2003]. Genetic and trophic factor manipulations have enhanced repair processes of inner ear neurosensory epithelium [Kopke et al., 2001b; Izumikawa et al., 2005]. Also, new methods have been tested for inner ear drug delivery including middle ear perfusion, use of catheters and wicks for round window membrane (RWM), cochlea, and vestibule [Kopke et al., 2001a; Jones et al., 2004; Izumikawa et al., 2005].

Safe, precise delivery of potentially therapeutic molecules remains a current challenge in otology/neurotology. We have been examining a new approach to inner ear drug delivery: SNP being pulled by magnetic forces, carrying a therapeutic payload into the inner ear in minutes. The RWM uniquely serves as portal of entry to cells of interest, i.e. sensory hair cells (HC), supporting cells, neurons, stria vascularis tissues. Small molecules, peptides, proteins, and viruses have been shown to pass through the RWM [Witte and Kasperbauer, 2000; Korver et al., 2002; Suzuki et al., 2003; Wang et al., 2003]. However, the passage of these molecules can be inefficient and highly variable [Juhn et al., 1988; Hoffer et al., 2001]. Additionally, most of these experiments involving passage of larger molecules through RWMs have been done in small animals, but humans have RWMs that are five to six times thicker than these animal models. Therefore, the larger molecules may not traverse the thick human RWM without the use of additional forces. The purposes of the preliminary studies reported here were to determine the feasibility of driving SNP and a payload across the RWM and the feasibility of driving the ossicular chain at a useful level with SNP embedded into the ossicular epithelium using externally applied magnetic forces. Our initial results with in vitro modeling, organotypic culture modeling, in vivo studies, and evaluation with fresh human temporal bones suggest the following: (1) SNP can be pulled through a tripartite in vitro membrane model, living guinea pig and rat RWM, and fresh cadaver RWM in less than 60 min by a magnetic force of ~0.3 tesla; (2) the magnetic gradient-forced transport supersedes diffusion or active forces of RWM transport; (3) SNP and PLGA particles appear biocompatible to inner ear tissues and to the RWM; (4) a payload has also been transported across the RWM in vivo, and (5) a sinusoidal magnetic field applied to implanted SNP resulted in ossicular displacements comparable to 90 dB SPL.

Materials and Methods

Synthesis of Nanoparticles

Our initial synthesis of magnetite (Fe_3O_4) utilized a procedure modified from Massart [Massart, 1981; Lian et al., 2004] in which the magnetite was prepared in an atmosphere saturated with nitro-

gen [Dormer et al., 2005]. Silica was tested as a biocompatible encapsulant for the magnetite and as a means to prospectively add both steric stabilization and a surface for derivatization of the particles.

For polymeric encapsulation of SNP into a larger composite nanoparticle, we hypothesized that oleic acid-coated magnetite nanoparticles (Liquid Research Ltd., Bangor, UK) and PLGA (Absorbable Polymers International, Pelham, Ala., USA) could be combined using previously published emulsification chemistry [Gupta and Gupta, 2005]. PLGA nanoparticles were formed using a double emulsion solvent evaporation technique [Prabha et al., 2002]. Following formulation of PLGA nanoparticles, dynamic light scattering (DLS) measurements determined hydrated particle size dispersion (HPP5001 High Performance Particle Analyzer, Malvern Instruments, Malvern, UK). Electron micrographs were taken also to determine particle size (H7600 Transmission Electron Microscope, Hitachi, Pleasanton, Calif., USA).

Electron Spin Resonance Spectroscopy

Aqueous 5,5-dimethyl-1-pyrroline- N-oxide (DMPO) was reacted with activated charcoal and then filtered. A baseline curve was made with DMPO. To determine if silica-coated SNP had reactive iron surfaces, a Fenton-type reaction was performed with 10 m*M* H_2O_2 added to a solution containing the DMPO spin trap and the SNP. Interaction of the SNP with the Fenton system was tested under three conditions: (1) the DMPO spin trap with 10 m*M* H_2O_2; (2) the addition of the SNP to the DMPO + H_2O_2 reaction system above, and (3) a positive control obtained by adding 60 μl of ferrous sulfate to the reaction seen in system 2 above. Spectra were obtained with the basic reaction system with the addition of 60, 180, and 300 μl SNP added to DMPO + H_2O_2, respectively (NanoBioMagnetics Inc., Edmond, Okla., USA).

Cell Growth Kinetics

A cell culture study of particle biocompatibility was performed. Madin-Darby canine kidney epithelial cells (MDCK) were seeded on the mucosal side of a porcine small intestine submucosa (SIS) membrane (Cook Biotech, West Lafayette, Ind., USA) at a seeding density of 4.8×10^5 cells/cm^2. Dextran-coated SNP (Nanomag-D NH2, Micromod, Germany) were added to the growth medium of the MDCK cells (1 mg/ml). Cells were counted at days 1, 2, 3, 5, 7, 9, 11, and 14 using a hemocytometer (Fisher Scientific, Pittsburgh, Pa., USA). On each of these days, cells were counted in 3 separate wells (n = 3).

Organotypic Culture Biocompatibility

Biocompatibility of SNP and PLGA nanoparticles containing SNP was tested using exposure to organotypic cell cultures of Corti's organ. Corti's organ was explanted from postnatal day 3 mouse pups and cultured for 24 h with standard Dulbecco's Modified Eagle's Medium (DMEM) at 37°C in 5% CO_2 similar to previously described methods [Nicotera et al., 2004]. Next the DMEM was replaced with fresh medium containing SNP (100 μg/ml) or PLGA particles with oleic acid-coated SNP embedded (1 mg/ml, 100 μg/ml, 1 μg/ml). That medium was replaced with fresh particle-free DMEM after 48 h. SNP cultures were maintained for 3–7 days (8 cultures for each time point). The PLGA cultures (4 samples at each of the three concentrations) were maintained in culture for an additional 3 days.

On the last day, the tissues were fixed in 4% paraformaldehyde and stained with tetramethylrhodamine B isothiocyanate (TRITC)- or fluoroscein isothiocyanate (FITC)-phalloidin to identify HC, cuticular plates, and stereocilia bundles under a light microscope as previously described [Kopke et al., 1997]. Specimens were mounted in mounting medium for fluorescence (VECTOR H-1000) and examined under a fluorescence microscope (Olympus BX51) with appropriate filter sets (excitation, 540 nm; emission, 573 nm) for TRITC and FITC (excitation, 495 nm; emission, 520 nm). Each explant of Corti's organ was examined in its full length. HC were identified by the bright FITC/TRITC phalloidin staining of the HC stereocilia bundles and cuticular plates, whereas missing HC were identified by the absence of cuticular plates and stereocilia bundles and the formation of supporting cell scars.

Magnetic Transport – in vitro RWM Model

Figure 1a illustrates our in vitro RWM model, a tripartite cell culture membrane constructed and cultured as previously described except that MDCK and fibroblasts were used instead of smooth muscle and urothelial cells [Zhang et al., 2000]. First, epithelial cells (MDCK) were cultured on one side of a small intestine submucosal membrane (Cook Biotech, West Lafayette, Ind., USA). Next, SWISS 3T3 fibroblasts were cultured on the contralateral side of the SIS membrane and allowed 2 days to penetrate the membrane. MDCK were then cultured on the free membrane surface and allowed 5 days to become confluent, as confirmed by measuring increased transmembrane electrical resistance (Epithelial Volt-Ohmmeter, WPI Inc., New Haven, Conn., USA) across the membrane until a peak in resistance was measured on day 4 before conducting the experiments.

Solutions of dextran-coated SNP clusters, 130 nm average diameter, or PLGA-embedded SNP, 160 nm diameter (1 mg/ml concentration) were placed on the upper surface of the RWM model. Individual NdFeB cylindrical magnets (Magstar Technologies) 6.35 × 6.35 mm were positioned so the centers of adjacent magnets were 2 cm apart. A plastic holder (12.8 × 8.6 × 3.1 cm) positioned the magnets directly under the culture wells of a 24-well plate. The magnetic field density measured at the surface of each of these magnets using a gauss meter (Model 5080, SYPRIS, Orlando, Fla., USA) averaged 0.41 tesla.

The SIS membranes with cultured cells were harvested at day 7 and fixed in 10% formalin, placed in 3% agar and stored in 10% formalin for subsequent histological sectioning at 4–5 μm. Sections were stained with Masson's trichrome (fig. 1b) and observed under light microscopy for signs of toxicity and positions of SNP en passage through the RWM. Transmission electron micrographs were taken on the fluid under the culture well inserts to verify magnetic gradient-forced transport of SNP across the RWM model.

Magnetic Transport – in vivo RWM Models

Adult Sprague-Dawley rats (n = 8) or albino guinea pigs (*Cavia porcellus*; n = 3) (Harlan, Indianapolis, Ind., USA) were anesthetized with a ketamine/xylazine ratio of 100/10 mg/kg for rats and 70/7 mg/kg for guinea pigs, i.m. The bulla was opened to expose the RWM. SNP, either dextran-coated 130-nm clusters of 20–30 nm (NanomagD, Micromod GmbH, Rostock, Germany) or silica-coated, 20–30 nm in diameter from our own synthesis, or PLGA-embedded SNP 160 nm in diameter (1 mg/ml) were placed in the RWM niche (1 μl for rats, 3 μl for guinea pigs). The RWM of the experimental ear was positioned horizontally facing upwards

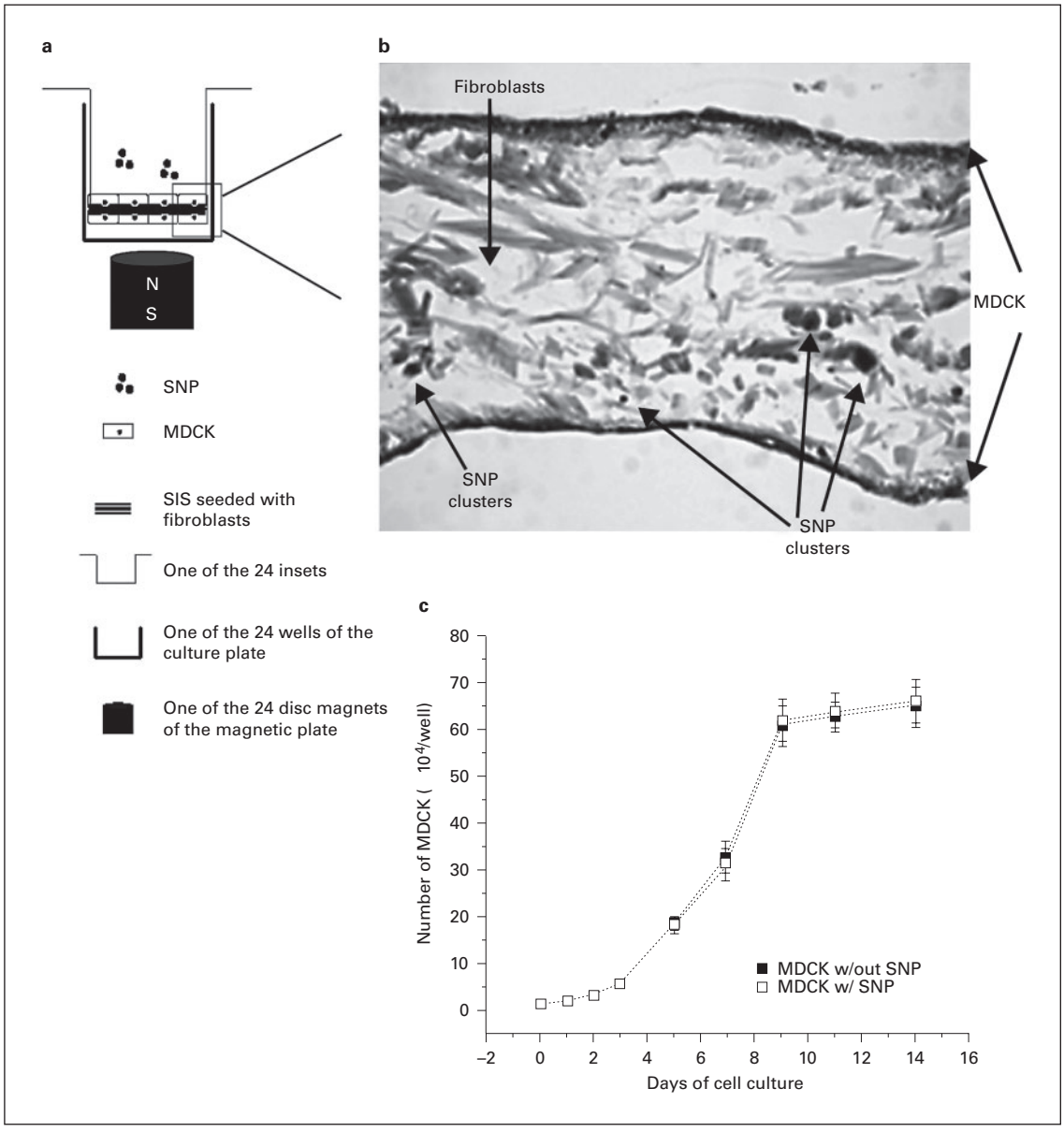

Fig. 1. a Schematic representation of 3 layers in the RWM model: a layer of fibroblasts sandwiched between 2 layers of MDCK cells. The diagram also shows the magnetic delivery system, a NdFeB magnet positioned under individual culture plate wells allowing for translational pulling of SNP across the membrane. **b** Photomicrograph of a cross-section of the RWM model showing stages of translational movement of the SNP. The cross-section shows MDCK cells on both sides of the SIS membrane and fibroblasts seeded within the SIS membrane. The SNP movement was captured on day 5 of cell culture. **c** Biocompatibility indicator growth plot showing that SNP (dextran-coated SNP, 1 mg/ml) have no effect on cell proliferation in MDCK cell culture. The cells were counted on days 1, 2, 3, 5, 7, 9, 11 and 14 of culture. Error bars represent standard deviation.

and the animal placed on the center surface of a 4-inch cube NdFeB48 magnet (Magnetic Sales, Culver City, Calif., USA). The distance from the RWM to the magnet pole face was 2.5 cm for rats and 3 cm for guinea pigs providing ~0.3 tesla for 20 min. The remaining SNP solution was then aspirated from the niche and replaced with a fresh solution (process was repeated two times for 60 min total exposure). Control animals went through the same protocol but without the magnetic field. The area of the basal turn and the apex, but not the RWM niche, was irrigated and aspirated dry. The bony wall on the basal turn of the cochlea was thinned

using an 18-gauge needle and a small hole made. A 30-gauge blunt-tip needle was inserted to the basal turn of the cochlea, and perilymph (10 μl for rats, 16 μl for guinea pigs) was withdrawn and saved for transmission electron microscopy (TEM). Fresh needles, syringes, and tubing were used for perilymph aspirations. The RWM was removed after fixation and also prepared for TEM.

The perilymph collected was washed twice with double-distilled water on a magnet to remove the salt content. The resulting 5-μl liquid was examined with TEM for nanoparticles. A small drop was put on glow-discharged formvar- and carbon-coated copper on nickel mesh grids. Samples were allowed to settle for 30 s, then wicked and rinsed 4 times with one drop of distilled/deionized water. RWM tissues were first rinsed in 0.1 *M* cacodylate buffer, then dehydrated through a series of acetones and finally rinsed in propylene oxide. After going through a series of propylene oxide/resin exchanges, samples were embedded in 8/2 resin. Transverse sections, 90 nm thick, were cut and put on 400 mesh copper grids that were glow discharged. Both perilymph and RWM samples were examined by TEM (H7600, Hitachi, Pleasanton, Calif., USA), and 2K × 2K digital images were taken (Megaplus ES 3.0, Advanced Microscopy Techniques, Danvers, Mass., USA). For each perilymph sample an average of 20 meshes from 2 grids were examined for nanoparticles. For RWM samples, 4 grids from each membrane sample were examined.

In order to quantify our observations for the guinea pig in vivo transport experiment, a 5-μl drop of control or magnet-exposed guinea pig perilymphatic fluid from a total of 2 animals was placed on the formvar grid. The particles evenly disperse and do not aggregate in fluid (data not shown). Fifteen randomly selected fields were observed and fifteen images were taken at 5000 × magnification, similar to figure 2g and i. The number of observed particles on each photograph was counted and compared between control and experimental samples. A two-tailed Student's t test was used to determine if the particle count means between the two samples were statistically different.

Magnetic Transport – Human Temporal Bone

SNP synthesized by NanoBioMagnetics Inc. were suspended in normal saline (0.2 mg/ml) and 5.5 μl was placed in the round window niche of human fresh frozen temporal bones (n = 2). Bones were placed approximately 1 inch from the pole face of a 4-inch cube NdFeB magnet external to the skull with the RWM parallel to the pole and exposed to approximately 0.3 tesla for 20 min. Next, the residual solution was removed from the niche and the procedure repeated twice for a total magnetic exposure of 60 min. After copious irrigation of the cochlear surface a cochleostomy was performed and 15 μl of perilymph aspirated using a 27-gauge needle and microsyringe for identification of SNP that were transported across the RWM. The same protocol was followed on a control temporal bone (no magnetic field). Both conventional TEM and electron energy loss spectroscopy (EELS) of particles prepared on formvar grids as previously described [Mamedova et al., 2005] were used to locate SNP in the sampled perilymphatic fluids. Conventional TEM techniques were used to locate approximately 10-nm electron dense spheres and confirm their elemental composition using the EELS feature searching at 708 eV for the iron L electron shell. The energy filtering option on the TEM microscope (CEM 902, Zeiss, Oberkochen, Germany) was used to photograph the iron-containing nanoparticles.

Ossicular Movements

SNP were silica coated and the silica surface was derivatized by the attachment of amino groups using 3-aminopropyltrimethoxysilane for conjugation with FITC [Dormer et al., 2005]. Intracellular location of fluorescent nanoparticles was subsequently done using scanning confocal microscopy. Guinea pigs were anesthetized and implanted with a sterile saline solution (50–75 μl) of SNP sonicated 3–4 min before placement either on the lateral wall of the surgically exposed incus (n = 9) or on the tympanic membrane (n = 2).

Each animal's head was laid on the pole face of a 4-inch cube NdFeB magnet (~0.30 tesla), the implanted ear facing up. Three aliquots of SNP were sequentially placed on the epithelium, then exposed to the magnet for 20 min. The animals recovered for 8–15 days and then were again anesthetized for laser Doppler single point interferometry measurements of velocity and conversion into displacements (Models OFV501 and 3000, Polytec PI, Tustin, Calif., USA) in response to an electromagnetic field. In a recumbent position, the incus was again exposed, and a 1 × 1-mm piece of reflective tape placed at the implant site. Interferometry measurements were made in response to a 6.5-mH coil activated at 500 or 1000 Hz, 5–8 V peak-to-peak (Model 80 Function Generator, Wavetek, San Diego, Calif., USA; Model 2706 Precision Amplifier, Bruel & Kjaer, Denmark).

Histological confirmation of the SNP implants was made by first decalcifying the incus, followed by transverse sectioning of the epithelium at 5 μm and observation using laser scanning confocal microscopy (Model TCS SP2, Leica, Mannheim, Germany).

Animal Care and Use

The experimental protocols were approved by the Institutional Animal Care and Use Committee, University of Oklahoma HSC. The study was performed in accordance with the Public Health Service Policy on Human Care and Use of Laboratory Animals, the National Institutes of Health Guide for the Care and Use of Laboratory Animals, the Animal Welfare Act and the principles of the Declaration of Helsinki.

Results

Synthesis of Nanoparticles

Figure 2a shows a TEM of PLGA particles. The PLGA particles had an average size of 99 ± 44 nm which was comparable with a size of 175 nm and a polydispersity index of 0.045 from DLS. Figure 2b shows a TEM of oleic acid-coated SNP incorporated into the PLGA microparticles. These particles had an average size of 85 ± 32 nm. The average size of the particles as measured via DLS was ~180 nm with a polydispersity index of ~0.1. The oleic acid-coated SNP appeared to range in size from 5 to 15 nm and incorporation of the SNP did not influence the size of the PLGA particles. As can be seen in figure 2c, the SNP have slightly aggregated together inside the polymer. This aggregation is most likely a result of the sonication process and not an artifact of evaporat-

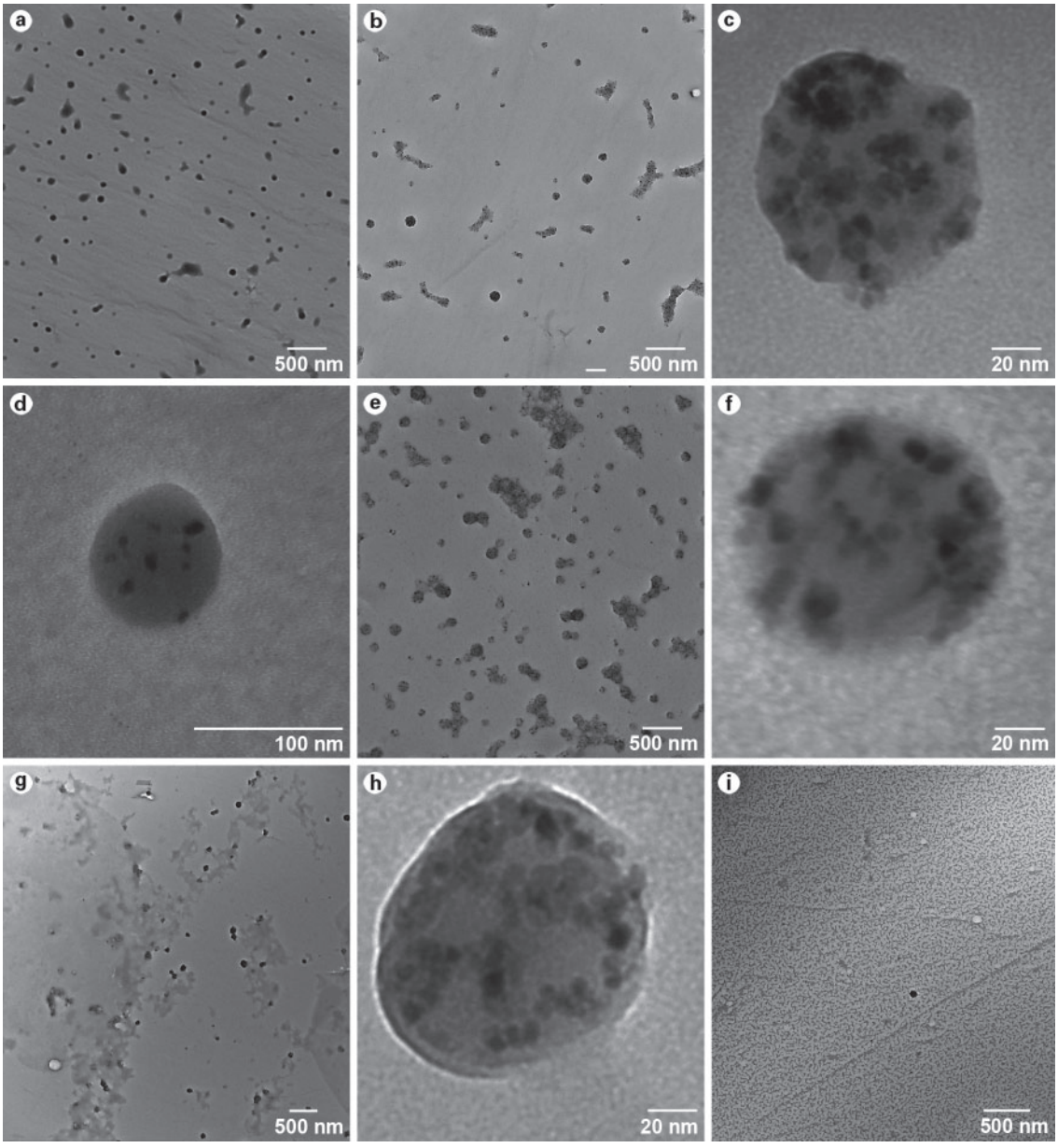

Fig. 2. TEM. **a** PLGA particles. Magnification 7000×. **b** PLGA particles with magnetite incorporated inside. Magnification 8000×. **c** PLGA particles with magnetite incorporated inside. Magnification 100000×. **d** PLGA particles made with a lower concentration of oleic acid-coated magnetite. Magnification 80000×. **e** PLGA particles with magnetite after passing through the RWM model. Magnification 7000×. **f** PLGA particles with magnetite after passing through the RWM model. Magnification 70000×. **g** PLGA particles with magnetite after passing through the RWM of a guinea pig. Magnification 5000×. **h** PLGA particles with magnetite incorporated inside from guinea pig perilymph. Magnification 100000×. **i** TEM of perilymphatic fluid from animal without magnet exposure demonstrating very few particles.

ing the particles on the TEM plate. The oleic acid-coated SNP embedded in the PLGA were not freely mobile. Thus aggregation of the magnetite is not expected when the particles are dried on the TEM grid. When a lower concentration of magnetite was used (1 vs. 5 mg/ml) in the formation of the PLGA microparticles, fewer magnetite particles were incorporated into the polymer and did not aggregate (fig. 2d).

Figure 2e, f shows TEM images of the magnetite-containing PLGA after having passed through the RWM model. TEM of a solution control experiment where no magnetic forces were employed demonstrated no particles in multiple TEM fields. In perilymphatic fluid samples from animals exposed to magnetic forces numerous particles were observed in multiple TEM fields as shown in figure 2g, h, whereas there were very few particles seen in fluid from animals not exposed to magnetic forces (fig. 2i). Quantitatively, the mean number of particles for the experimental (magnet exposed) sample was 51.2 ± 13.1 particles per photograph and the mean particle count for the control (no magnet exposure) samples was 1.8 ± 1.8 ($p < 0.001$).

Biocompatibility

ESR studies of silica-coated paramagnetic nanoparticles in a Fenton system revealed no evidence of free iron in the silica-encapsulated nanoparticles. There was no spectral evidence of free radical activity, supporting that the silica encapsulation of the nanoparticles prevented iron exposure and generation of free radicals.

As can be seen in figure 1c, the cell growth kinetics curve for MDCK cells grown in culture on SIS membranes was identical for cells cultured without particles or cells cultured with a concentration of 1 mg/ml of Nanomag-D NH_2 dextran particles.

Application of particles to organotypic cultures of mouse organ of Corti revealed little detectable HC loss or supporting cell scar formation with either the SNP (n = 8 at each time point) or the polymer-encapsulated oleic acid-coated paramagnetic nanoparticles (4 at each concentration). Very little or no HC loss was observed nor were replacement supporting cell scars detected (similar to control cultures not exposed to particles) at the light microscopic level in any of the cultures even at 1 mg/ml concentrations and at the longest time periods of culture. Representative photomicrographs of organotypic cultures are seen in figure 3.

TEM and light microscopy of explanted RWM (fig. 4a–c) and in vitro tripartite SIS membrane (fig. 1b), respectively, revealed no evidence of cell death, necrosis, inflammation or other obvious pathology on initial studies. Similar indicators of biocompatibility were noted for the particles incorporated in the middle ear mucosa of guinea pig ossicles [Dormer et al., 2005].

Magnetic Gradient Transport

A total of 9 SIS membrane inserts, 6 experimental and 3 controls, were utilized to assess magnetic gradient transport with and without magnetic forces. TEM observations detected a large number of SNP with a polymer payload in all 6 experimental inserts as seen in figure 2e, f. On the other hand, in the control membranes without magnetic forces no SNP were detected (data not shown). The concentration of SNP was 10^{12} particles/ml and 100 μl was applied to each insert.

TEM of fresh human cadaveric cochlear aspirate also readily demonstrated the particles of interest, whereas none were seen in the specimens not exposed to magnetic forces. These SNP were rapidly pulled through the human RWM in fresh frozen cadaveric human temporal bone and detected in the inner ear perilymphatic fluid. EELS confirmed that the particles contained iron. Perilymphatic fluid from temporal bones exposed to nanoparticles but no magnetic forces were devoid of these particles (fig. 5a, b).

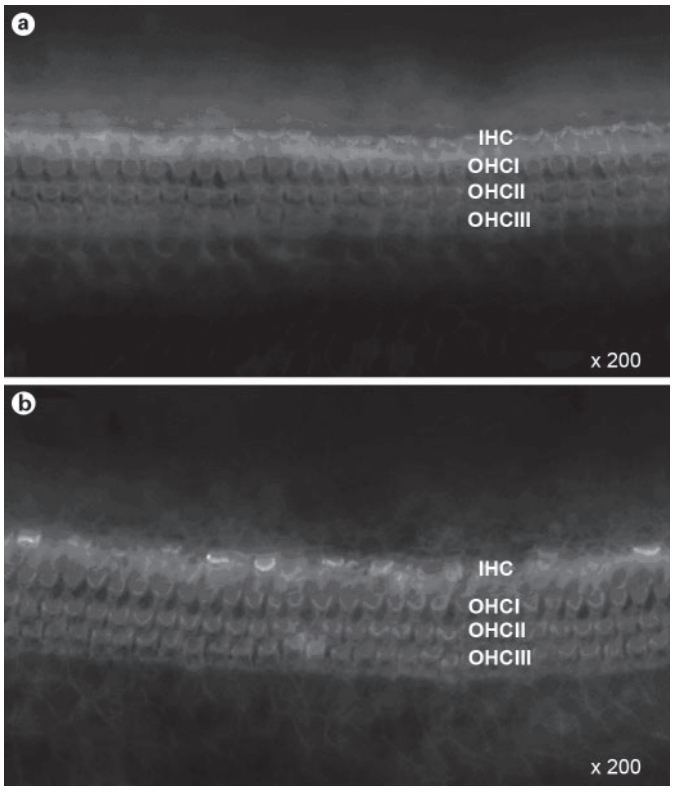

Fig. 3. Representative photomicrograph of cultured organ of Corti from postnatal day 3 mouse pups (5 days in vitro). Three rows of outer HC (OHC) and one row of inner HC (IHC) are shown. TRITC-phalloidin staining. **a** Control. **b** PLGA-SNP (1 mg/ml, 48 h) treated. At the light microscopic level, control and particle-exposed cultures all evidenced little, if any, HC loss. Magnification 200×.

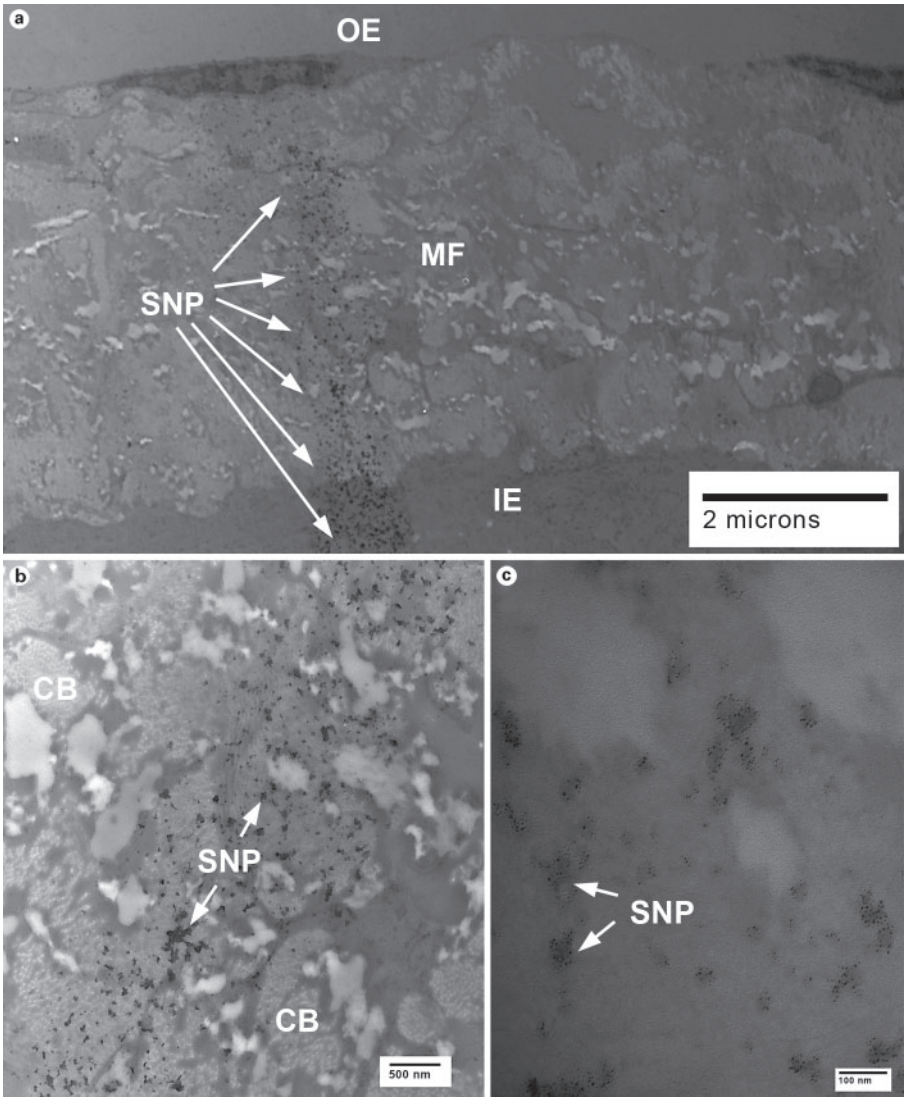

Fig. 4. SNP passing through RWM. TEM image of RWM from a rat exposed to magnet field for 60 min. Particles placed on the RWM in solution were drawn into and through the RWM with a magnetic gradient. Particles from samples from controls not exposed to magnetic forces were found only on the surface of the RWM (data not shown). **a** A low power magnification (1500×) view shows the RWM and SNP passing through three layers of the RWM (outer epithelium, middle fibrous layer, and into inner epithelium). **b** A high power view (6000×) shows the distribution of SNP within the RWM fibrous layer among collagen bundles. **c** A higher power view (40000×) shows the individual dextran-coated SNP clusters in the tissue. OE = Outer epithelium; MF = middle fibrous layer; IE = inner epithelium; CB = collagen bundle.

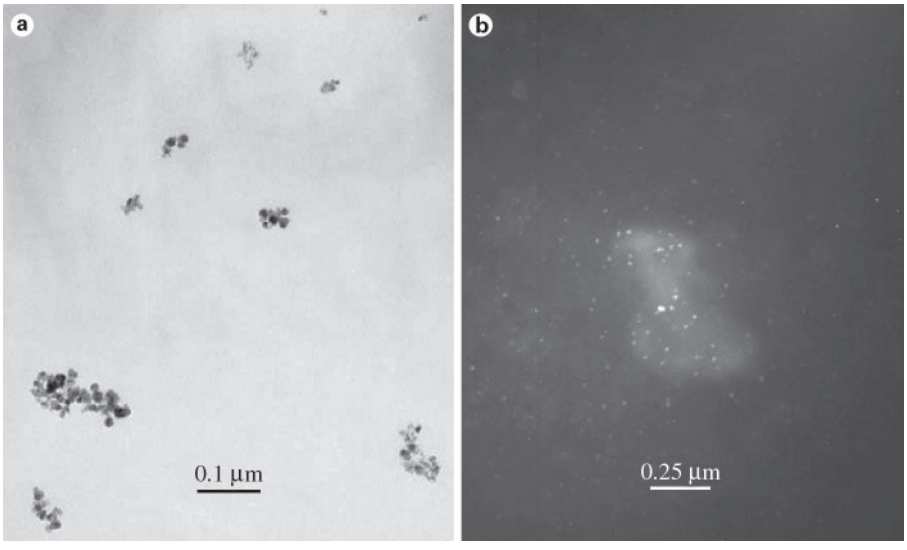

Fig. 5. These magnetic nanoparticles were rapidly pulled through the human RWM along a magnetic gradient in fresh cadaveric human temporal bone and detected in the inner ear perilymphatic fluid. **a** TEM of perilymphatic fluid aspirated from the cochlea of magnet-exposed temporal bone demonstrating particles. Original negative (85000×). **b** EELS confirms that the particles contain iron (bright dots). Perilymphatic fluid from temporal bone exposed to nanoparticles but no magnetic forces was devoid of these particles.

Ossicular Displacement

Silica-coated SNP, average diameter of 16 nm, with a zeta potential of –15 to –20 mV were internalized into epithelia of the tympanic membrane or that covering the incus. The density of SNP at the incus implant site was visible without magnification 8 days following implantation and the FITC-labeled SNP were visible under scanning confocal laser microscopy [fig. 6, 7 in Dormer et al., 2005]. Histopathology revealed no inflammatory response, no giant cells or evidence of apoptosis following 2–15 days of implantation. In this preliminary study, the displacements of the (intact) ossicular chain and tympanic membrane, as measured using single point interferometry, were comparable to 90 dB SPL displacements of the human middle ear [table 1, Dormer et al., 2005]. Frequency doubling occurred as the SNP responded to both polarities of the reversing electromagnetic field. This confirmed the superparamagnetic property of the magnetite SNP.

Discussion

The earliest use of external magnetic field to deliver clinical agents was in 1951, involving catheters for selective angiography. Magnetic microspheres were mostly studied until nanotechnology emerged in the late 1980s. Long-term deposition of iron in vivo is not a toxicity concern, as assessed epidemiologically in miners of hematite whose lung concentrations over lifetimes were 100–1000 times above those produced by drug targeting [Ranney, 1987]. Neither is adverse immunogenetic response a concern as iron is one of the most regulated cellular elements. Today, surface modifications can stabilize SNP in physiological solutions, protect against oxidation, provide functional groups for further derivitization and, in the case of polymeric encapsulation, carry and protect payloads en route to target tissues whereupon biodegradation will release payloads [Neuberger et al., 2005]. Future successes of SNP applications in nanomedicine, like other biomaterials, will be related to the extent of complete physicochemical characterizations (e.g. zeta potential) since surface chemistry dictates cell differentiation [Gupta and Gupta, 2005; Keselowsky and Garcia, 2005].

Middle Ear Biomechanics

For the first time it was shown that SNP, chronically implanted in a tissue, could be used to generate force, although performance data are lacking in this feasibility study [Dormer et al., 2005]. Current implantable middle ear hearing devices (IMEHD) under development or in clinical trials employ active electronic actuators consisting of motors, solenoid type drivers, piezoelectric crystals or magnets driven by an external magnetic field [Huttenbrink, 1999]. Reduced surgical and device risk, lower cost and direct drive benefit may be an advantage of tissue-indwelling, biocompatible SPN. Magnetite nanoparticles caused ossicular displacements in guinea pigs that were comparable to those in human temporal bones in response to a 90-dB SPL sound source. Nevertheless, the mass of the guinea pig ossicular chain is substantially less than in the human and was relatively easy to displace using an external magnetic field. Others have used magnetic particles to exert piconewton forces influencing (bone) cell differentiation [Cartmell et al., 2004]. RGD-coated microparticles bound to integrin receptors on primary human osteoblasts and an external magnetic field oscillated the cells in 2-D monolayer culture or 3-D constructs. Varying load-bearing matrices resulted.

Inner Ear Targeted Delivery

Of the prospective applications in nanomedicine, targeted delivery of therapeutics and enhanced MRI imaging, both utilizing nanoparticulate Fe_3O_4, may have the greatest clinical impact [Shinkai and Ito, 2004]. Delivering therapeutics only to target tissues may reduce both side effects and cost while improving treatment. Targeting of SNP by an external magnetic field had initially been explored for intravascular delivery. However, traversing the RWM provides a unique nanomedicine application where delivery particles will not be removed by reticuloendothelial organs. Like vascular targeting across the endothelium, inner ear delivery is independent of the membrane status and highly dependent on homogeneity of the magnetic field gradient in the target volume.

Substances with limited access to the inner ear may traverse (permeabilize) the RWM carrying a payload of drugs or genes to the inner ear. We have explored this targeted delivery for the first time utilizing SPN [Lee et al., 2004]. Our in vitro RWM model was used to initially identify candidate SNP for optimal targeted delivery to the inner ear (fig. 1a–c). In vivo testing in rat and guinea pig subsequently validated the RWM model, and we are currently refining the payload release from the biodegradable PLGA in perilymph. The model served to emulate the human RWM, penetrable to SNP, using external magnetic forces. Our results showed that cluster type aggregates (130 nm) containing 10 nm SPN were biocompatible and might be considered as carriers for therapeutic substances or as nonviral vectors for gene therapy. There

was no observable effect of the SPN on growth and proliferation of human epithelial cells in culture. The SPN crossed the tripartite RWM model much more rapidly than diffusion because of the forces from an external magnetic field. It is not surprising that a small number of particles were detected in perilymph of a guinea pig not exposed to magnetic forces since these particles are small enough to diffuse through the RWM or to be transported through active processes. However, the particles were much more evident after exposure to a magnetic gradient. Future studies are aimed at gathering additional quantitative information.

PLGA nanospheres have been used previously as nonviral vectors of DNA and other biologically active compounds. Labhasetwar and others tested biodegradable nanoparticles (~200 nm) consisting of PLGA and PVA [Panyam et al., 2002, 2004; Sahoo et al., 2004]. Particles have been loaded with wt-p53 plasmid DNA that transfected a breast cancer cell line [Prabha and Labhasetwar, 2004]. Sustained gene expression resulted from the slow intracellular release of the encapsulated DNA. Cellular uptake of PLGA particles 10–800 nm in diameter was confirmed by fluorescence of 6-coumarin and confocal microscopy [Qaddoumi et al., 2004]. Endocytosis appears to be involved in internalization and cationic surface treatment is facilitatory. PLGA nanoparticles (<200 nm) coated with a PVA-chitosan blend produce a cationic shell with the ability to electrostatically bind DNA to a nanosphere [Kumar et al., 2004a, b].

Therapeutic Perspectives

Inner ear medicine represents an expanding field that will benefit from improved targeted delivery strategies for a wide range of therapeutic small molecules, peptides, proteins, oligonucleotides and larger molecules containing genetic information. With the growing understanding of the molecular basis for traumatic, toxic, ischemic, inflammatory, infectious, and degenerative pathologies of the inner ear, specific efficient targeted delivery of mechanism-based therapeutics appears promising. In addition, plasmid gene delivery through an efficient, minimally invasive, safe method may increase the possibility of clinical auditory HC replacement with restoration of hearing. Here, in preliminary studies using materials comparable to those FDA approved and used clinically [Shinkai and Ito, 2004], we have demonstrated that readily achievable magnetic gradients can be created to enhance the delivery of paramagnetic nanoparticles with a biodegradable polymer payload into the mammalian inner ear.

Acknowledgements

Gratitude is expressed to Eric Howard, Associate Professor of Cell Biology, OUHSC, for his invaluable assistance in these ongoing studies.

This study was partially funded by The Shulsky Fund for Medicine and Research, New York City (via the Oklahoma City Community Foundation), the National Institute for Deafness and other Communicative Disorders (SBIR DC05528-01), the Office of Naval Research and INTEGRIS Baptist Medical Center, Oklahoma City.

K.J.D. and D.G. are stockholders in NanoBioMagnetics Inc.

References

Adams JC: Clinical implications of inflammatory cytokines in the cochlea: a technical note. Otol Neurotol 2002;23:316–322.

Aubert-Pouessel A, Venier-Julienne MC, Saulnier P, Sergent M, Benoit JP: Preparation of PLGA microparticles by an emulsion-extraction process using glycofurol as polymer solvent. Pharm Res 2004;21:2384–2391.

Bala I, Hariharan S, Kumar M: PLGA nanoparticles in drug delivery: the state of the art. Crit Rev Ther Drug Carrier Syst 2004;21:387–422.

Cartmell S, Magnay J, El Haj A, Dobson J: Use of magnetic particles to apply mechanical forces for bone tissue engineering purposes. Int Conf Fine Particle Magnetism, London 2004, pp 41–42.

Dormer KJ: Implantable electronic otologic devices for hearing restoration; in Finn WE, Lopresti PG (ed): Handbook of Neuroprosthetic Research Methods. Boca Raton, CRC Press, 2003, pp 237–261.

Dormer K, Seeney C, Lewelling K, Lian GD, Gibson D, Johnson M: Epithelial internalization of superparamagnetic nanoparticles and response to external magnetic field. Biomaterials 2005;26:2061–2072.

Funhoff AM, van Nostrum CF, Lok MC, Fretz MM, Crommelin DJA, Hennink WE: Poly(3-guanidinopropyl methacrylate): a novel cationic polymer for gene delivery. Bioconjug Chem 2004;15:1212–1220.

Gupta AK, Gupta M: Synthesis and surface engineering of iron oxide nanoparticles for biomedical applications. Biomaterials 2005;26:3995–4021.

Hoffer ME, Allen K, Kopke RD, Weisskopf P, Gottshall K, Wester D: Transtympanic versus sustained-release administration of gentamicin: kinetics, morphology, and function. Laryngoscope 2001;111:1343–1357.

Huang T, Cheng AG, Stupak H, Liu W, Kim A, Staecker H, Lefebvre PP, Malgrange B, Kopke R, Moonen G, Van de Water TR: Oxidative stress-induced apoptosis of cochlear sensory cells: otoprotective strategies. Int J Dev Neurosci 2000;18:259–270.

Huttenbrink KB: Current status and critical reflections on implantable hearing aids. Am J Otol 1999;20:409–415.

Izumikawa M, Minoda R, Kawamoto K, Abrashkin KA, Swiderski DL, Dolan DF, Brough DE, Raphael Y: Auditory hair cell replacement and hearing improvement by Atoh1 gene therapy in deaf mammals. Nat Med 2005, advanced online publication.

Jeong JR, Lee SJ, Kim JD, Shin SC: Magnetic properties of Fe_3O_4 nanoparticles encapsulated with poly(D,L-lactide-co-glycolide). IEEE T Magn 2004;40:3015–3017.

Jiang HL, Jin JF, Hu YQ, Zhu KJ: Improvement of protein loading and modulation of protein release from poly(lactide-co-glycolide) microspheres by complexation of proteins with polyanions. J Microencapsul 2004;21:615–624.

Jones GE, Jackson RL, Liu J, Costello M, Ge X, Coleman JKM, Boasen JF, Harper EA, Kuzdak NE, Kopke RD: Three methods of inner ear trophic factor delivery to recover vestibular function and morphology from gentamicin-induced vestibular toxicity in the guinea pig. Abstracts 27th Annu Midwinter Res Meet, Assoc Res Otolaryngol, Daytona Beach, 2004.

Juhn SK, Hamaguchi Y, Goycoolea M: Review of round window membrane permeability. Acta Otolaryngol Suppl 1988;457:43–48.

Keselowsky BG, Garcia AJ: Quantitative methods for analysis of integrin binding and focal adhesion formation on biomaterial surfaces. Biomaterials 2005;26:413–418.

Kopke RD, Coleman JK, Liu J, Campbell KC, Riffenburgh RH: Candidate's thesis: enhancing intrinsic cochlear stress defenses to reduce noise-induced hearing loss. Laryngoscope 2002;112:1515–1532.

Kopke RD, Hoffer ME, Wester D, O'Leary MJ, Jackson RL: Targeted topical steroid therapy in sudden sensorineural hearing loss. Otol Neurotol 2001a;22:475–479.

Kopke RD, Jackson RL, Li GM, Rasmussen MD, Hoffer ME, Frenz DA, Costello M, Schultheiss P, Van de Water TR: Growth factor treatment enhances vestibular hair cell renewal and results in improved vestibular function. Proc Natl Acad Sci USA 2001b;98:5886–5891.

Kopke RD, Liu W, Gabaizadeh R, Jacono A, Feghali J, Spray D, Garcia P, Steinman H, Malgrange B, Ruben RJ, Rybak L, Van de Water TR: Use of organotypic cultures of Corti's organ to study the protective effects of antioxidant molecules on cisplatin-induced damage of auditory hair cells. Am J Otol 1997;18:559–571.

Korver KD, Rybak LP, Whitworth C, Campbell KM: Round window application of D-methionine provides complete cisplatin otoprotection. Otolaryngol Head Neck Surg 2002;126:683–689.

Kumar M, Bakowsky U, Lehr CM: Preparation and characterization of cationic PLGA nanospheres as DNA carriers. Biomaterials 2004a;25:1771–1777.

Kumar M, Mohapatra SS, Kong X, Jena PK, Bakowsky U, Lehr CM: Cationic poly(lactide-co-glycolide) nanoparticles as efficient in vivo gene transfection agents. J Nanosci Nanotechnol 2004b;4:990–994.

Lee SJ, Jeong JR, Shin SC, Kim JC, Chang YH, Chang YM, Kim JD: Nanoparticles of magnetic ferric oxides encapsulated with poly(D,L lactide-co-glycolide) and their applications to magnetic resonance imaging contrast agent. JMMM 2004;272–76:2432–2433.

Lian G, Lewelling K, Johnson M, Gibson D, Dormer K, Seeney C: Fe_3O_4 magnetite nanoparticles coated by silica for biomedical applications. Microsc Microanal 2004;10(suppl 2):3.

Mamedova N, Kopke R, Liu J, Jackson R, Costello M, Gibson D, Dormer K: Feasibility of superparamagnetic nanoparticles for drug delivery to the inner ear. Abstracts 28th Annu Midwinter Res Meet – Assoc Res Otolaryngol, New Orleans 2005.

Massart R: Preparation of aqueous magnetic liquids in alkaline and acidic media. IEEE T Magn 1981;17:1247–1248.

Neuberger T, Schopf B, Hofmann H, Hofmann M, von Rechenberg B: Superparamagnetic nanoparticles for biomedical applications: possibilities and limitations of a new drug delivery system. JMMM 2005;1:483–496.

Nicotera TM, Ding D, McFadden SL, Salvemini D, Salvi R: Paraquat-induced hair cell damage and protection with the superoxide dismutase mimetic M40403. Audiol Neurootol 2004;9:353–362.

Pankhurst QA, Connolly J, Jones SK, Dobson J: Applications of magnetic nanopaticles in Biomedicine. J Phys D Appl Phys 2003;36:R161–R181.

Panyam J, Dali MA, Sahoo SK, Ma WX, Chakravarthi SS, Amidon GL, Levy RJ, Labhasetwar V: Polymer degradation and in vitro release of a model protein from poly(D,L-lactide-co-glycolide) nano- and microparticles. J Control Release 2003;92:173–187.

Panyam J, Williams D, Dash A, Leslie-Pelecky D, Labhasetwar V: Solid-state solubility influences encapsulation and release of hydrophobic drugs from PLGA/PLA nanoparticles. J Pharm Sci 2004;93:1804–1814.

Panyam J, Zhou WZ, Prabha S, Sahoo SK, Labhasetwar V: Rapid endo-lysosomal escape of poly(DL-lactide-co-glycolide) nanoparticles: implications for drug and gene delivery. FASEB J 2002;16:1217–1226.

Prabha S, Labhasetwar V: Nanoparticle-mediated wild-type p53 gene delivery results in sustained antiproliferative activity in breast cancer cells. Mol Pharm 2004;1:211–219.

Prabha S, Zhou WZ, Panyam J, Labhasetwar V: Size-dependency of nanoparticle-mediated gene transfection: studies with fractionated nanoparticles. Int J Pharm 2002;244:105–115.

Puig-De-Morales M, Grabulosa M, Alcaraz M, Mullol J, Maksym GN, Fredberg JJ, Navajas D: Measurement of cell microrheology by magnetic twisting cytometry with frequency domain demodulation. J Appl Physiol 2001;91:1152–1159.

Qaddoumi MG, Ueda H, Yang J, Davda J, Labhasetwar V, Lee VHL: The characteristics and mechanisms of uptake of PLGA nanoparticles in rabbit conjunctival epithelial cell layers. Pharm Res 2004;21:641–648.

Ranney DF: Magnetically controlled devices and biomodulation; in Tyle P (ed): Drug Delivery Devices. New York, NY, Marcel Dekker, 1988, pp 325–368.

Ravi R, Somani SM, Rybak LP: Mechanism of cisplatin ototoxicity – antioxidant system. Pharmacol Toxicol 1995;76:386–394.

Ryan AF, Harris JP, Keithley EM: Immune-mediated hearing loss: basic mechanisms and options for therapy. Acta Otolaryngol 2002;122:38–43.

Sahoo SK, Ma W, Labhasetwar V: Efficacy of transferrin-conjugated paclitaxel-loaded nanoparticles in a murine model of prostate cancer. Int J Cancer 2004;112:335–340.

Seidman M, Van de Water T: Pharmacologic manipulation of the labyrinth with novel and traditional agents delivered to the inner ear. Ear Nose Throat J 2003;82:276–280, 282–283, 287–288.

Shinkai M, Ito A: Functional magnetic particles for medical application. Adv Biochem Eng Biotechnol 2004;91:191–220.

Song BB, Anderson DJ, Schacht J: Protection from gentamicin ototoxicity by iron chelators in guinea pig in vivo. J Pharmacol Exp Ther 1997;282:369–377.

Suzuki M, Yamasoba T, Suzukawa K, Kaga K: Adenoviral vector gene delivery via the round window membrane in guinea pigs. Neuroreport 2003;14:1951–1955.

Wang J, Van de Water TR, Bonny C, de Ribaupierre F, Puel JL, Zine A: A peptide inhibitor of c-Jun N-terminal kinase protects against both aminoglycoside and acoustic trauma-induced auditory hair cell death and hearing loss. J Neurosci 2003;23:8596–8607.

Witte MC, Kasperbauer JL: Round window membrane permeability to transforming growth factor-alpha: an in vitro study. Otolaryngol Head Neck Surg 2000;123:91–96.

Yamamoto H, Kuno Y, Sugimoto S, Takeuchi H, Kawashima Y: Surface-modified PLGA nanosphere with chitosan improved pulmonary delivery of calcitonin by mucoadhesion and opening of the intercellular tight junctions. J Control Release 2005;102:373–381.

Zhang YY, Kropp BP, Moore P, Cowan R, Furness PD, Kolligian ME, Frey P, Cheng EY: Coculture of bladder urothelial and smooth muscle cells on small intestinal submucosa: potential applications for tissue engineering technology. J Urol 2000;164:928–934.

KARGER

Yamamoto et al., 2002]. These include soluble tropic factors such as growth factors, which are released into the extracellular fluid. Neurites can respond to gradients of these soluble factors with directional growth [e.g. Cao and Shoichet, 2003; Gillespie, 2003; Yoshikawa and Thomas, 2004]. Patterns of extracellular matrix (ECM) molecules such as laminin, fibronectin or collagen, which may be components of extracellular structures or be bound to their surfaces, can provide additional cues [e.g. Gillespie, 2003; Gallo and Letourneau, 2004; Hari et al., 2004; Oster et al., 2004; Yoshikawa and Thomas, 2004]. A wide variety of molecules that reside on the surfaces of cells, such as components of the ephrin/Eph bidirectional signaling system [Marquardt et al., 2005], can provide directional signals at the cellular and the subcellular level.

Many known neurite guidance molecules have been localized to regions or cells of the developing cochlea that are appropriate for a role in regulating neurite growth, providing the substrates for guidance of afferent and efferent projections. Neurotropic growth factors present in the developing organ of Corti include neutrotrophin-3 (NT-3), brain-derived neurotrophic factor and acidic fibroblast growth factors (FGF-1), all of which are produced by hair cells [Luo et al., 1993; Pirvola et al., 1992, 1994; Ernfors et al., 1994]. Many ECM molecules including fibronectin, laminin, tenascin and various collagens occur in the organ [e.g. Woolf et al., 1992; Tsuprun and Santi, 1999, 2001; Whitlon et al., 1999]. Several ephrins and Eph receptors have also been identified in the developing inner ear [Bianchi and Liu, 1999; van Heumen et al., 2000; Pickles et al., 2002].

Identifying the role played by these individual molecules in spiral ganglion (SG) neurite guidance has proven to be more difficult. Gene deletion studies have provided information, but can result in the death of neurons, e.g. tropic molecules that also provide trophic support [Ernfors et al., 1994; Farinas et al., 1994; Fritzsch et al., 1997a, 1998], or even the organism, e.g. many ECM molecules [George et al., 1993]. While in vitro techniques clearly have their limitations, they can be used to probe different developmental periods independently, in a way that gene deletion studies often cannot. Studies of neurons in culture have the additional advantage that the environment in which neurites are extending can be precisely controlled. In particular, they allow potential guidance factors to be presented in controlled patterns.

This is critical since, in order for a substance to provide directional information to advancing neurites, it must be differentially distributed. Variation in distribution can take many forms, from abrupt gradients in concentration that are essentially step-like at the dimension of the sampling growth cone, to gradual gradients that extend over many times the sensing radius of the neuron. For example, recent evidence indicates that gradients of soluble neurotropic factors can contribute to neurite guidance over distances of more than 10 mm [Cao and Shoichet, 2003]. Distribution of insoluble substances may be punctate, or can occur in patterns that relate to the underlying structure of the tissue. For example, in rodents, fibronectin appears to occur in tracts that run beneath the hair cells, during the first postnatal week [Woolf et al., 1992]. Cell surface molecules can be confined to individual cells or to cellular regions, or may be broadly distributed across tissues.

We have taken advantage of methods for micropatterning guidance molecules to directly assess SG neurite guidance in culture. Insoluble molecules have been patterned as edges, stripes and puncta. Soluble factors have been represented as discrete fluid gradients or localized cellular sources. Taken together, our studies suggest that SG neurites can respond directionally to differentially distributed guidance factors.

Methods

Culture of SG Neurons

Surgical procedures were approved by the local animal subject committee in accordance with the guidelines laid down by the NIH regarding the care and use of animals for experimental procedures. Three- to five-day-old (P3–P5) rat pups were decapitated and the skulls opened midsagitally under sterile conditions. The membranous labyrinth was exposed by peeling off the cartilaginous cochlear capsule under a dissecting microscope. The stria vascularis and the organ of Corti were removed in order to expose the spiral ganglia. The SG was excised from the entire length of the cochlea and divided into explants that were approximately 300 × 300 μm.

Culture procedures were based on those developed by Van De Water and Ruben [1971] and have been described in detail elsewhere [e.g. Brors et al., 2003]. Briefly, individual explants were cultured on surfaces coated with poly-*L*-lysine (PLL). Additional molecules were applied to this surface in various patterns as described below. The tissue was initially incubated in attachment media consisting of DMEM, 10% FCS, 5% HEPES and 30 units/ml penicillin for 24 h at 37°C, 5% CO_2. After 24 h, the culture medium was changed to maintenance media consisting of DMEM supplemented with 1 × N2 and 5 g/l glucose. Cultures were maintained for 72–96 h in maintenance media. Various soluble factors were included as described below.

Fixation and Immunohistochemistry

After culture in maintenance media, explants were fixed with 4% paraformaldehyde for 20 min and then washed with PBS. The samples were blocked with 1% donkey serum for 10 min at room temperature to reduce nonspecific binding. Specimens were incubated with rabbit polyclonal anti-200 kDa neurofilament antibody

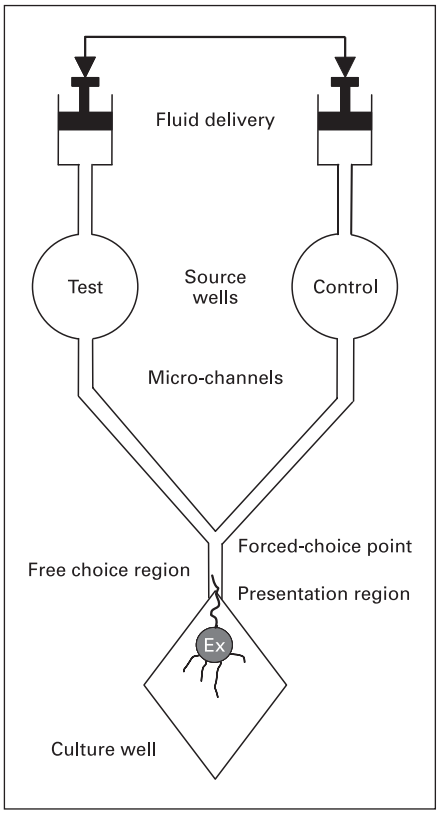

Fig. 1. Schematic diagram of a microfluidic device for creation of a fluid gradient and choice point for growing neurites. The device is generated by photolithography and molding. Test and control fluids are forced through a microchannel network at equal rates. They meet at the forced-choice point of a 'Y', and then flow in parallel through a free-choice presentation region to the tissue culture well.

(Sigma-Aldrich) diluted 1:500 at 4°C overnight. Explants were then incubated in donkey antirabbit secondary antibody (Jackson ImmunoResearch) diluted 1:100 in PBS. Either fluorescent or DAB labeling was used to visualize the secondary antibody. Immunolabeling controls in which rabbit serum was substituted for the primary antibody exhibited no labeling. Neurites were digitally imaged on a fluorescence inverted microscope (Olympus).

Microfabrication

Photolithographic techniques used to generate molds for microfluidic devices and for masks used in surface patterning have been described in detail elsewhere [Wittig et al., 2005]. Briefly, mold patterns were generated as negative images in Canvas 5.0 (Deneba Systems, Inc.) and printed as high-resolution transparencies with multiple patterns. The transparencies were used to expose the desired areas of positive photoresist (SU-8 100 or SU-8 1000, Microchem Corp.) spun into a uniform layer of the desired thickness on a 4-inch silicon wafer to ultraviolet light. When a second layer and transparency were required, they were aligned to the initial exposed pattern, which had become translucent.

After exposure, the photoresist was developed, and the mold master was cleaned, baked and dried. It was then attached to an aluminum plate prior to silicon wafer removal. The pattern was then molded in polydimethylsiloxane (Sylgard 184, Dow Corning) and cured to the desired level of elasticity.

Results

Soluble Guidance Cues

A microfluidic device for the evaluation of soluble guidance cues in fluid was developed by Wittig et al. [2005]. The device was fabricated and tested for production of fluid gradients with a fluorescent dye. A schematic of the device is illustrated in figure 1. Fluid is delivered at equal rates from two source wells by identical, physically ganged syringes. The resulting fluid gradients are illustrated in figure 2. As the two fluid streams unite at the union of the microchannel 'Y' a steep gradient is formed across the 100-μm width of the stem of the Y. Dye concentration transitions from >95% of peak concentration to <5% of peak concentration in 20–35 μm. This gradient is maintained until the fluid streams exit the narrow stem of the 'Y' into an expanding culture well, when the gradient becomes increasingly diffuse. Thus in an experiment using a biologically active diffusible mediator on one side of the device, neurites extending from an SG explant toward the microchannel encounter at first a diffuse and then, as they enter the microchannel, a sharp fluid gradient of the factor.

SG explants presented with a choice between NT-3 and control media showed a strong preference for growth in NT-3. This resulted in changes in neurite direction within the diffuse gradient at the exit from the 'Y', in preferential growth of neurites on the NT-3 side of the stem of the 'Y' and growth into the NT-3 side of the 'Y' bifurcation of a majority of neurites, as illustrated in figure 3. When NT-3 was presented from both delivery wells, no preference for side was observed (data not shown).

Insoluble Guidance Cues

A variety of strategies were employed to produce restricted distributions of substrate-bound guidance cues. Initially, silicone masks were fabricated with a single longitudinal gap. When fitted into a tissue culture well, the mask blocked all but a single stripe of culture surface, to which substances could be attached from solution by incubation. This method produced an abrupt edge of the attached guidance cue over ~20 μm at the edge of the stripe. SG explants could be placed outside of or on the

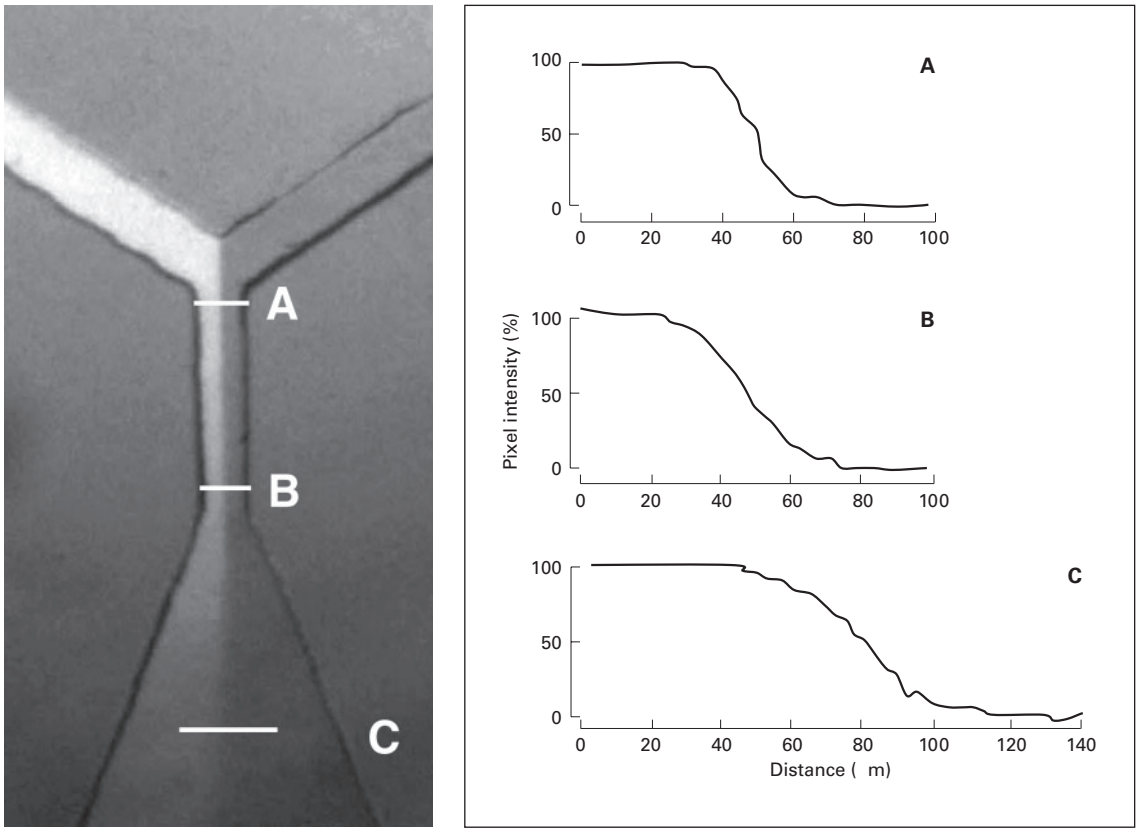

Fig. 2. Test of the fluid gradients produced by delivery of a fluorescent dye versus clear fluid to the forced-choice (**A**), free-choice (**B**) and presentation (**C**) regions of the device. A sharp gradient is created in the forced-choice and free-choice regions. A diffuse gradient is created when the microchannel exits into the presentation region, in both the horizontal and vertical dimensions. Adapted from Wittig et al. [2005].

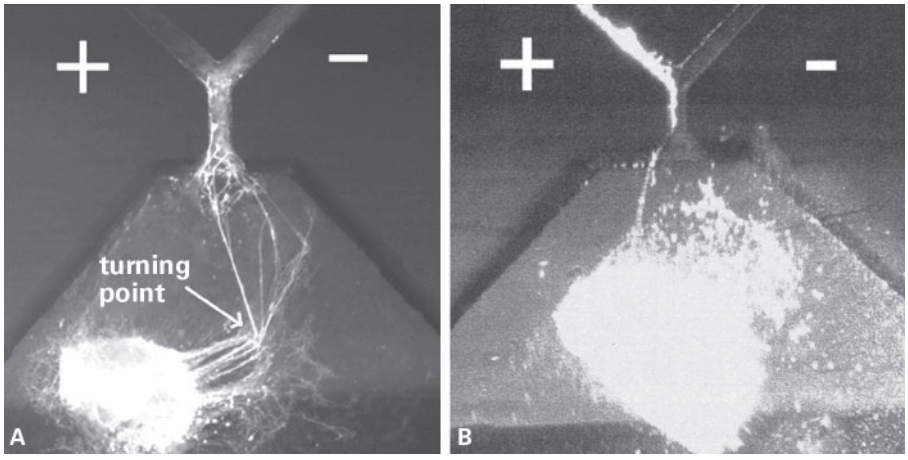

Fig. 3. Neonatal rat SG explants grown in the microchannel device for 72 h, with delivery of 10 ng/ml NT-3 in neuronal media (+) versus media alone (–). The explants were subsequently fixed and stained with antineurofilament antibody to visualize neurites. **A** A sharp inflection in neurite projection toward the microchannel can be observed. **B** Neurites and associated cells are preferentially observed on the side of the free-choice region that contains NT-3, and in the NT-3-containing microchannel beyond the forced-choice point. Adapted from Wittig et al. [2005].

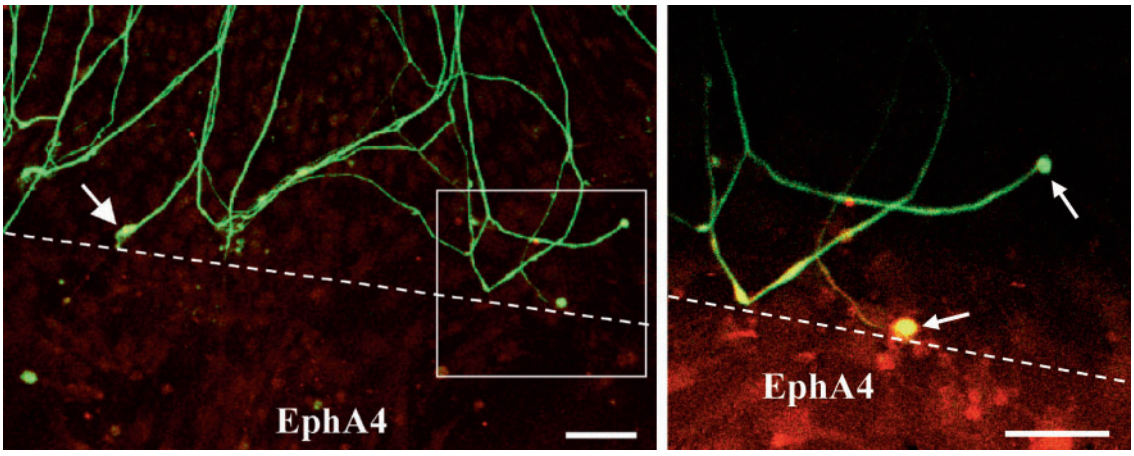

Fig. 4. Neonatal rat SG neurites (green) at the edge of a stripe of EphA4 (dashed line) exhibit growth cone collapse (arrows), termination of extension, and reversal of growth trajectory. From Brors et al. [2003].

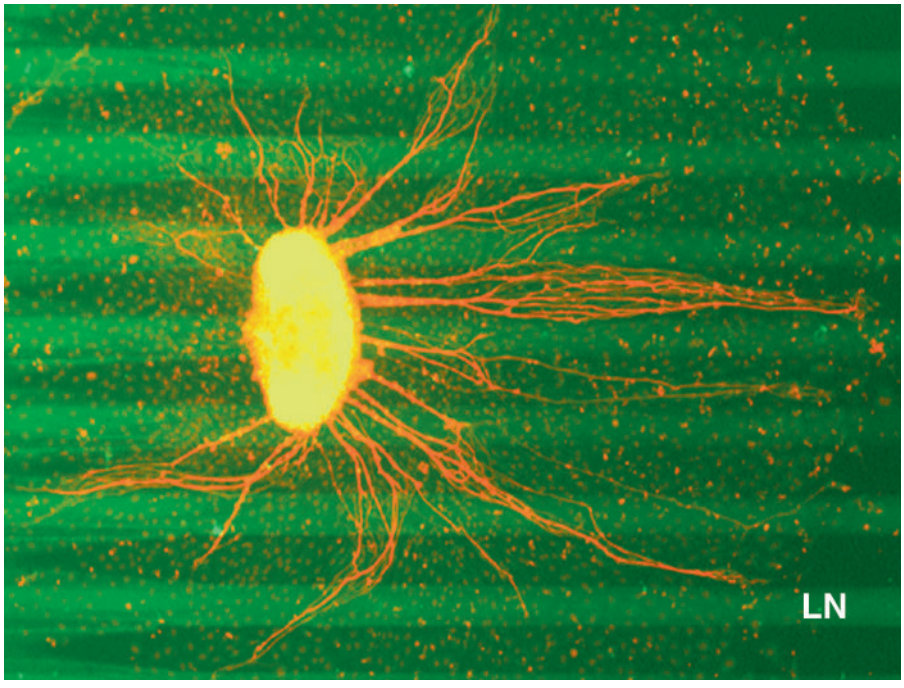

Fig. 5. Neurites from a neonatal SG explant (red), grown on a pattern of laminin stripes (green). The neurites demonstrate a strong preference to grow off of laminin. Adapted from Evans et al. [2005].

stripe, to evaluate their response to positive or negative edges, respectively.

This method was used to evaluate the responses of SG neurites to boundaries of the ECM molecule fibronectin [Aletsee et al., 2000], and the Eph receptor EphA4 [Brors et al., 2003]. Fibronectin boundaries proved to inhibit neurite growth, producing a strong tendency for neurites to stop and/or turn in response to a positive edge (data not shown). EphA4 was actively repulsive, invariably causing neurites to exhibit growth cone collapse and reversal of growth trajectory (fig. 4). No response to a neutral control protein (bovine serum albumin, BSA) was observed (data not shown).

To simulate linear tracts of ECM molecules in the organ of Corti, photolithographic microfabrication techniques were used to manufacture a mask with repeating

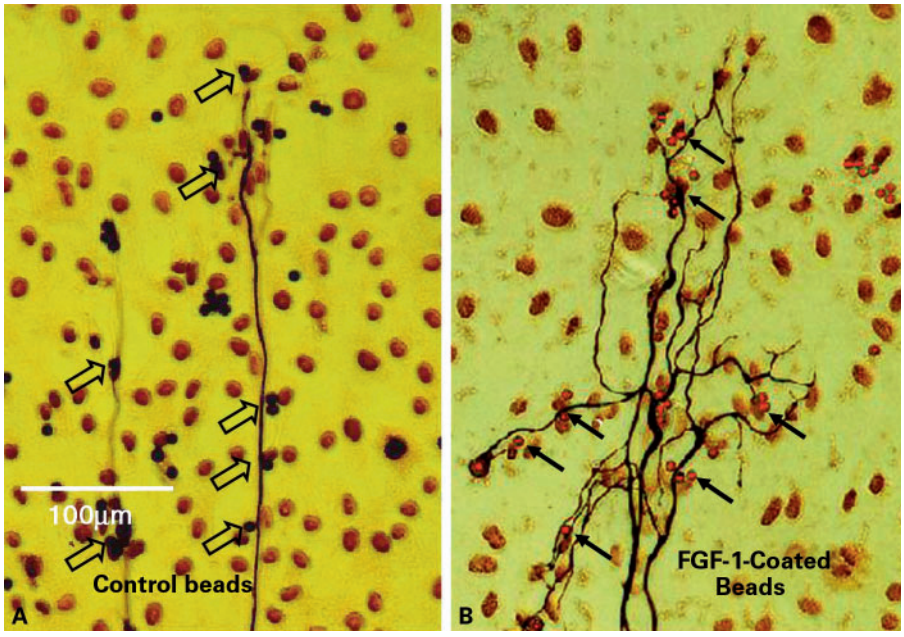

Fig. 6. Interaction of neurites from an SG explant with point sources of FGF-1. **A** The neurites cultured with control beads (open arrows) follow a simple trajectory. **B** The neurites encounter a cluster of FGF-1-coated beads (solid arrows). They exhibit extensive branching. Analysis of numerous such contacts revealed a significant increase in branching ($p < 0.01$). From Aletsee et al. [2003].

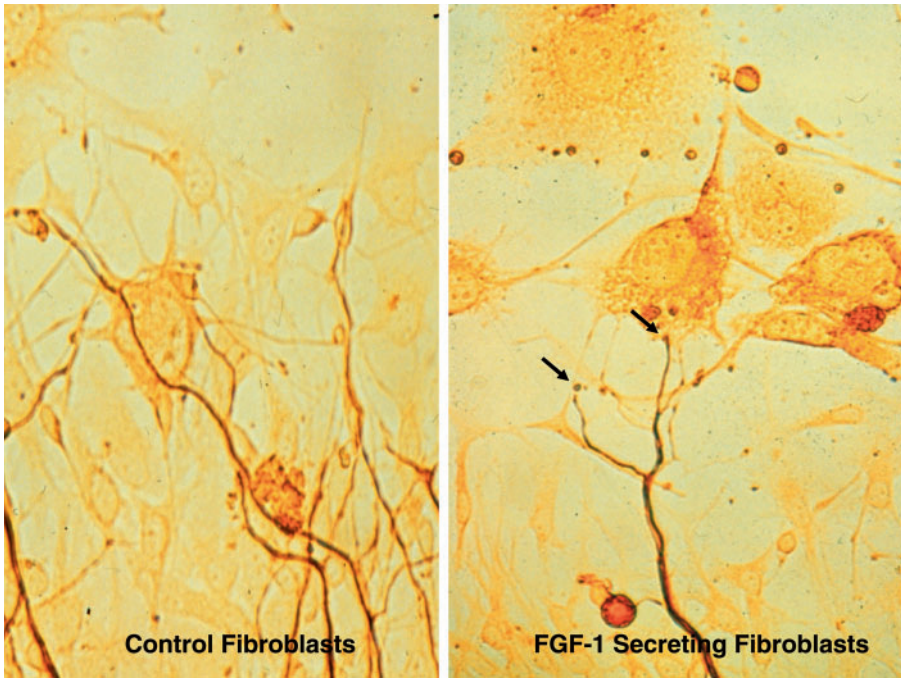

Fig. 7. Response of SG neurites to a cellular source of FGF-1. In the left panel, neurites grow over control mouse 3T3 fibroblasts. In the right panel, neurites encountering 3T3 cells that have been stably engineered to express human FGF-1 on the cell surface branch and form bouton-like terminations (arrows) on the cells. From Dazert et al. [1998].

microchannels that, after placement on a culture surface, could be filled with fluid containing an ECM molecule, for incubation [Evans et al., 2005]. After removal of the mask and application of PLL to coat the regions between the ECM stripes, this resulted in a pattern of narrow, repeating stripes of the cue.

When SG explants were grown on patterns of laminin, they showed a highly significant ($p < 0.001$), dose-dependent tendency for preferential growth. When stripes were produced by incubation with low concentrations of laminin, the neurites were preferentially found on laminin. At higher concentrations, the reverse was seen. In the example illustrated in figure 5, neurites exhibit a strong pref-

erence to grow off of stripes produced by incubation with 40 μg/ml of laminin. In the figure it can be noted that especially neurites approaching the laminin stripes at angles below about 45° tended to grow off of laminin onto PLL. In contrast, neurites preferred PLL to fibronectin at all concentrations, while control stripes of BSA had no effect (data not shown).

Cells that display guidance cues on their surfaces can act as punctate sources. For example, during the first postnatal week, rat hair cells produce high levels of FGF-1. Aletsee et al. [2003] modeled this phenomenon using 2- to 3-μm Sepharose microbeads coated with FGF-1, a growth factor that often binds to ECM molecules. SG neurites that encountered beads coated with BSA showed no response. Neurites that encountered FGF-1-coated beads exhibited extensive branching, although they did not terminate on the beads (fig. 6).

Dazert et al. [1998] used an alternative method to model FGF-1 production by hair cells. They co-cultured SG explants with 3T3 fibroblasts that were stably transfected to produce human FGF-1. The cells were placed peripheral to the explants, and were sufficiently different in morphology (larger and more spread out) from cells migrating out of the explants that they could easily be distinguished. In the construct used for transfection, the FGF-1 signal peptide was replaced with that for FGF-3, so that the FGF-1 remained bound to the cell surface rather than being secreted into the surrounding medium. While SG neurites showed a tendency to grow over control fibroblasts, they exhibited branching in response to FGF-1-producing cells. Moreover, they also formed bouton-like contacts on the cells (fig. 7).

Discussion

The results presented in this review demonstrate that patterning of neuronal guidance cues, on a microscale that is relevant to sampling by growth cone filopodia, provides a means by which to investigate SG neurite guidance in culture. Using a variety of methods it was possible to produce spatial patterns of cues, as experimental models of distributions that occur in the developing cochlea. In particular, patterning methods based upon photolithographic techniques allowed precise micropatterning. These methods were derived from many previous studies in other systems.

Stripe assays have a long history of use in the evaluation of neurite pathfinding. For example, Walter et al. [1987] created stripes using the cell membranes from homogenates of different target tissues. They employed a silicon mask with parallel channels similar to that used in the present study. The mask was placed to selectively block (in a striped pattern) the insertion of a membrane suspension into a capillary pore filter when suction was applied beneath the filter. Chick retinal ganglion explants were then cultured on this surface after the matrix was removed and a different membrane suspension was used to fill the empty stripes on the filter. More biochemically specific studies have used purified proteins as substrata. Employing methods similar to those of the present study, based on photolithographic techniques, Vielmetter and Stuermer [1989], Nguyen-Ba-Charvet et al. [2001], Weinl et al. [2003], and Jain et al. [2004] evaluated the responses of primarily retinal neurites to stripes of various substrates.

Our use of photolithography to generate microfluidic networks was also based upon a rich prior history. Methods for the rapid production of microfluidic systems using a positive relief microchannel structure on silicon molded with polydimethylsiloxane were outline by Duffy et al. [1998]. This technique formed the basis for a network used to create complex concentration gradients [Dertinger et al., 2001, 2002] with laminar fluid flow through microchannels. Previous microfluidic designs permanently bonded fluidic delivery tubes, microchannel layers, and surface layers such that each unit could be used only once [Duffy et al., 1998; Dertinger et al., 2001]. We used a compression plate to make each unit reusable across experiments. The compression plate incorporates a fluidic delivery system, simplifying connection of hydraulic pumps (syringe pumps) to the cell culture plate. An additional innovation was to apply the microchannel device to extending neurites.

Using micropatterning, we have found that neonatal SG neurites are sensitive to spatial patterns of a number of potential guidance cues. In particular, SG neurites appeared to display directional growth in response to both diffuse and sharp spatial differences in the concentration of NT-3. Diffuse differences appeared to induce turning, while a near-step difference in concentration produced a tendency for growth restricted to the NT-3 side. While these behaviors can be interpreted to reflect directional responses of SG neurites, an alternate possibility is preferential survival. It is possible that when neurites grew into media without NT-3, the associated neuron died, leaving only neurites in the NT-3 region. We feel that this explanation is less likely than directional behavior, since we and others have found that the requirement for NT-3 is not complete for postnatal P3–P5 neurites extending

from SG explants. That is, SG neurons in explants harvested at this age do not die obligatorily without neurotrophin support. Rather, many neurons in SG explants survive and project neurites in media without any neurotrophic factor present [e.g. Aletsee et al., 2001a].

SG neurites also responded to point sources of FGF-1 with branching and/or termination. They exhibited avoidance of ECM molecules, and could be guided over long distances by linear ECM patterns. Finally, SG neurites were actively repulsed by the Eph receptor EphA4.

Neurotrophic growth factors such as the neurotrophins or FGFs have been previously implicated in cochlear neuronal survival. For example, gene deletion studies have identified the importance of NT-3 for embryonic SG neuron survival [Farinas et al., 1994; Fritzsch et al., 1997a, b], and FGF treatment has been effective in rescuing dissociated SG neurons or increasing SG neurite numbers in culture [Lefebvre et al., 1992; Malgrange et al., 1996a; Aletsee et al., 2001a]. However, evidence for a guidance role of these factors has been less direct. Fritzsch et al. [1997a] concluded, based on innervation patterns detected in NT-3 null mice, that basalward turning of type II SG neurons within the organ of Corti occurs in response to an NT-3 gradient. Malgrange et al. [1996b] found that SG neurites are preferentially found on that side of a semipermeable membrane upon which NT-3 is present, although it should be noted that growth conditions on the two sides differed in other ways. Our data are consistent with these earlier results and conclusions. They provide more direct evidence that developing SG neurites will grow up a diffuse NT-3 fluid gradient, even in the absence of a physical barrier segregating the factor. Gradients may also influence SG neurons in other ways. Based on recordings from cultured SG neurons after neurotrophin treatment, Davis [2003] has speculated that neurotrophin gradients may help to shape the physiological properties of SG neurons at different cochlear locations.

Because FGF-1 null mice exhibit embryonic lethality, development of cochlear innervation in the absence of FGF-1 has not been evaluated. However, strong expression of FGF-1 by cochlear hair cells during the first postnatal week in rodents [Luo et al., 1993] occurs during a period of active synaptogenesis [Lenoir et al., 1980] and terminal innervation in the organ of Corti [Echteler, 1992; Echteler and Nofsinger, 2000]. This suggests that FGF-1 may play a role in innervation of the organ. Previous studies have indicated that FGFs in solution can support SG neuron survival and promote the growth of neurites. However, the response of SG neurites to point sources of FGF-1 suggests that this factor may also serve as a termination and branching cue.

Many neurons respond to ECM molecules via integrin receptors. We have previously shown that SG neurites are stimulated by uniform surfaces of ECM molecules such as laminin and fibronectin, and that this stimulation is mediated by integrins [Aletsee et al., 2001b; Kim et al., 2005]. However, ECM molecules are not uniformly distributed in the developing cochlea. In particular, the developing organ of Corti contains tracts of ECM matrix molecules that run beneath the hair cells [Woolf et al., 1992]. The data reviewed here suggest that depending upon the ECM molecule and amount, such tracts may attract growing neurites, or the boundaries of such tracts may serve to restrict the growth of neurites into certain regions of the organ, or to channel dendrites alongside or between adjacent tracts. Similarly EphA4, which occurs on the upper and lower elements of the osseous spiral lamina [van Heumen et al., 2000], may serve to funnel extending neurites within the lamina and toward the organ of Corti.

All of the observations reviewed here were obtained in vitro, and potential differences between the culture and the in vivo environments must be taken into consideration when interpreting the data. However, in vitro methods have allowed us to simplify the environment of extending SG neurites, and to control the distributions of possible guidance cues that they encounter. Microfabrication and cellular techniques have permitted us to produce gradients of guidance cues over distances much smaller than the sensing radius of the neural growth cone. We have also been able to study particular periods of development in isolation. In doing so, we have identified a number of signals that have the potential to influence the trajectory of developing SG neurites.

The data also have implications for the regrowth of deafferented SG neurites toward the electrodes of a cochlear implant (CI) [Brors et al., 2002]. The spatial resolution of CIs is low compared to the intact cochlea, which has many thousands of independent neural channels. It may be possible to increase the number of usable CI channels by attracting the neurites of surviving SG neurons toward the electrode array. If neurites could be directed to the electrodes in a controlled manner, allowing stimulation with very small electrical fields, it might be possible to increase the number of effectively separate channels dramatically, to several hundred. This could greatly increase CI frequency resolution. While there are distinct differences between neonatal and adult neurons [Koeberle and Bahr, 2004], lessons learned on developing neu-

rons provide a starting point for research on mature dendrites. The survival of deafferented adult SG neurons can be enhanced by exogenous neurotrophins [e.g. Staecker et al., 1996], suggesting that other responses may also be possible. Research on the guidance of adult SG neurites is currently underway.

Acknowledgements

Supported by grant DC00139 from the NIH/NIDCD, the Research Service of the VA, the National Organization for Hearing Research, the Deafness Research Foundation, and the Deutsche Forschungsgemeinschaft. The assistance of Sangeeta Bhatia and Elliot Hui in microfabrication of molds for the linear array masks is gratefully acknowledged.

References

Aletsee C, Beros A, Mullen L, Palacios C, Pak K, Dazert S, Ryan AF: Ras/MEK but not p38 signaling mediates neurite extension from spiral ganglion neurons. JARO 2001a;2:377–387.

Aletsee C, Beros A, Mullen L, Palacios S, Pak K, Dazert S, Ryan AF: The disintegrin kistrin inhibits neurite extension from spiral ganglion explants cultured on laminin. Audiol Neurotol 2001b;6:57–65.

Aletsee C, Brors D, Mlynski R, Ryan AF, Dazert S: Branching of spiral ganglion neurites is induced by focal application of fibroblast growth factor-1. Laryngoscope 2003;113:791–796.

Aletsee C, Kim D, Dazert S, Ryan AF: Fibronectin boundaries influence the outgrowth of spiral ganglion neurons in vitro. Abstr ARO 2000;23:130.

Bianchi LM, Liu H: Comparison of ephrin-A ligand and EphA receptor distribution in the developing inner ear. Anat Rec 1999;254:127–134.

Brors D, Aletsee C, Schwager C, Mlynski R, Hansen S, Schafers M, Ryan AF, Dazert S: Interaction of spiral ganglion neuron processes with alloplastic materials in vitro. Hear Res 2002;167:110–121.

Brors D, Bodmer D, Pak K, Aletsee C, Schafers M, Dazert S, Ryan AF: EphA4 provides repulsive signals to developing cochlear ganglion neuritis mediated through ephrin-B2 and -B3. J Comp Neurol 2003;462:90–100.

Cao X, Shoichet MS: Investigating the synergistic effect of combined neurotrophic factor concentration gradients to guide axonal growth. Neuroscience 2003;122:381–389.

Davis RL: Gradients of neurotrophins, ion channels, and tuning in the cochlea. Neuroscientist 2003;9:311–316.

Dazert S, Kim D, Luo L, Aletsee C, Garfunkel S, Maciag T, Baird A, Ryan AF: Focal delivery of fibroblast growth factor-1 by transfected cells induces spiral ganglion neurite targeting in vitro. J Cell Physiol 1998;177:123–129.

Dertinger SK, Chiu DT, Jeon NL, Whitesides GM: Generation of gradients having complex shapes using microfluidic networks. Anal Chem 2001;73:1240–1246.

Dertinger SK, Jiang X, Li Z, Murthy VN, Whitesides GM: Gradients of substrate-bound laminin orient axonal specification of neurons. Proc Natl Acad Sci USA 2002;99:12542–12547.

Duffy DC, McDonald JC, Schueller OJ, Whitesides GM: Rapid prototyping of microfluidic systems in poly(dimethylsiloxane). Anal Chem 1998;70:4974–4984.

Echteler SM: Developmental segregation in the afferent projections to mammalian auditory hair cells. Proc Natl Acad Sci USA 1992;89:6324–6327.

Echteler SM, Nofsinger YC: Development of ganglion cell topography in the postnatal cochlea. J Comp Neurol 2000;425:436–446.

Ernfors P, Lee KF, Jaenisch R: Mice lacking brain-derived neurotrophic factor develop with sensory deficits. Nature 1994;368:147–150.

Evans A, Pak K, Mullen L, Bhatia S, Ryan AF: Micropatterning of extracellular matrix molecules reveals preference by cochlear ganglion neurites, submitted.

Farinas I, Jones KR, Backus C, Wang XY, Reichardt LF: Severe sensory and sympathetic deficits in mice lacking neurotrophin-3. Nature 1994;369:658–661.

Fritzsch B, Barbacid M, Silos-Santiago I: The combined effects of trkB and trkC mutations on the innervation of the inner ear. Int J Dev Neurosci 1998;16:493–505.

Fritzsch B, Farinas I, Reichardt LF: Lack of neurotrophin 3 causes losses of both classes of spiral ganglion neurons in the cochlea in a region-specific fashion. J Neurosci 1997a;17:6213–6225.

Fritzsch B, Silos-Santiago I, Bianchi L, Farinas I: Effects of neurotrophin and neurotrophin receptor disruption on the afferent inner ear innervation. Semin Cell Dev Biol 1997b;8:277–284.

Gallo G, Letourneau PC: Regulation of growth cone actin filaments by guidance cues. J Neurobiol 2004;58:92–102.

George EL, Georges-Labouesse EN, Patel-King RS, Rayburn H, Hynes RO: Defects in mesoderm, neural tube and vascular development in mouse embryos lacking fibronectin. Development 1993;119:1079–1091.

Gillespie LN: Regulation of axonal growth and guidance by the neurotrophin family of neurotrophic factors. Clin Exp Pharmacol Physiol 2003;30:724–733.

Hari A, Djohar B, Skutella T, Montazeri S: Neurotrophins and extracellular matrix molecules modulate sensory axon outgrowth. Int J Dev Neurosci 2004;22:113–117.

Jain A, Brady-Kalnay SM, Bellamkonda RV: Modulation of Rho GTPase activity alleviates chondroitin sulfate proteoglycan-dependent inhibition of neurite extension. J Neurosci Res 2004;77:299–307.

Kim D, Pak K, Aletsee C, Mullen L, Dazert S, Ryan AF: Fibronectin enhances spiral ganglion neurite outgrowth in vitro. Hear Res, submitted.

Koeberle PD, Bahr M: Growth and guidance cues for regenerating axons: where have they gone? J Neurobiol 2004;59:162–180.

Lefebvre P, Weber T, Rigo J, Staecker H, Moonen G, Van De Water T: Peripheral and central target-derived trophic factor(s) effects on auditory neurons. Hear Res 1992;58:185–192.

Lenoir M, Shnerson A, Pujol R: Cochlear receptor development in the rat with emphasis on synaptogenesis. Anat Embryol 1980;160:253–262.

Luo L, Koutnouyan H, Baird A, Ryan, AF: Expression of mRNA encoding acidic and basic FGF in the adult and developing cochlea. Hear Res 1993;69:182–193.

Malgrange B, Lefebvre PP, Martin D, Staecker H, Van de Water TR, Moonen G: NT-3 has a tropic effect on process outgrowth by postnatal auditory neurones in vitro. Neuroreport 1996b;7:2495–2499.

Malgrange B, Lefebvre P, Van De Water TR, Staecker H, Moonen G: Effects of neurotrophins on early auditory neurones in cell culture. Neuroreport 1996a;7:913–917.

Marquardt T, Shirasaki R, Ghosh S, Andrews SE, Carter N, Hunter T, Pfaff SL: Coexpressed EphA receptors and ephrin-A ligands mediate opposing actions on growth cone navigation from distinct membrane domains. Cell 2005;121:127–139.

Nguyen-Ba-Charvet KT, Brose K, Marillat V, Sotelo C, Tessier-Lavigne M, Chedotal A: Sensory axon response to substrate-bound Slit2 is modulated by laminin and cyclic GMP. Mol Cell Neurosci 2001;17:1048–1058.

Oster SF, Deiner M, Birgbauer E, Sretavan DW: Ganglion cell axon pathfinding in the retina and optic nerve. Semin Cell Dev Biol 2004;15:125–136.

Pickles JO, Claxton C, Van Heumen WR: Complementary and layered expression of Ephs and ephrins in developing mouse inner ear. J Comp Neurol 2002;449:207–216.

Pirvola U, Arumae U, Moshnyakov M, Palgi J, Saarma M, Ylikoski J: Coordinated expression and function of neurotrophins and their receptors in the rat inner ear during target innervation. Hear Res 1994;75:131–144.

Pirvola U, Ylikoski J, Palgi J, Lehtonen E, Arumae U, Saarma M: Brain-derived neurotrophic factor and neurotrophin 3 mRNAs in the peripheral target fields of developing inner ear ganglia. Proc Natl Acad Sci USA 1992;89:9915–9919.

Staecker H, Kopke R, Malgrange B, Lefebvre P, Van De Water TR: NT-3 and/or BDNF therapy prevents loss of auditory neurons following loss of hair cells. Neuroreport 1996;7:889–894.

Tessarollo L, Coppola V, Fritzsch B: NT-3 replacement with brain-derived neurotrophic factor redirects vestibular nerve fibers to the cochlea. J Neurosci 2004;10:2575–2584.

Tsuprun V, Santi P: Ultrastructure and immunohistochemical identification of the extracellular matrix of the chinchilla cochlea. Hear Res 1999;129:35–49.

Tsuprun V, Santi P: Proteoglycan arrays in the cochlear basement membrane. Hear Res 2001;157:65–76.

Van De Water TR, Ruben RJ: Organ culture of the mammalian inner ear. Acta Otolaryngol 1971;71:303–312.

van Heumen WR, Claxton C, Pickles JO: Expression of EphA4 in developing inner ears of the mouse and guinea pig. Hear Res 2000;139:42–50.

Vielmetter J, Stuermer CA: Goldfish retinal axons respond to position-specific properties of tectal cell membranes in vitro. Neuron 1989;2:1331–1339.

Walter J, Kern-Veits B, Huf J, Stolze B, Bonhoeffer F: Recognition of position-specific properties of tectal cell membranes by retinal axons in vitro. Development 1987;101:685–696.

Weinl C, Drescher U, Lang S, Bonhoeffer F, Loschinger J: On the turning of Xenopus retinal axons induced by ephrin-A5. Development 2003;130:1635–1643.

Whitlon D, Zhang X, Pecelunas K, Greiner M: A temporospatial map of adhesive molecules in the organ of Corti of the mouse cochlea. J Neurocytol 1999;28:955–968.

Wittig J, Ryan AF, Asbeck P: A reusable microfluidic plate with alternate-choice architecture for assessing growth preference in tissue culture. J Neurosci Meth 2005;144:79–89.

Woolf N, Koehrn FJ, Ryan AF: Expression of fibronectin in the developing inner ear of the gerbil and rat. Dev Brain Res 1992;65:21–33.

Yamamoto N, Tamada A, Murakami F: Wiring of the brain by a range of guidance cues. Prog Neurobiol 2002;68:393–407.

Yoshikawa S, Thomas JB: Secreted cell signaling molecules in axon guidance. Curr Opin Neurobiol 2004;14:45–50.

Audiology & Neurotology

Author Index Vol. 11, No. 2, 2006

Subject Index Vol. 11, No. 2, 2006

KARGER

Fax +41 61 306 12 34
E-Mail karger@karger.ch
www.karger.com

Accessible online at:
www.karger.com/aud